FUNCTIONAL CHARACTERIZATION OF A HUMAN ODORANT RECEPTOR

THÈSE N^{O} 3386 (2005)

PRÉSENTÉE À LA FACULTÉ SCIENCES DE BASE

Institut des sciences et ingénierie chimiques

SECTION DE CHIMIE ET GÉNIE CHIMIQUE

ÉCOLE POLYTECHNIQUE FÉDÉRALE DE LAUSANNE

POUR L'OBTENTION DU GRADE DE DOCTEUR ÈS SCIENCES

PAR

Valérie JACQUIER

ingénieure physicienne diplômée EPF
de nationalité suisse et originaire de Vernayaz (VS)

acceptée sur proposition du jury:

Prof. H. Vogel, directeur de thèse
Prof. H. Breer, rapporteur
Dr H. Hirling, rapporteur
Dr L. Salomé, rapporteur

Lausanne, EPFL
2006

Abstract

Olfaction appears to be mediated by a large family of odorant receptors (ORs) that accounts for $\sim 1\,\%$ of the human genome [1–4]. The functional characterization of these receptors has so far been hindered by their poor functional expression in the plasma membrane of heterologous cells.

In order to investigate the problem of inefficient OR membrane targeting, sequential stages in the life cycle of the human OR17-40 were monitored. The modification of the receptor by different tags enabled the direct visualization of its biogenesis and trafficking in HEK293 cells. A multi-color labelling approach, which involved fluorescent subcellular markers as well as the spectral separation of membrane-inserted and intracellularly located receptors, indicated that high over-expression led to the accumulation of the receptor in the ER, whereas low expression levels improved its membrane targeting. To increase the efficiency of OR-mediated signalling, fluorescence-activated cell sorting of a functional OR17-40 - GFP fusion protein was used to separate low from high expressing cells, thus increasing the fraction of odorant-responsive cells up to 80 % of the total cell population.

Selectively labelled cell surface receptors accumulated over time in intracellular compartments, indicating constitutive receptor internalization. This process, which was independent of receptor activation, occurred along the clathrin-mediated pathway. Moreover, the imaging of single receptors in the plasma membrane indicated that, in absence of ligand, part of the receptors are already confined within small domains of $195 \pm 10\,\mathrm{nm}$. This fraction, which increased upon agonist or antagonist binding, probably corresponds to receptors located in clathrin-coated pre-pits.

Odorant molecules structurally related to the cognate agonist helional were tested for their ability to activate OR17-40. It was found that an aldehyde group connected to an aromatic ring via a carbon chain of defined length and containing a methyl group in alpha or beta position is necessary for activating the receptor. In addition, first evidence for an OR17-40-specific antagonism was provided.

Finally, OR17-40 activation was monitored in cell-derived native vesicles, opening new ways for assay miniaturization and the development of odorant screenings in a micro-array format.

Version Abrégée

Les odeurs seraient transmises au cerveau par une vaste famille de récepteurs olfactifs (ORs) représentant environ 1 % du génome humain [1–4]. La caractérisation de ces récepteurs a été jusqu'ici retardée par le faible taux d'expres-sion fonctionnelle dans la membrane plasmique de cellules hétérologues.

Dans le but d'étudier le problème du mauvais transport des récepteurs olfactifs à la membrane plasmique, différentes étapes dans la vie du récepteur olfactif humain OR17-40 ont été suivies. La modification du récepteur par l'addition de différents peptides ont permis de visualiser directement sa biogénè-se et son adressage à la membrane dans des cellules HEK293. Un marquage multicolore comprenant des marqueurs cellulaires fluorescents ainsi que la séparation spectrale des récepteurs insérés dans la membrane et des récepteurs situés dans le cytoplasme a indiqué qu'une haute sur-expression conduit à l'accumulation du récepteur dans le réticulum endoplasmique, alors que le transport du récepteur à la membrane plasmique est meilleur dans les cellules à faible taux d'expression. Pour renforcer le signal induit par le récepteur, le tri de cellules en fluorescence exploitant une chimère fonctionelle OR17-40 - GFP a été utilisé pour séparer les cellules à faible taux d'expression des cellules à haute sur-expression, ce qui a permis d'enrichir la fraction des cellules répondant au ligand jusqu'à 80 % de la population totale.

Il est montré que les récepteurs se trouvant à la membrane plasmique et qui ont été marqués spécifiquement s'accumulent au cours du temps dans des compartiments intracellulaires, indiquant l'internalisation constitutive du récepteur. Ce processus, qui est indépendant de l'activation du récepteur, a lieu par la voie médiée par la clathrine. De plus, l'étude de la diffusion de récepteurs uniques dans la membrane plasmique a indiqué qu'en absence de ligand, une partie des récepteurs est confinée à l'intérieur de domaines de 195 $\pm$ 10 nm, qui correspondent probablement à des précurseurs de puits recouverts de clathrine, et que cette fraction augmente après l'addition d'un agoniste ou d'un antagoniste.

Des molécules odorantes structurellement similaires à l'agoniste helional ont été testées pour leur capacité à activer OR17-40. Il est montré qu'un groupe

aldehyde relié à un cycle aromatique par une chaîne carbonique de longueur définie et contenant un groupe méthyle en position alpha ou beta est nécessaire pour activer le récepteur. De plus, un premier exemple d'antagonis-me spécifique à OR17-40 est fourni.

Finalement, l'activation d'OR17-40 a été observée dans des vésicules natives produites à partir de cellules, ouvrant la voie à la miniaturisation de tests pour le screening de molécules odorantes.

Contents

Chapter 1

General Introduction

The sense of smell is essential for the survival of most animals. It enables the identification and evaluation of food, territories, predators and reproductive partners by detecting molecules of immense chemical variety, ranging from acids, alcohols, aldehydes, esters, to aromatic and heterocyclic molecules. The vast capacity of chemical recognition is thought to be based on a large family of olfactory receptors (ORs) comprising up to thousand different subtypes [1–6]. These receptors are predicted to be heptahelical transmembrane proteins, which initiate the chemoelectrical transduction of odorant signals via G protein-coupled cascades in olfactory sensory neurons (OSNs) [1].

1.1 The Olfactory System

In most animals, two different olfactory systems have been developed: the main and the accessory olfactory systems [6, 7]. The common or main olfactory system enables the sensing of the environment, involved for example in food and prey detection, and is remarkable for its breadth and discriminatory capacity. The accessory olfactory system, called the vomeronasal system, is involved in the mating of a partner. It is highly specialized in recognizing pheromones, species-specific molecules produced by one sex and perceived by the other, and gives information on the geographic location of the mate and its reproductive state [6, 7].

In both olfactory systems, sensing is initiated by the binding of molecules to receptors encoded by a multigene family. Odors, typically small volatile molecules carried by the respiratory air stream, bind to ORs located in the cilia of olfactory sensory neurons in the nasal epithelium (Figure 1.1) [7–9]. These neurons are bipolar, with a single, unbranched axon projecting to the olfactory bulb and a short dendrite advancing into the nasal cavity [3, 7]. In the human nose, there

are more than five million olfactory neurons that are regenerated all three to six months [10], as toxic molecules reaching the nose lead to cell death.

In OSNs, ORs are mostly concentrated at the cell surface membrane of the cilia at the tip of the dendrite, where the sensory transduction takes place [8]. They are also present at axon terminals, where they are thought to play a role in the guidance of developing olfactory axons [11]. Indeed, in the olfactory bulb, the axons of OSNs expressing the same OR converge to a single "target" called a glomerulus [5, 12]. Glomeruli are spherical conglomerates of neuropil, which measure about 50 to 100 μm in diameter and which consist of the incoming axons of OSNs and the dendrites of the main projection cell in the bulb, the mitral cell [7]. From there, the signals are transmitted to the primary olfactory cortex and forwarded both to higher cortical areas, where the conscious perception of odors takes place, and to the limbic system, where emotions are created [3, 5] (Figure 1.1).

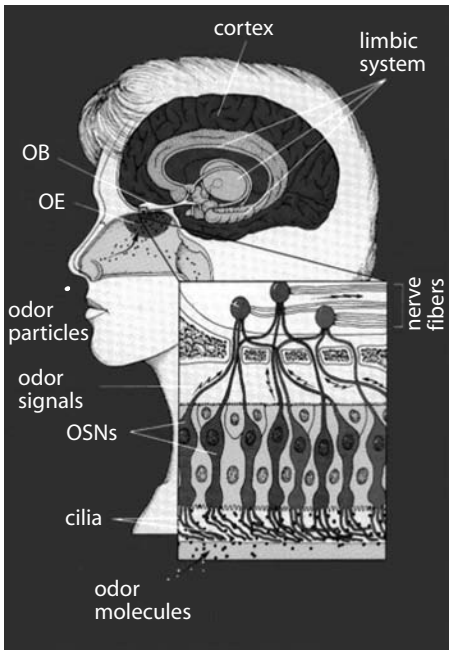

Figure 1.1: The olfactory system. *Olfactory sensory neurons (OSNs) in the olfactory epithelium (OE) detect odorant molecules carried by the respiratory air stream. The olfactory signals are then transmitted to high brain centers via the main olfactory bulb (OB).*

1.2 Odorant Receptors

1.2.1 Odorant Receptor Genes

ORs are encoded by the largest gene family, accounting for about 1 % of the human genome [5, 7, 8]. They have no introns in their coding sequence, which facilitates their identification from genomic DNA [9]. In human, about 900 OR genes were identified, but two-third of these turned out to be non-functional or "pseudogenes", due to frameshifts, internal deletions or incomplete coding regions, leaving 347 putative functional ORs [13]. The large number of human pseudogenes, as compared to about 20 % in rodents [4], suggests that olfaction became less important in the course of higher primate evolution [9].

ORs can bind either water-soluble or airborne ligands. Accordingly, their corresponding genes can be divided into two classes: Class I genes code for ORs binding water-soluble odorants, and Class II genes for ORs recognizing airborne ligands [9]. Class I genes are similar to fish OR genes, whereas Class II genes are unique to terrestrial vertebrates [4].

Human OR genes are located on almost all chromosomes, and are typically organized in clusters of ten or more members, but are randomly located inside one cluster [9, 14]. Transcriptional orientation can be either way, and intergenic distances are variable [14].

1.2.2 Structural Features of Odorant Receptors

ORs display the characteristic structural features of G protein-coupled receptors (GPCRs), such as seven α-helical transmembrane domains connected by intracellular and extracellular loops of different lengths, and various conserved short sequences [7]. They belong to the family A of GPCRs, which includes most GPCRs, such as rhodopsin and catecholamine receptors [3]. Family A GPCRs share two cysteines in the first and second extracellular loops that form a disulfide bridge, and an Asp-Arg-Tyr sequence (DRY motif) in the second intracellular loop [3, 15]. However, a putative palmitoylation site, which is typical for family A GPCRs and should allow the formation of a fourth cytoplasmic loop [15], is lacking in most ORs [3]. There are other characteristics specific to ORs, such as an unusually long second extracellular loop, an extra pair of conserved cysteines in that loop, and additional short conserved sequences [6].

Within the OR family, there is a range of similarity from less than 40 % to over 90 % identity, which allows the classification of OR sequences in different subfamilies [13]. In the third, fourth and fifth transmembrane regions, the se-

quences are very variable (Figure 1.2). In three-dimensional models of family A GPCRs, such as adrenergic receptors [16] or rhodopsin [17], these three α-helices are thought to form a pocket corresponding to the ligand binding site [18]. The variability observed among ORs in this region provides the first molecular basis for understanding the diversity and the large number of odorants that can be detected and discriminated [7].

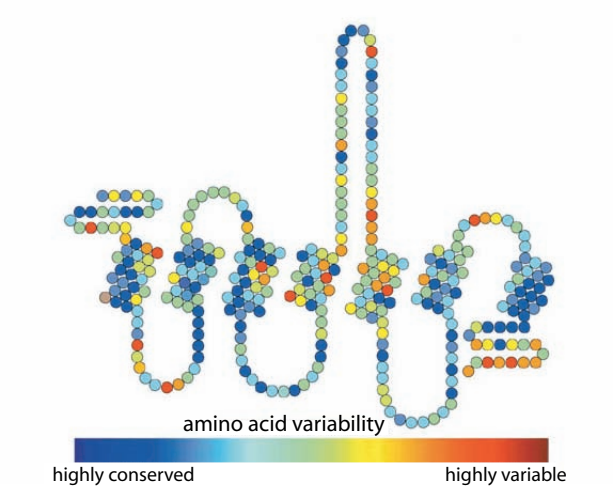

Figure 1.2: Seven-transmembrane domain structure of an OR. *The extra- and intracellular ends are relatively short. The degree of amino acid conservation in the consensus sequence is represented as a color in the rainbow spectrum, with blue being highly conserved and red highly variable (taken from [4]).*

1.3 Olfactory Signalling Pathways

1.3.1 GPCR Signalling

As all other GPCRs, odorant receptors activate a G protein upon agonist binding. The G protein is a heterotrimeric protein comprising the subunits α, β, and γ. The G_α subunit complexes the nucleotide guanosine diphosphate (GDP) in its inactive state and guanosine triphosphate (GTP) when it is activated [19]. The GTP-complexed G_α dissociates from the $G_{\beta\gamma}$ subunit, which is then activated. Both G_α and $G_{\beta\gamma}$ interact with downstream effectors, leading to a cellular response [19]. G protein activation is terminated by GTP hydrolysis on the G_α subunit, followed by the reunification of the heterotrimeric G protein. GTP hydrolysis is often accelerated by other proteins called regulators of G protein signalling (RGS) [20, 21].

The Extended Ternary Complex Model — In the earliest model for GPCR activation, the ternary complex model, receptor, ligand and G protein form a complex leading to the activation of the G protein (Figure 1.3*A*). However, studies based on constitutively active mutants of the β-adrenergic receptor led to a revised model for GPCR activation, called the extended ternary complex model (Figure 1.3*B*) [22]. In this model, the receptor exists in a equilibrium between an inactive (R) and an active (R*) conformation. Only R* can interact with the G protein, but both R and R* can bind ligands.

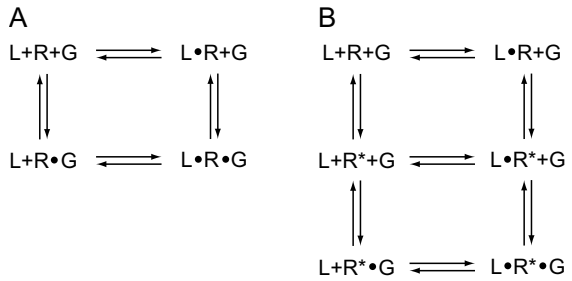

Figure 1.3: Models for GPCR activation. *(*A*) Ternary complex model. (*B*) Extended ternary complex model, which includes an activated receptor state R*. R, receptor; L, ligand; G, G protein (taken from [22]).*

Ligands can be divided into full, partial and inverse agonists, as well as antagonists [23]. Full agonists have a preference for the R* state, so that their binding shifts the R $\rightleftarrows$ R* equilibrium to the right, increasing the amount of active G proteins. They elicit the maximal response upon binding to the receptor, whereas partial agonists, which also prefer R* over R, do not fully shift the equilibrium and only evoke a partial response. Inverse agonists have a higher affinity for R and shift the equilibrium towards R, thus lowering the basal activity of the receptors. Antagonists exclude the binding of agonists by binding to both R and R*, without changing the conformational equilibrium of the receptor.

Signal Transduction Pathways — G proteins act as transducing units and transmit the signal from the activated receptor to the effector. The α- as well as the $\beta\gamma$-subunits can interact with different effectors and thereby activate different signalling pathways (Table 1.1).

The two most important G protein-coupled signalling pathways are the cAMP signalling pathway and the DAG/IP_3 signalling pathway.

The cAMP signalling pathway The cAMP signalling pathway uses cyclic adenosine monophosphate (cAMP) as a second messenger. cAMP is synthesized

Subunit	Family	Main subtypes	Primary effector
α	α_s	$G_{\alpha s}$, $G_{\alpha olf}$	Adenylate cyclase ↑
	$\alpha_{i/o}$	$G_{\alpha i1}$, $G_{\alpha i2}$, $G_{\alpha i2}$	Adenylate cyclase ↓
		$G_{\alpha oA}$, $G_{\alpha_{oB}}$	K^+ channels ↑
		$G_{\alpha t1}$, $G_{\alpha_{t2}}$	Ca^{2+} channels ↓
		$G_{\alpha z}$	Cyclic GMP phosphodiesterase ↑
	αq	$G_{\alpha q}$, $G_{\alpha 11}$, $G_{\alpha 14}$,	Phospholipase C ↑
		$G_{\alpha 15}$, $G_{\alpha 16}$	
	$\alpha 12$	$G_{\alpha 12}$, $G_{\alpha 13}$	?
β	$\beta_{1\text{-}5\ (6?)}$	Different assemblies	Adenylate cyclase ↑/↓
		of β- and γ-subunits	Phsopholipase ↑
			Phosphatidylinositol 3-kinase ↑
γ	$\gamma_{1\text{-}11\ (12?)}$		Protein kinase C ↑
			Protein kinase D ↑
			GPCR kinases ↑
			Ca^{2+}, K^+ (and Na^+) channels

Table 1.1: Heterotrimeric G proteins and their effectors. *The arrows indicate up- or down-regulation of the effector (taken from [19]).*

from the intracellular ATP by a plasma membrane-bound enzyme, the adenylyl cyclase, and is rapidly and continuously degraded by cAMP phosphodiesterases [24].

There are at least 8 isoforms of mammalian adenylyl cyclases, most of which are regulated by both G proteins and calcium [24]. GPCRs acting through the cAMP pathway can either stimulate an adenylyl cyclase via a stimulatory G protein ($G_{\alpha s}$ or $G_{\alpha olf}$), or inhibit it via an inhibitory G protein ($G_{\alpha i}$). The adenylyl cyclase can also be stimulated or inhibited by the $\beta\gamma$-subunit of the G protein (Table 1.1). Both $G_{\alpha s}$ and $G_{\alpha i}$ are sensitive to two bacterial toxins, *Cholera toxin* and *Pertussis toxin* [25, 26].

The stimulation of the adenylyl cyclase leads to a rapid increase of the cAMP level in the cytosol and activates protein kinase A, which in turn phosphorylates a variety of proteins.

The DAG/IP_3 signalling pathway The other main signalling pathway uses both diacylglycerol (DAG) and inositol-triphosphate (IP_3) as second messengers. GPCRs acting through this pathway are coupled to G proteins of the $G_{\alpha q/11}$ family, which activate the plasma membrane enzyme phospholipase C type β (PLC_β) [27]. PLC_β cleaves the lipid phosphatidyl-inositol-4,5-bisphosphate (PIP_2) into DAG and IP_3. IP_3 directly binds to calcium channels in the endoplasmic reticulum,

leading to a fast increase in the cytosolic concentration of calcium. DAG activates the protein kinase C (PKC), which phosphorylates many proteins. The DAG/IP_3 signalling pathway is illustrated in Figure 1.4.

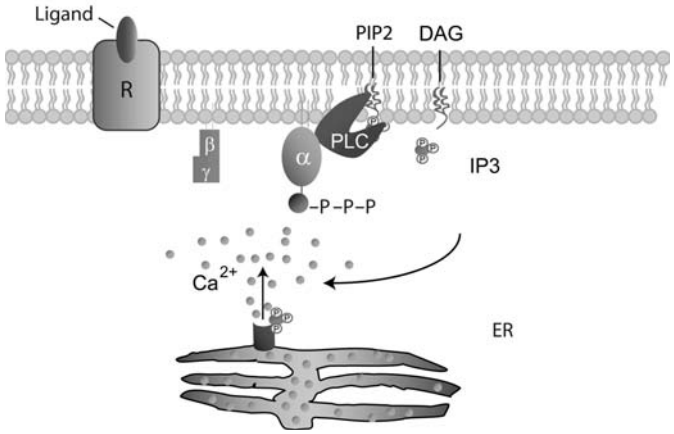

Figure 1.4: The DAG/IP_3 signalling pathway. *Upon activation of the receptor (R), the heterotrimeric G protein dissociates and interacts with a phospholipase C β (PLC), which cleaves the lipid phosphatidyl-inositol-4,5-biphosphate (PIP_2) into diacylglycerol (DAG) and inositol-triphosphate (IP_3). IP_3 opens calcium channels in the endoplasmic reticulum (ER), leading to an increase in the intracellular calcium ion concentration.*

1.3.2 Odorant Receptor Activation

Once an odorant receptor has bound an agonist, a cascade of events is initiated inside the neuron, transforming the signal of ligand binding into a change in the membrane potential (Figure 1.5) [7, 9, 28].

The ligand-bound receptor activates a G protein (an olfactory-specific subtype, G_{olf}), which in turn activates an adenylyl cyclase type III (ACIII) [9]. The cyclase converts ATP into cyclic AMP (cAMP), that binds to a cyclic nucleotide-gated (CNG) ion channel. The channel opens and conducts cations such as Na^+ and Ca^{2+} [4,29]. If enough channels are open for a sufficient time, an action potential is generated and propagated along the axon [7]. The membrane depolarization is also increased by an efflux of chloride ions: Calcium ions entering the cell via the CNG channels activate another type of ion channel, the chloride permeable ion channels. This enables OSNs to amplify the signal initiated by the odorant binding [29].

Studies on genetically modified mice in which G_{olf}, ACIII or the CNG channel have been deleted ([30–32]) indicate that the cAMP pathway is the common

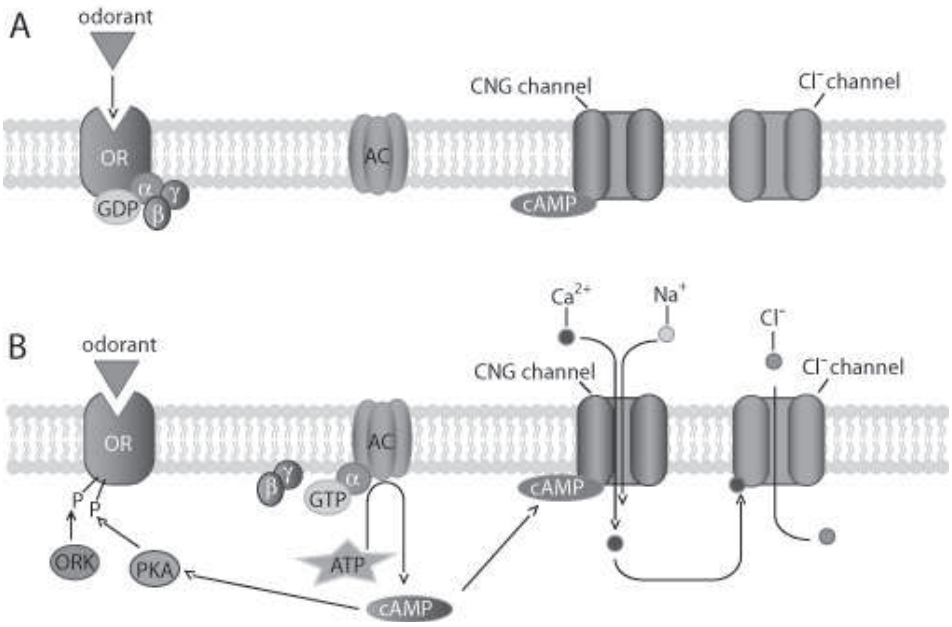

Figure 1.5: Schematic view of the cyclic nucleotide transduction pathway in OSNs. *Within the cilia of the OSNs a cascade of enzymatic activity transduces the binding of an odorant molecule to a receptor into an electrical signal that can be transmitted to the brain. OR, odorant receptor; AC, adenylyl cyclase; CNG channel, cyclic nucleotide-gated channel; PDE, phosphodiesterase; PKA, protein kinase A; ORK, olfactory receptor kinase; α, β, γ, G protein subunits (modified from [4]). (*A*) Resting state of the receptor. (*B*) Receptor activation.*

pathway for all OSNs. Whether IP_3 or other second messengers have modulatory roles remains to be proven [7, 33].

In invertebrates, which can have both excitatory and inhibitory responses to odors, olfaction seems to be mediated by several pathways [34, 35]. In lobsters, the main pathway seems to involve inositol phosphates [36] and in *Drosophila* and the moth, there is also strong evidence for IP_3 as a second messenger [37]. The final target of this cascade, the analogue of the CNG channel in vertebrates, remains to be identified.

1.4 Down-Regulation of OR Activation

1.4.1 GPCR endocytosis

GPCR endocytosis regulates receptor signalling by controlling the amount of receptors and ligands on the cell surface and extracellular medium [38]. The usual process of GPCR endocytosis, called "homologous desensitization", involves the

phosphorylation of activated receptors by a specific family of G protein-coupled receptor kinases (GRKs), followed by the interaction of phosphorylated receptors with cytoplasmic proteins called arrestins [39]. Four isoforms of arrestins have been identified, but only two isoforms, β-arrestin 1 (β-arr1) and β-arrestin 2 (β-arr2), are ubiquitously expressed in mammalian cells [39]. Arrestin-bound receptors are unable to couple to heterotrimeric G proteins, disrupting the pathway of GPCR-mediated signal transduction at the earliest stage. Moreover, binding of β-arrestins targets many, although not necessarily all, GPCRs to the clathrin-mediated pathway of endocytosis by interacting directly with clathrin and the adaptor protein AP-2, two components of the endocytic machinery involved in the formation of clathrin-coated pits [39–41].

Clathrin-Dependent Endocytosis — Clathrin-dependent endocytosis occurs at specific sites on the plasma membrane after the formation of a complex structure, called a coated pit, which concentrates surface proteins for internalization [42]. The clathrin-coated pits contain two major structural proteins, clathrin and the adaptor protein AP-2, as well as several other proteins. Coated-pit formation is thought to be initiated by the binding of AP-2 molecules to a docking site or receptor in the plasma membrane, followed by clathrin assembly [39, 42]. The formed pits progressively invaginate and are finally released into the cytosol as free clathrin-coated vesicles (Figure 1.6), a process which requires the GTPase dynamin [43]. In the cytosol, the vesicles fuse with endosomes where the ligand is separated from the receptor and the receptor is dephosphorylated. Receptors are then either recycled to the plasma membrane, or degraded in lysosomes [44].

GPCRs are divided into two classes based on their affinities for β-arrestins [45]. Class A receptors, such as β_2-adrenergic receptor, known to recycle and resensitize rapidly, preferentially bind to β-arrestin 2 and form low-affinity complexes, which dissociate upon internalization of the receptor. In contrast, class B receptors, such as angiotensin II type 1a and vasopressin 2 receptors, which recycle and resensitize slowly, possess similar affinities for both β-arrestins and form high-affinity complexes leading to the internalization of a stable receptor-β-arrestin complex. Clusters of phosphorylated residues in the receptor C-terminal part seem to be responsible for the ability of class B receptors to bind β-arrestins with very high affinity [46]. Such clusters are absent from the C-terminus of class A receptors [46].

Clathrin-Independent Endocytosis — The internalization of some GPCRs, such as the the angiotensin II type 1a receptor [47], the M2 muscarinic acetylcholine

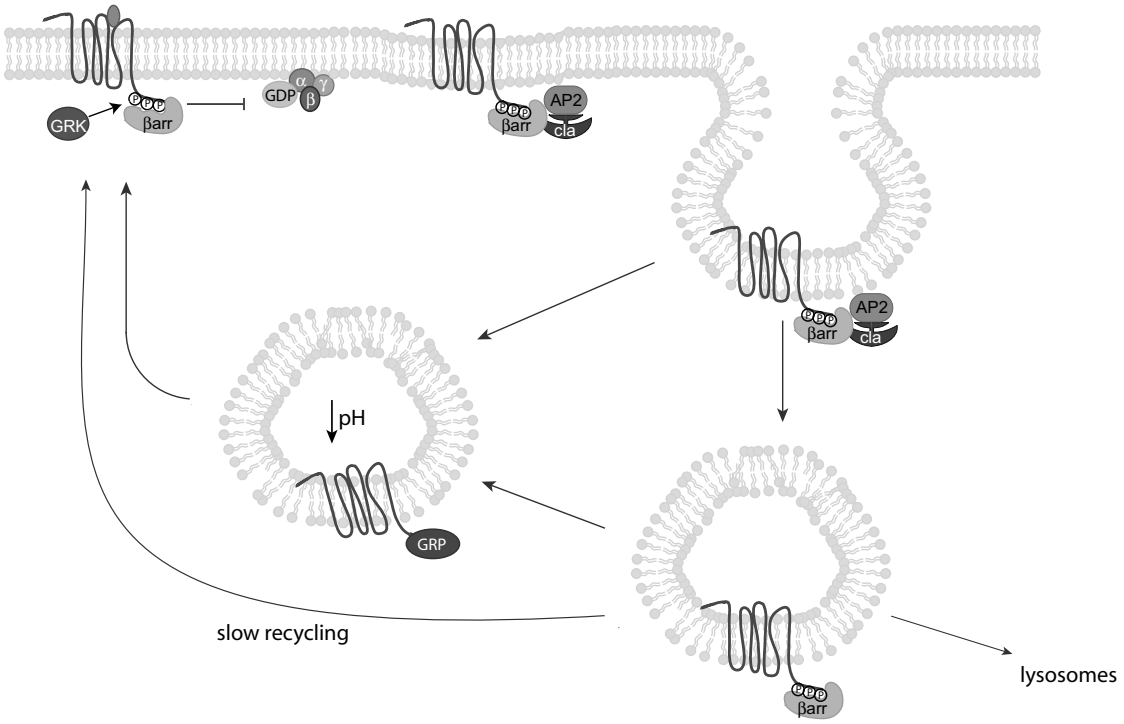

Figure 1.6: Model for GPCR desensitization and internalization. *GPCR activation leads to GRK-dependent phosphorylation of the receptor, which facilitates the binding of β-arrestins. β-arrestins, via their association with the adaptor protein AP-2, target GPCRs to clathrin-coated pits. GPCRs are subsequently internalized in clathrin-coated vesicles and are either recycled back to the plasma membrane after dephosphorylation or are targeted to lysosomes for degradation. GRK, G protein-coupled receptor kinase; P, phosphate group; βarr, β-arrestin; AP2, AP-2 heterotetrameric adaptor complex; cla, clathrin; GRP, G protein-coupled receptor phosphatase.*

receptor [48] or D1 and D2 dopamine receptors [49], does not require β-arrestin or dynamin. This indicates that some GPCRs follow alternative endocytic pathways, which are still not fully characterized [39].

Clathrin-independent pathways may be mediated through lipid rafts or through caveolae [50,51]. Lipid rafts are dynamic, detergent-resistant regions of the plasma membrane which are enriched in cholesterol, glycosphingolipids and glycosylphosphatidylinositol (GPI)-anchored proteins, while caveolae are small flask-shaped plas-
ma membrane invaginations which contain the same lipid components as rafts as well as caveolin [50, 52]. Several GPCRs have been shown to signal in lipid rafts/caveolae [53–55]. Moreover, several chemokine receptors, which are also internalized via clathrin-independent pathways, have been found in raft mem-

branes [51]. The mechanism by which caveolae or lipid rafts mediate receptor endocytosis is not known [50], but once internalized, GPCRs enter a compartment called the caveosome and fuse with early endosomes, which are also a component of the clathrin-mediated pathway [51].

1.4.2 OR-Specific Inhibition of Signalling

OSNs developed many different negative feedback systems to terminate their response to an odorant, a process which is important in order to respond to new ligands. During odor responses, the rise of intracellular Ca^{2+} concentration decreases the sensitivity of cyclic nucleotide-gated ion channels to cAMP [7, 9], leading to their inactivation. Regulators of G-protein signalling (RGS) decrease adenylyl cyclase activity [7]. Moreover, cAMP activates protein kinase A (PKA), which leads to the phosphorylation of serine and threonine residues of ORs [9], promoting their internalization. Odorant-induced desensitization was also shown to be mediated by G protein-coupled receptor kinase 3 (GRK3) [56, 57] and by β-arrestin-2 [58], which are enriched in the dendritic knobs and cilia of the OSNs [58].

1.5 Odor Coding

Several findings indicate that each OSN expresses only one OR gene in mammals [59–62], although an exception was found for a specific pair of ORs that are co-expressed in some rat OSNs [63]. The olfactory epithelium can be divided into four expression zones. OSNs expressing the same OR are located inside the same zone, where they are randomly distributed among OSNs expressing other ORs [61]. In the olfactory bulb, the axons of neurons expressing the same OR converge to two or at most a few glomeruli (Figure 1.7), which are arranged symmetrically between the medial and lateral halves of the bulb [12, 64, 65].

This suggests that olfactory information is first roughly organized into four large sets in the nose and then reorganized in the olfactory bulb into a sensory map, which is identical in different individuals [4, 64]. In both the nose and bulb, information derived from different ORs is strictly segregated: Each OSN in the nose and each glomerulus in the olfactory bulb receives the input from one particular OR. The glomerular convergence of OSNs expressing the same OR type probably leads to an increase in the signal-to-noise ratio [4].

The studies of Malnic and co-workers provided evidence that the mammalian olfactory system uses a combinatorial receptor coding scheme to encode odor identity and to discriminate odors [2, 66]. As shown in Figure 1.8, an odorant receptor

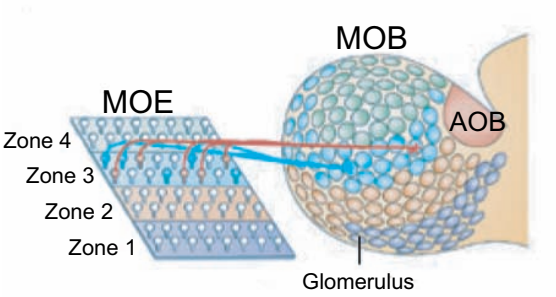

Figure 1.7: Patterns of connectivity between olfactory epithelium and olfactory bulb. *The olfactory epithelium can be subdivided in four zones of equal surface area. A given OR gene is expressed in OSNs which are located within a zone. Their axons converge onto one or a few glomeruli in each of the two halves of the bulb. MOE, main olfactory epithelium; MOB, main olfactory bulb; AOB, accessory olfactory bulb (taken from [4]).*

can be activated by different odorant molecules, and, conversely, an odorant molecule can activate more than one type of receptor, so that each odor leads to a specific pattern of activation.

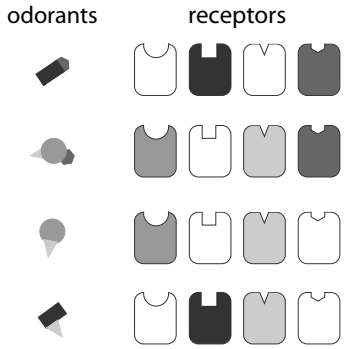

Figure 1.8: Combinatorial receptor codes for odorants. *The receptors shown in color are those that bind the odorant on the left. Each OR can bind several odorants, and each odorant can activate a set of ORs (modified from [66]).*

1.6 Pairing Odors with Odorant Receptors

It took seven years from the discovery of the OR super-family to the first experimental evidence that ORs indeed mediate odorant signals, mostly because odorant receptors proved to be extremely difficult to express in heterologous cells. In fact, ORs are retained in the endoplasmic reticulum due to inefficient folding and are

poorly coupled to ER export machinery in non-native systems [67]. For this reason, most ORs are still orphan receptors, i.e. their native ligands are yet not known. Four strategies, described in the following, have been used to "de-orphanize" odorant receptors.

A first approach used genetic studies in *Caenorhabditis elegans* and indicated that an *odr-10* mutant lacked a seven-transmembrane receptor and was unable to detect diacetyl [68]. This OR-odorant interaction was subsequently confirmed by the heterologous expression of ODR-10 in HEK293 cells, where the activation of the receptor by diacetyl was monitored using calcium imaging [69].

Another strategy, which made use of an adenovirus-mediated gene transfer followed by electrophysiological detection of odorant-mediated responses, led to the identification of octanal as an agonist for the rat I7 receptor [70] and enabled the finding of an odorant with some antagonistic activity [70, 71]. This approach was also used to identify lyral as an agonist for MOR23 [72].

A third approach for de-orphanizing ORs is to use gene targeting to co-express the green fluorescent protein (GFP) in OSNs that endogenously express a given OR gene. Cells are then isolated from the epithelium, loaded with a calcium-sensitive fluorescent dye, and the green neurons which express both the OR and GFP are identified and imaged for their responses to odorants. This method enabled the discovery of acetophenone and benzaldehyde as agonists for the mouse M71 receptor [73]. Furthermore, when the M71 coding region was replaced by rat I7, responses to acetophenone and benzaldehyde were no longer seen and the cells became, as expected, responsive to octanal [73].

Finally, also based on the rat I7-octanal pair, a heterologous expression system was developed in human embryonic kidney (HEK293) cells [74]. To improve the translocation of the OR to the plasma membrane of these cells, the N-terminal part of rhodopsin (first 20 amino acids) was fused to the OR. G-protein subunits that couple promiscuously to GPCRs were over-expressed in order to artificially couple the OR to the IP_3/Ca^{2+} signalling pathway, allowing calcium imaging measurements.

An analogous HEK293 expression system, but with different OR protein modifications (the $5HT_3$ membrane import signal sequence followed by a *c-myc* epitope was fused to the OR N-terminus) enabled the de-orphanization of the first human OR: Helional was paired with OR17-40 [75]. This interaction was confirmed by electrophysiological measurements in engineered *Xenopus laevis* oocytes [75].

1.7 Aim and Scope of this Thesis

In order to establish a functional expression system for odorant receptors and develop cell-based assays to study their specificity and sensitivity for odorant molecules, this thesis focuses on the functional analysis of the human odorant receptor OR17-40.

For the direct visualization of the receptor in living cells, different OR17-40 fusion proteins enabling expression and subcellular localization studies were constructed and functionally characterized (Chapter 3). To investigate the cellular mechanisms responsible for its poor surface membrane targeting, the biogenesis and membrane trafficking of OR17-40 was followed using a novel fluorescence labelling strategy, which allowed the optical discrimination between membrane-inserted receptors and all translated receptors (Chapter 4). The selective labelling of cell surface receptors also provided a tool for studying the effect of agonist or antagonist binding on the lateral diffusion of OR17-40 in HEK293 cell plasma membranes (Chapter 5).

For efficient screenings of large odorant collections in microtiter plates, a calcium imaging-based functional assay was developed (Chapter 6). Using chemical derivatives of the cognate ligand helional, this assay enabled the investigation of the structural properties of odorant molecules essential for OR17-40 binding and/or activation.

Finally, a novel strategy for the miniaturization of functional odorant screening assays based on cell-derived native vesicles containing different OR subtypes is described (Chapter 7).

Chapter 2

Experimental Techniques and Procedures

This chapter deals with the materials and general methods used throughout this work, unless otherwise stated. It includes the standard techniques for cell cultures, transient and stable protein expression, calcium ion signalling, ACP labelling, fluorescence confocal microscopy, and FACS analysis.

2.1 Materials

Dulbecco's modified Eagle's medium (DMEM), fetal calf serum (FCS), Dulbecco's phosphate-buffered saline (D-PBS) and Lipofectamine2000 were from Invitrogen (Breda, NL). Hygromycin B was from Calbiochem (Darmstadt, D). Puromycin and penicillin/streptomycin were from Sigma (Buchs, CH).

The monoclonal anti-c-myc, Cy3 conjugate clone 9E10 was purchased from Sigma (Buchs, CH). Paraformaldehyde was from Fluka (Buchs, CH).

The fluorescent indicator dyes Fluo-3 and FuraRed were from Molecular Probes (Eugene, OR, USA) and the Calcium 3 assay kit from Molecular Devices (Munich, D).

2.2 Cell Cultures and Transfection

2.2.1 HEK293 Cells

Human embryonic kidney cells (HEK293 cells) were cultured in Dulbecco's modified Eagle medium (DMEM) supplemented with 2.2 % or 10 % fetal calf serum (FCS). The cultures were grown at 37 ^{o}C in a humidified 5 % CO_2 atmosphere and were split at regular time intervals.

Sixteen to twenty hours before transfection, exponentially growing cells cultured in DMEM containing 2.2 % FCS were seeded either on sterile 25 mm glass cover slides (Hecht Assistent, Sondheim-Rhoen, D) or on 8-well chambered coverglass slides (Lab-Tek, Naperville, IL, USA). Cells were transfected using the calcium phosphate precipitation method [76], unless otherwise specified.

2.2.2 *Odora* Cells

Non-differentiated *odora* cells were grown in Dulbecco's modified Eagle medium (DMEM) supplemented with 10 % fetal calf serum and 100 U/ml penicillin - 100 μg/ml streptomycin (PenStrep) in a humidified 95 % air, 5 % CO_2 incubator at 34 °C. For differentiation, cells were cultured in DMEM/PenStrep medium containing 10 % FCS and 1 μg/ml insulin, 20 μM dopamine and 100 μM ascorbic acid (dopamine stabilizer) in a humidified 95 % air, 7 % CO_2 incubator at 39 °C for 5 to 7 days.

Differentiated *odora* cells were transfected using Lipofectamine2000 according to the manufacturer's instructions, with 2.5 μg DNA and 10 μl Lipofectamine2000 per milliliter of cells.

2.3 Stable Cell Line Selection

Exponentially growing HEK293 cells were seeded in a 12-well plate and each well was transfected with 2.5 μg receptor DNA and 2.5 μg $G_{\alpha q}$ DNA using the calcium phosphate precipitation method. 48 h after transfection, the medium was replaced by the selection medium (DMEM containing 10 % FCS, puromycin (20 μg/ml) and hygromycin B (200 μg/ml)). Confluently growing cells were split in 6-well plates and then expanded in 75 cm^2 culture flasks containing the selection medium.

2.4 Immunocytochemistry

Cells expressing the c-Myc - OR17-40 construct together with a nuclear-targeted GFP, or the c-Myc - OR17-40 - GFP construct, were fixed for 5 min in PBS containing 4 % paraformaldehyde. Cells were washed with PBS, blocked for 20 min with PBS containing 1 % fetal calf serum and incubated for 1 h with the monoclonal anti-c-myc, Cy3 conjugate clone 9E10, at a 1:50 dilution. Cells were then washed three times with PBS and visualized by laser-scanning confocal microscopy. The excitation was at 543 nm, and the emission was recorded using a 560 nm long pass filter.

2.5 ACP Labelling

Cells stably or transiently expressing ACP - OR17-40 or ACP - OR17-40 - GFP and grown either on sterile 25 mm glass cover slides or on 8-well chambered coverglass slides, were labelled with Cy5 (5 μM CoA-Cy5, 1 μM AcpS and 10 mM $MgCl_2$ in D-PBS) for 30 min. The labelling was performed at room temperature, unless otherwise specified. Cells were then washed three times with D-PBS and visualized by laser-scanning confocal microscopy. The excitation was at 633 nm, and the emission was recorded using a 650 nm long pass filter.

2.6 Fluorescence Confocal Microscopy

Laser-scanning confocal micrographs were recorded using a 453/488 nm Ar-Kr laser line or a 543 or 633 nm He-Ne laser line on a Zeiss LSM 510 microscope (Zeiss, Jena, D) with a 63 x water (1.2 numerical aperture) objective. Detection and distinction of fluorescence signals was achieved by appropriate filter sets using a multi-tracking mode. Table 2.1 lists the filter sets when using one fluorophore in single-tracking mode and Table 2.2 lists the filter sets when using two fluorophores in multi-tracking mode. If possible, an additional dichroic mirror was used for the multi-tracking mode to split the fluorescence emission into two channels.

	Excitation Line	Dichroic Mirror	Emission Filter
ECFP	458 nm	HFT 458	LP 475
EGFP, EYFP, Alexa488	488 nm	HFT 488	LP 505
Cy3, rhodamine	543 nm	HFT 543	LP 560
Cy5, CypHer	633 nm	HFT 633	LP 650

Table 2.1: Filter sets for one fluorophore and single-tracking mode.

2.7 FACS Analysis

Cells expressing OR17-40 - GFP, ACP - OR17-40 or ACP - OR17-40 - GFP labelled with CoA-Cy5 were very briefly trypsinized, centrifuged for 4 min at 1,200 rpm in DMEM containing 10 % FCS, resuspended in PBS and collected by centrifugation. The pellet was finally resuspended in PBS at a density of about $1x10^6$ cells/ml. Fluorescence measurements were performed on a CyAn ADP LX 9 Color analyser (DakoCytomation, FortCollins, CO, USA), using the 488 nm and 633 nm excitation lines. The GFP fluorescence was detected in the FL1 (FITC) channel and the

	Excitation Line	Dichroic Mirror (HFT)	Beam Splitter (NFT)	Emission Filter
Cy3 and	543 nm			BP 560-615
Cy5	633 nm	UV/488/543/633	635 vis	LP 650
ECFP and	458 nm	458	-	BP 465-495
EYFP	488 nm	488	-	BP 510-560
EGFP and	488 nm			BP 505-550
Cy3	543 nm	488/543	545	LP 560
EGFP	488 nm			BP 505-550
and Cy5	633 nm	UV/488/543/633	635 vis	LP 650

Table 2.2: Filter sets for two fluorophores and multi-tracking mode.

Cy5 signal in the FL8 (APC) channel. Analysis (Summit, DakoCytomation) was performed on viable cells only, as determined by a gate on forward and side scatter.

2.8 Single-Cell Calcium Imaging

Twenty-four to forty-eight hours after transfection, cells grown on 25 mm glass cover slides were loaded by incubation at 37 °C for 30 min in serum-free DMEM containing the calcium ion indicator dyes Fluo-3-AM (3 μM) and FuraRed-AM (5 μM). The dye loading medium was then exchanged against DMEM containing 10 % FCS and incubation at 37 °C was continued for another 30 min in order to allow for cleavage of the ester. Calcium signalling measurements were performed on a laser-scanning confocal microscope. Both dyes were excited at 488 nm and the increase in Fluo-3 fluorescence intensity and decrease in FuraRed fluorescence intensity were recorded and separated with appropriate filters (Fluo-3: BP 505-550 nm; FuraRed: LP 560 nm).

For each experiment, odorant compounds were freshly diluted in D-PBS from a stock solution of 1 M in DMSO and 100 μl was manually applied with a micropipette into the chamber. After each ligand application, ATP (100 μM final concentration) was added to the cells, as a control for the ability of the cells to increase the Ca^{2+} ion concentration in general. ATP activates the P_2y-type of ATP receptor, which is present in HEK293 cells and which couples to the IP_3 pathway [77].

2.9 Ca^{2+} - FLEX Assay

Twenty-four hours prior to the calcium imaging assay, cells stably expressing the receptor and $G_{\alpha q}$ were seeded in black wall/clear bottom 96-well plates (Greiner) at a 80 % confluence. On the day of measurement, cells were loaded for 1 h at 37 °C with a calcium-sensitive dye (Calcium 3 assay kit, Molecular Devices) following the manufacturer's instructions. The change in fluorescence intensity of the calcium dye upon agonist addition was recorded on the fluorescence plate reader FLEXstation (Molecular Devices). The FLEXstation's integrated 8-channel pipettor delivered 50 μl of 5x-concentrated odorant compounds within 2 seconds simultaneously to 8 wells containing 200 μl of cells. The intensity of fluorescence emission at 515 nm, following excitation at 485 nm, was monitored from the 8 wells simultaneously, during 250 s. After 180 s, 25 μl of a 11x-concentrated (1,1 mM) solution of ATP was added to the wells.

Agonist response amplitudes were determined from the peak fluorescence, baseline-corrected traces and normalized to the ATP response amplitude. The amplitudes thus obtained were averaged over 9 to 20 wells expressing the same construct and receiving the same stimulus. EC_{50} values and curves were derived from the fit with the Hill-equation:

$$f(x) = m_0 + ((m_1 * (x^{nH}))/((C^{nH}) + x^{nH}))$$

with m_0 = minimum, m_1 = maximum, C = EC_{50} and nH = Hill coefficient.

Chapter 3

Expression of the Human Odorant Receptor OR17-40 in Heterologous Cells

3.1 Introduction

As described in Chapter 1, the functional expression of ORs using OSNs, adenovirus-infected olfactory epithelia, and genetically engineered animals were successful for a limited number of ORs. Nevertheless, these model systems have practical limitations. For example, odorant-responsive OSNs are difficult to maintain in primary culture [78], viral-mediated gene transfer does not consistently yield functional OR expression [79], and creating genetically engineered animals for each member of the OR super-family would be expensive and would not be suitable for high-throughput applications.

For these reasons, efficient heterologous expression systems need to be developed. The choice of a suitable cell line is influenced by two conditions: On one hand it should allow the functional expression of ORs, and on the other hand provide the molecular components of the signal transduction machinery to couple OR activation to a cellular response.

HEK293 cells have been used for the functional expression of several odorant receptors [74, 75, 80]. These cells are easy to handle and allow the monitoring of odorant responses by the activation of the DAG/IP_3 signalling pathway followed by an intracellular calcium ion release, which can be detected using calcium-sensitive indicator dyes [75, 79]. Alternatively, some odorant receptors were expressed in a cell line derived from the rat epithelium [81, 82], *odora* (*o*lfactory-*d*erived *o*dorant *r*eceptor *a*ctivatable), which can be induced to differentiate into cells that have the

same properties as mature OSNs. Differentiated *odora* cells were shown to express the olfactory G protein G_{olf}, the adenylyl cyclase type III (ACIII), and the β subunit of the olfactory cyclic nucleotide-gated channel (oCNGβ) [81], and can be used for studying OR activation by monitoring the calcium influx through the CNG channel with calcium-sensitive indicator dyes. ORs were shown to be expressed in the plasma membrane of differentiated *odora* cells, while in undifferentiated *odora* cells, ORs were not properly translocated, even though the receptors were released to the Golgi apparatus and endosomes [82]. The efficient translocation of ORs to the plasma membrane is thus an essential aspect in developing functional assays for the study of OR activation.

For some GPCRs, accessory proteins are required for correct receptor targeting to the cell surface [83]. For instance, NinaA was found to mediate cell surface expression of Rhodopsin 1 in *Drosophila melanogaster*, while RanBP2 promotes the translocation of mammalian cone opsin [84]. A novel family of chaperone proteins, called RAMPs for *r*eceptor *a*ctivity *m*odifying *p*roteins, has been found to interact with the *c*alcitonin *r*eceptor-*l*ike *r*eceptor (CRLR), assisting in the transport of CRLR to the cell surface, and defining the glycosylation state and recognition properties of the receptor [85]. The M10 and M1 family of MHC class I proteins and β2 microglobulin are helper proteins for the putative mammalian pheromone receptors V2Rs [86], and OR83b, an atypical odorant receptor found in *Drosophila*, was recently shown to interact with *Drosophila* odorant receptors [87].

Similarly, several accessory proteins were found to enhance the plasma membrane translocation of some mammalian odorant receptors in native and heterologous cells. ODR-4, a membrane protein that is expressed exclusively on intracellular membranes of chemosensory neurons, was shown to be required for the translocation of a subset of odorant receptors (e.g. ODR-10) to the cilia of olfactory neurons in *C. elegans* [88]. Its co-expression enhanced the surface expression of an epitope-tagged rat odorant receptor in undifferentiated *odora* cells, as well as in CHO cells [82]. This indicates that ODR-4 is able to improve plasma membrane trafficking of a mammalian OR, although its co-expression did not have any effect on the surface expression of another rat odorant receptor, OR5 [82].

Very recently, three other accessory proteins were found by screening modified LongSAGE (serial analysis of gene expression) libraries from single olfactory neurons and from neurons of the vomeronasal organ of mouse [89]. Candidate genes with open reading frames (ORFs) that encode membrane-associated proteins or with similarities to known chaperones were cloned from olfactory epithelium cDNAs. Each cDNA was co-transfected with a mouse OR (mOR203-1) tagged with an epitope into HEK23 cells, and OR cell surface expression was measured by im-

munocytochemistry. Two unrelated clones enhanced both the number and staining intensity of mOR203-1 cell surface expression: RTP1, (*r*eceptor *t*ransporting *p*rotein *1*) and REEP1 (*r*eceptor *e*xpression *e*nhancing *p*rotein *1*). RTP2, a close relative of RTP1 was also found to enhance cell surface expression. The effect of the co-expression of these proteins was investigated on three other mouse odorant receptors and on the rat I7 receptor. The surface expression of the rat I7 was significantly lower than for the other ORs tested, but still enhanced by the accessory proteins [89].

In addition to accessory proteins, the formation of homo- or heterodimers might play a role in OR trafficking [90, 91]. For example, by hiding specific ER retention signals, oligomerization might favor the entry of the completed proteins in the export system, thus allowing its correct trafficking. A role for dimerization in GPCR export from the ER was first suggested by a series of studies on the metabotropic GABAb receptors [92]. When expressed alone, the GABAb R1 receptor is retained in the ER as an immature protein, while GABAb R2, although properly targeted to the plasma membrane, cannot bind GABA. When the two receptors are co-expressed, both reach the plasma membrane as a complex that can bind GABA [92]. Other examples of heterodimers are the T1R taste receptors: T1R3 is not functional when expressed alone in heterologous cells, but forms heterodimers with T1R2, thereby mediating sweet taste, or combines with T1R1 to form a receptor that is broadly responsive to L-amino acids and monosodium L-glutamate, which has an umami taste [4]. The heterodimerization of the NK1 receptor and the μ-opioid receptor was also shown to regulate receptor trafficking and resensitization [93].

The β_2-adrenergic receptor (β_2-AR) is expressed in OSNs, where it seems to be involved in axon guidance [11]. Recently, co-expression of β_2-AR, but not of other AR subtypes that are also expressed in neurons, was shown to increase the cell surface expression of a mouse odorant receptor (M71) in HEK293 cells [94]. Co-immunoprecipitation of the β_2-AR with the M71 receptor indicated that the two receptors physically interact.

In this chapter, the expression and subcellular localization of the human OR17-40 receptor in HEK293 cells and in differentiated *odora* cells with and without the co-expression of the accessory proteins ODR-4, β_2-AR, and RTPs are reported.

To enable such studies, the receptor needs to be visualized in living cells. The classical way of labelling would be by means of antibodies. In recent years however, new techniques have been developed, e.g. incorporation of non-natural fluorescent amino acids [95] or fusion to autofluorescent proteins [96]. In addition, post-

translational *in vivo* labelling methods have been introduced, where the fluorescent label is covalently or non-covalently attached to a fusion tag or fusion protein [97–102].

In the present study, we have chosen three different approaches for labelling OR17-40 in cells: (i) A C-terminal fusion to the green fluorescent protein (GFP) was used for the real-time visualization of the receptor in living cells, (ii) an N-terminal fusion of an epitope tag allowed the detection of the receptor by a fluorescent antibody on fixed cells, and (iii) the acyl carrier protein (ACP) fused to the receptor N-terminus enabled enzymatic post-translational labelling with fluorescent substrates in living cells. The technical aspects of these approaches and their use for comparing expression and plasma membrane trafficking of OR17-40 in different cell lines are discussed in detail in this chapter.

3.2 Experimental Procedures

3.2.1 Materials

OR17-40 cDNA was a kind gift from H. Hatt (Ruhr-Universität, Bochum, D). ODR-4 was kindly provided by C. Bargmann (University of California, San Francisco, USA). The *odora* cell line was a kind gift from D. Hunter (Tufts University, Boston, USA).

The synthetic oligonucleotides were purchased from MWG (Ebersberg, D). pBluescript II KS+ and the QuickChange site-directed mutagenesis kit were from Stratagene (La Jolla, CA, USA). pEAK8 was from Edge BioSystems (Gaithersburg, MD, USA). pEGFP-N1 and pEGFPnuc were from Clontech (Palo Alto, CA, USA). Restriction enzymes were purchased from New England Biolabs (Ipswich, MA, USA). DNA sequencing was done by Microsynth (Balgach, CH).

Octadecyl rhodamine B (R18) dye was from Molecular Probes (Eugene, OR, USA). pACP-NK1, CoA-Cy5 and AcpS were a kind gift from N. George and K. Johnsson (LIP-ISIC, EPFL, CH).

Cell culturing, cell transfection and preparation, immunocytochemistry, ACP labelling, fluorescence confocal microscopy, and single-cell calcium imaging, were performed as described in Chapter 2.

3.2.2 cDNA Constructs of OR17-40

wild-type OR17-40 — For a better plasma membrane localization of the odorant receptor, the 20 first amino acids of the bovine rhodopsin [74] followed by

a *Nde*I site were added at the receptor N-terminus by PCR using the following primers: OR17-40-fo: 5'- TCT GAT ATC GC ACC ATG AAC GGG ACC GAG GGC CCA AAC TTC TAC GTG CCT TTC TCC AAC AAG ACG GGC GTG GTG CAT ATG CAG CCA GAA TCT GGG GCC AAT GGA ACA GTC ATT GCT GAG -3'; OR17-40-rev: 5'- CGC GAT CGA TGC GGC CGC TCA AGC CAG TGA CCG CCT CCC TGT GAG -3'; and the resulting 1.1 kb *Eco*RV - *Not*I fragment was subcloned both into the cloning vector pBluescript II KS+ and into the mammalian expression vector pEAK8, yielding pBS::OR17-40 and pEAK8::OR17-40, respectively.

OR17-40 - GFP — pEAK8::OR17-40 - GFP was obtained by replacing the stop codon of OR17-40 by a *Bam*HI site using site-directed mutagenesis on pBS::OR17-40. GFP was amplified by PCR from pEGFP-N1 using the following primers: GFP-fo: 5'- CGC GGA TCC ATG GTG AGC AAG GGC GAG GAG CTG -3'; GFP-rev: 5'- CGC GAT CGA TGC GGC CGC TTA CTT GTA CAG CTC GTC CAT GCC -3'; and the resulting 750 bp *Bam*HI - *Not*I fragment was subcloned into pBS::OR17-40. OR17-40 - GFP was cut out with *Eco*RV and *Not*I and subcloned into pEAK8.

c-Myc - OR17-40 — pEAK8::c-Myc - OR17-40 was obtained by adding the sequence EQKLISEEDL (residues 410-419) of the human oncogene product *c-myc* between the rhodopsin membrane import sequence and the coding sequence of the receptor using site-directed mutagenesis and the following primers: myc-fo: 5'- GTG CCT TTC TCC AAC AAG ACG GGC GTG GTG CAT AT G GCA TCA ATG CAG AAG CTG ATC TCA GAG GAG GAC CTG GGA TCC CAG CCA GAA TCT GGG GCC AAT GGA ACA GTC -3'; myc-rev: 5'- GAC TGT TCC ATT GGC CCC AGA TTC TGG CTG GGA TCC CAG GTC CTC CTC TGA GAT CAG CTT CTG CAT TGA TGC CAT ATG CAC CAC GCC CGT CTT GTT GGA GAA AGG CAC -3'.

ACP - OR17-40 — For cloning of pEAK8::ACP - OR17-40, a *Bam*HI site was added between the rhodopsin membrane import sequence and the coding sequence of the receptor in pBS::OR17-40 using site-directed mutagenesis . The ACP fragment was amplified by PCR from pACP-NK1 using the following primers: ACP-fo: 5'- GGC ATC TC CAT ATG ATG AGC ACT ATC GAA GAA CGC GTT AAG -3'; ACP - rev: 5'- GTA GGA TCC CGC CTG GTG GCC GTT GAT GTA ATC AAT GGC -3'. The resulting 240 bp fragment was subcloned into pBS::OR17-40 digested with *Nde*I and *Bam*HI. ACP - OR17-40 was cut out with *Eco*RV and *Not*I and subcloned into pEAK8.

c-Myc - OR17-40 - GFP and ACP - OR17-40 - GFP — The double-tagged receptors c-Myc - OR17-40 -GFP and ACP - OR17-40 - GFP were obtained by di-

gesting pEAK8::c-Myc - OR17-40 or pEAK8::ACP - OR17-40 and pEAK8::OR17-40 - GFP with *Kpn*I and *Not*I and ligating the OR17-40 - GFP fragment into pEAK8::c-Myc- OR17-40 or pEAK8::ACP - OR17-40 respectively.

glyco - OR17-40 — To increase the glycosylation state of OR17-40, the amino acids 14 to 24 of the neurokinin 1 receptor (NISTNTSEPN) were added after the rhodopsin membrane import sequence in pBS::ACP - OR17-40 or in pBS::OR17-40 - GFP. This was done using site-directed mutagenesis and the following primers: glyco-fo: `5'- GGC CCA AAC TTC TAC GTG CCT TTC TCC AAC AAG ACG GGC GTG GTG ATT AAT ATC TCC ACT AAC ACC TCG GAA CCC AAT CAT ATG CAG CCA GAA TCT GGG GCC AAT GGA ACA GTC ATT GCT GAG -3'`; glyco - rev: `5'- CTC AGC AA T GAC TGT TCC ATT GGC CCC AGA TTC TGG CTG CAT ATG ATT GGG TTC CGA GG T GTT AGT GGA GAT ATT AAT CAC CAC GCC CGT CTT GTT GGA GAA AGG CAC GT A GAA GTT TGG GCC -3'`. glyco-ACP - OR17-40 and glyco OR17-40 - GFP were cut out with *Eco*RV and *Not*I and subcloned into pEAK8.

All plasmids were verified by restriction analysis and DNA sequencing. The different OR17-40 constructs are illustrated in Figure 3.1.

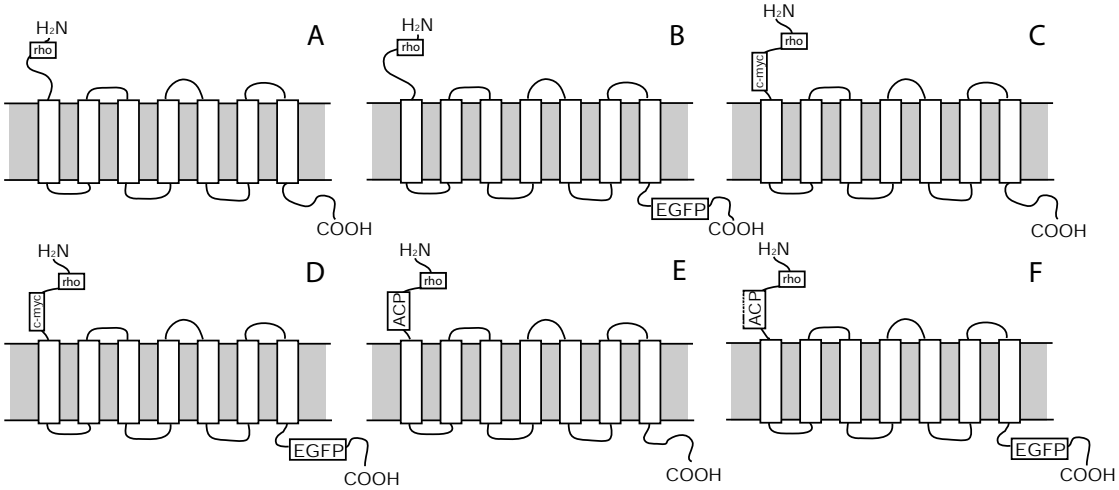

Figure 3.1: Membrane topology of the OR17-40 cDNA constructs showing the different C-terminal and N-terminal modifications. *(*A*) Wild-type OR17-40; (*B*) OR17-40 - GFP; (*C*) c-Myc - OR17-40; (*D*) c-Myc - OR17-40 - GFP; (*E*) ACP - OR17-40; (*F*) ACP - OR17-40 - GFP. Rho, bovine rhodopsin membrane import sequence; ACP, acyl carrier protein; EGFP, enhanced green fluorescent protein.*

3.2.3 ACP Labelling

The post-translational labelling method used for this work is based on the enzymatic modification of ACP by phosphopantetheine transferase (PPTase), leading to the transfer of 4'-phosphopantetheine from co-enzyme A (CoA) to a serine residue of ACP, which is genetically fused to the protein of interest (Figure 3.2). Fluorescent dyes attached to the phosphopantetheine on CoA are transferred to ACP together with 4'-phosphopantetheine during the labelling process. The ACP/PPTase pair used here is derived from *Escherichia coli*. PPTase from *E. coli* (AcpS) can be easily purified and possesses a relative narrow substrate specificity with respect to ACP [103].

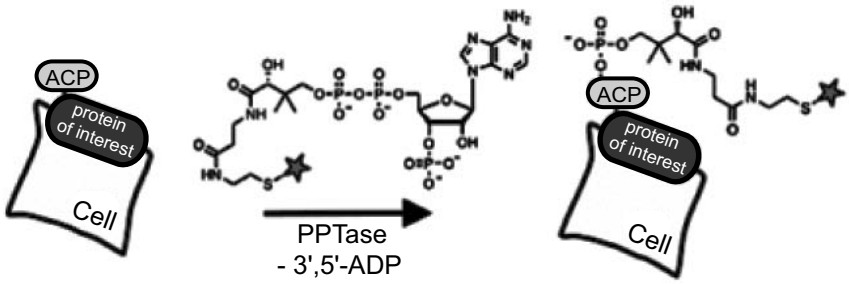

Figure 3.2: ACP labelling technique. *The fluorescent label (star) attached to CoA is transferred together with 4'-phosphopantetheine by PPTase to the ACP protein, which is genetically fused to the extracellular side of the protein of interest (taken from [99]).*

3.3 Results and Discussion

3.3.1 Subcellular Localization of OR17-40 in HEK293 Cells

Functionality of the Tagged OR17-40 Receptors — Studies on tagged odorant receptors have reported that N- or C-terminal modifications could impair receptor activity. For example, the addition of a small epitope tag on the C-terminus of the mouse mOR-EG receptor completely abolished its odorant responsiveness, probably by disrupting its coupling to G proteins [104]. In contrast, the C-terminal fusion of the rat I7 receptor to EGFP was shown not to affect ligand binding or downstream signalling [105], suggesting that different ORs do not tolerate in the same manner such modifications. Therefore, we first verified that the N- or C-terminal modification of OR17-40 by different tags did not abolish the receptor responsiveness to its cognate ligand helional.

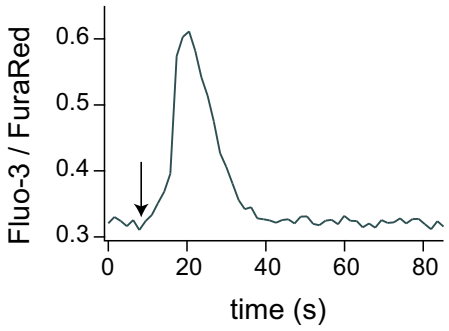

Figure 3.3: Single-cell calcium imaging of HEK293 cells expressing the wild-type OR17-40 receptor together with $G_{\alpha q}$. *Cells were loaded with the calcium ion indicator dyes Fluo-3 and FuraRed and stimulated with 100 μM helional at the time indicated by the arrow. Changes in fluorescence intensities were recorded using laser-scanning confocal microscopy.*

The co-expression of the G protein $G_{\alpha q}$ together with each of the receptor fusion constructs allowed the study of OR activation by calcium imaging. The addition of helional induced a transient intracellular calcium ion increase, which could be detected by the calcium-sensitive fluorescent dyes Fluo-3 and FuraRed, in HEK293 cells transiently expressing OR17-40 - GFP, c-Myc - OR17-40, ACP - OR17-40 or ACP - OR17-40 - GFP together with $G_{\alpha q}$. The kinetics of the calcium responses of the different constructs was similar to that of the wild-type receptor (Figure 3.3), whereas none of the constructs responded to the non-activating control substance piperonal [75]. We thus conclude that modifications at both the C- or N-terminus of the receptor do not affect OR-mediated signalling.

EGFP fusion — First subcellular localization studies of OR17-40 in HEK293 cells were performed using the C-terminal fusion of the receptor to EGFP, which has been shown to be well suited for studying GPCR localization and trafficking in living cells [106, 107].

As shown in Figure 3.4, OR17-40 - GFP is mainly expressed in intracellular membranes and, although part of the GFP fluorescence signal co-localizes with the fluorescence of the lipid dye octadecyl rhodamine B (R18), it is impossible to distinguish the membrane-inserted receptors from those which are trapped in intracellular compartments.

Immunocytochemistry — To only label the receptors which are correctly translocated to the plasma membrane, we fused a *c-myc* epitope to the N-terminus of OR17-40. This small (10 amino acids) modification with respect to the wild-type receptor is not likely to disturb its membrane trafficking. Moreover, the use of a

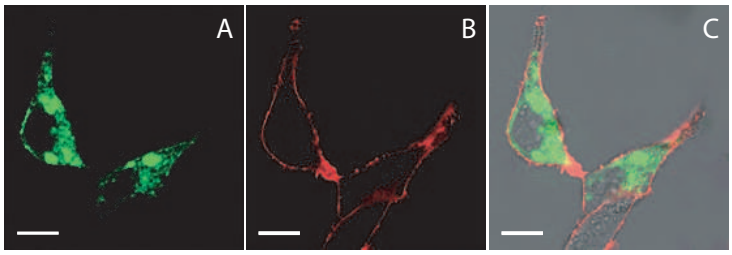

Figure 3.4: Subcellular localization of OR17-40 - GFP construct in HEK293 cells. *Fluorescence confocal micrographs showing OR17-40 - GFP fusion construct transiently expressed in HEK293 cells. The cell membrane is stained with R18 dye. (*A*) OR17-40 - GFP. (*B*) Membrane dye R18. (*C*) Transmission image of the same area with fluorescence micrographs* A *and* B *superimposed. Scale bar indicates 10 µm.*

fluorescent antibody raised against this extracellular epitope allows the selective visualization of the membrane-inserted receptors, thus avoiding background signal from intracellularly trapped receptors (Figure 3.5).

This labelling method proved to be very specific, since all antibody-labelled cells co-expressed the transfection marker GFPnuc (GFP with a nuclear import sequence). The number of cells exhibiting a detectable antibody labelling was low (about 5 to 10 % of the transfected cells). Many labelled cells had a rather faint membrane staining, reflecting a low level of membrane-inserted receptors, as compared to cells expressing a well-localized GPCR, the β_2-adrenergic receptor, also tagged with a *c-myc* epitope (data not shown).

It should be pointed out that, in order to avoid receptor internalization due to antibody cross-linking [108, 109], the cells need to be fixed prior to the incubation with the antibody. This method is therefore not suited for following receptor dynamics in living cells.

ACP labelling — The ACP labelling technique, which allows the selective fluorescence labelling of membrane proteins in living cells, enables real time-course studies to be performed. Figure 3.6 (*A-C*) shows Cy5-labelled ACP - OR17-40 in the plasma membrane of HEK293 cells.

Moreover, a double-tagged OR17-40 fusion construct, with ACP genetically fused to the receptor N-terminus and GFP to the C-terminus, allows the optical distinction of the cell surface receptors, by means of the Cy5 label, from the whole population of translated receptors participating to the GFP fluorescence. This also allows the comparison of the amount of well-translocated ORs in cells with different expression levels.

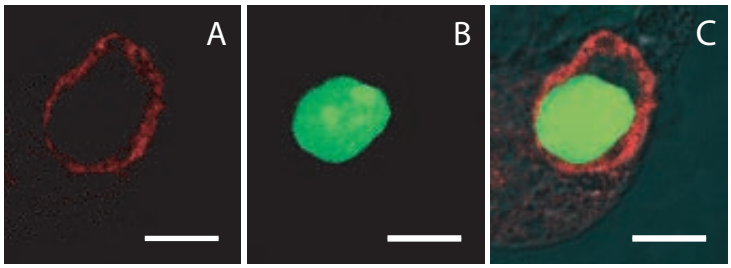

Figure 3.5: Subcellular localization of c-Myc - OR17-40 construct in HEK293 cells. *Fluorescence confocal micrographs showing non-permeabilized HEK293 cells transiently expressing c-Myc -OR17-40 construct together with a nuclear-targeted GFP and labelled with a Cy3-conjugated anti-c-myc antibody. (*A*) Anti-c-myc antibody. (*B*) GFP-stained nucleus. (*C*) Transmission image of the same area with fluorescence micrographs* A *and* B *superimposed. Scale bar indicates 10 µm.*

Figure 3.6 (*D-F*) shows the typical subcellular distribution of the double-tagged receptor construct in HEK293 cells. In general, although a limited amount of the translated ORs translocate to the plasma membrane, most of them are trapped in intracellular membranes. Interestingly, cells having a low expression level (low GFP fluorescence) exhibit a higher amount of membrane-inserted receptors, as revealed by a higher Cy5 fluorescence on the cell surface (Figure 3.6 (*G-I*)). It is likely that ORs are less efficiently folded due to a lack of chaperones and that they tend to aggregate in the ER of highly expressing cells. This will be discussed in more detail in Chapter 4, which deals with the trafficking of OR17-40. On the other hand, cells expressing ACP - OR17-40 - GFP and grown at 34 ^{o}C or 31 ^{o}C, in order to slow down OR biosynthesis and enhance folding efficiency, did not exhibit a better cell surface localization of the receptor (data not shown).

Furthermore, since the Cy5 fluorescence intensity in the membrane of cells expressing either ACP - OR17-40 - GFP or ACP - OR17-40 was similar, we can conclude that the fusion to GFP does not impair the membrane trafficking of the receptor.

Increasing the glycosylation state of the receptor — Recently, Katada *et al.* showed that the glycosylation of ORs was critical for their translocation to the plasma membrane of heterologous cells [104]. Indeed, removal of the N-terminal glycosylation site of mOR-EG, a mouse odorant receptor, completely impaired its membrane trafficking to the cell surface of HEK293 cells. On the other hand, cell surface expression of this receptor was greatly enhanced by the addition of extra N-terminal glycosylation sequences, for instance by the fusion of a bovine rhodopsin

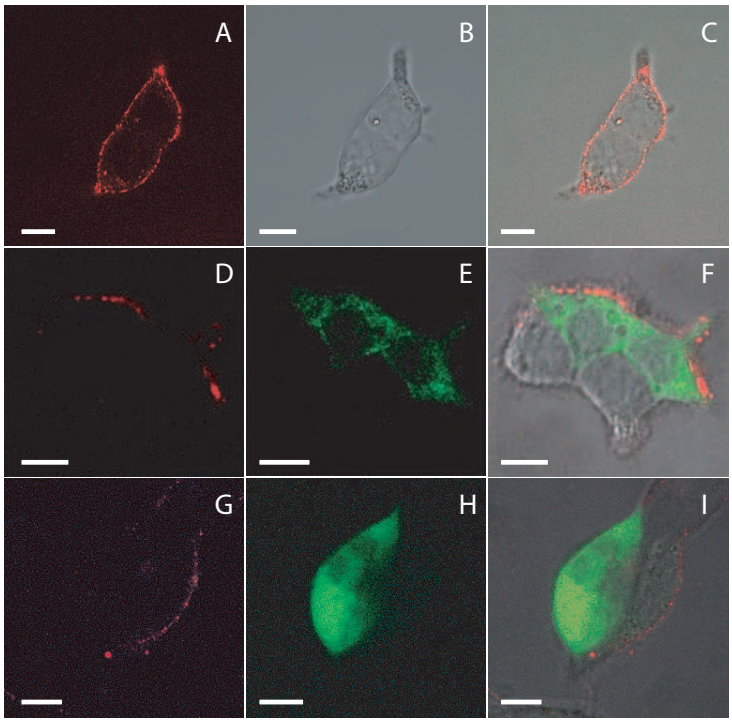

Figure 3.6: Subcellular localization of ACP - OR17-40 and ACP - OR17-40 -GFP fusion constructs in HEK293 cells. *Confocal micrographs showing HEK293 cells transiently expressing ACP - OR17-40 (*A, B, C*) or ACP - OR17-40 - GFP (*D, E, F *and* G, H, I*) and labelled with CoA-Cy5. (*A, D, G*) Cy5 channel. (*B*) Transmission channel. (*E, H*) GFP channel. (*C, F, I*) Transmission images of the same areas with fluorescence micrographs of the two other columns superimposed. Scale bar indicates 10 µm.*

membrane-import sequence, containing two additional glycosylation sites [104].

The neurokinin 1 receptor (NK1R), a GPCR which is very well translocated to the plasma membrane of HEK293 cells, has two glycosylation sites in its extracellular N-terminal part, that are located at positions 14 and 18 in the NK1R amino acid sequence. We therefore added the amino acid sequence NK1R(14-24) to the N-terminus of the ACP-OR17-40 or the OR17-40 - GFP fusion constructs,

just after the bovine rhodopsin membrane-import sequence.

The expression and subcellular localization of these receptor constructs transiently expressed in HEK293 were first investigated by confocal microscopy (Figure 3.7, *A* and *B*), which revealed that most of the receptors were still located intracellularly. For a more quantitative comparison of the plasma membrane expression of the modified and unmodified receptor constructs, we performed FACS analysis (Figure 3.7, *C* and *D*): Cells expressing glyco-ACP - OR17-40 and labelled with CoA-Cy5 did not exhibit a higher amount of cell surface receptors as compared with the unmodified receptor construct.

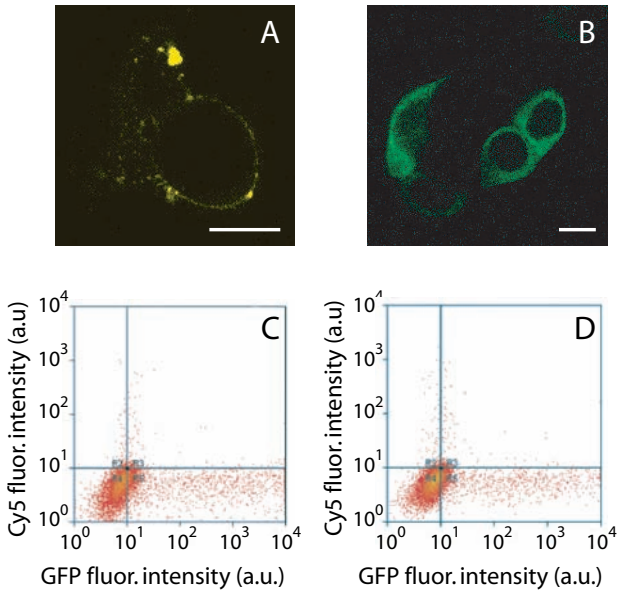

Figure 3.7: Subcellular localization of glyco-ACP - OR17-40 and glyco-OR17-40 - GFP fusion constructs in HEK293 cells. *(*A *and* B*) Confocal micrographs showing HEK293 cells transiently expressing Cy5-labelled glyco-ACP - OR17-40 (*A*) or ACP - OR17-40 - GFP (*B*). Scale bar indicates 10 µm. (*C *and* D*) FACS analysis performed on HEK293 cells transiently expressing glyco-ACP - OR17-40 and labelled with CoA-Cy5 (*D*) showed no higher cell surface receptor level as compared to the unmodified ACP - OR17-40 receptor construct (*C*).*

3.3.2 Subcellular Localization of OR17-40 in *Odora* Cells

The transient expression of OR17-40 in other heterologous cells, such as Chinese hamster ovary (CHO) cells, polarized MCCK cells, and neuronal N1E cells, yielded the same results as described for HEK293 cells (data not shown): Receptors were mainly retained in intracellular compartments.

The *odora* cell line, which is derived from the rat olfactory epithelium, was expected to provide a higher cell surface expression of the odorant receptors. As OR plasma membrane targeting was shown to require the differentiation of *odora* cells [82], OR17-40 was transiently expressed in *odora* cells that had been cultured for 5 to 7 days under differentiation conditions. Differentiated cells exhibited a bipolar morphology, with long processes extending over several tens of micrometers (Figure 3.8*B*), whereas undifferentiated cells had an epithelial morphology (Figure 3.8*A*).

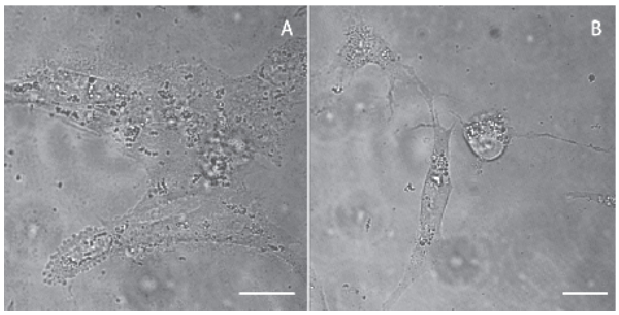

Figure 3.8: Morphology of *odora* cells. *Micrographs showing undifferentiated (*A*) and differentiated (*B*)* odora *cells. Scale bar indicates 20 µm.*

The subcellular localization of the OR17-40 - GFP fusion construct in differentiated *odora* cells is shown in Figure 3.9*A*. The cell surface expression of OR17-40 - GFP is not significantly improved in this cell line. A small fraction of receptors reaches the plasma membrane of differentiated *odora* cells, as detected by the fluorescence of Cy5-labelled ACP - OR17-40 (Figure 3.9*B*). In general, OR17-40 subcellular localization in *odora* cells is similar to the one seen in HEK293 cells, with the majority of the receptors located intracellularly.

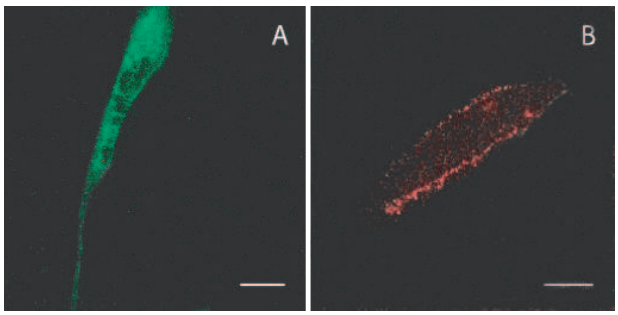

Figure 3.9: Subcellular localization of OR17-40 - GFP and ACP - OR17-40 fusion constructs in differentiated *odora* cells. *Confocal micrographs showing differentiated* odora *cells transiently expressing OR17-40 - GFP (*A*) or Cy5-labelled ACP - OR17-40 (*B*) fusion constructs. Scale bar indicates 20 µm.*

For this reason, and because HEK293 cells present several advantages over *odora* cells (easier cell culturing, no need of differentiation, better transfection efficiencies and lower autofluorescence), most of the experiments of this thesis will be performed on HEK293 cells.

3.3.3 Co-expression of OR17-40 with Helper Proteins

To investigate if ODR-4, β_2-AR or the RTP proteins would improve OR17-40 membrane trafficking in HEK293 cells, we co-expressed these proteins together with the ACP - OR17-40 - GFP double-tagged construct. In order to obtain data on a statistically relevant number of cells, we performed a fluorescence-activated cell sorting (FACS) analysis on Cy5-labelled cells. This approach enabled us to determine, on one hand, the total fluorescence intensity from all translated receptors via the GFP fluorescence emission in individual cells, and, on the other hand, the fluorescence intensity from the membrane-inserted receptors, through the Cy5 fluorescence emission.

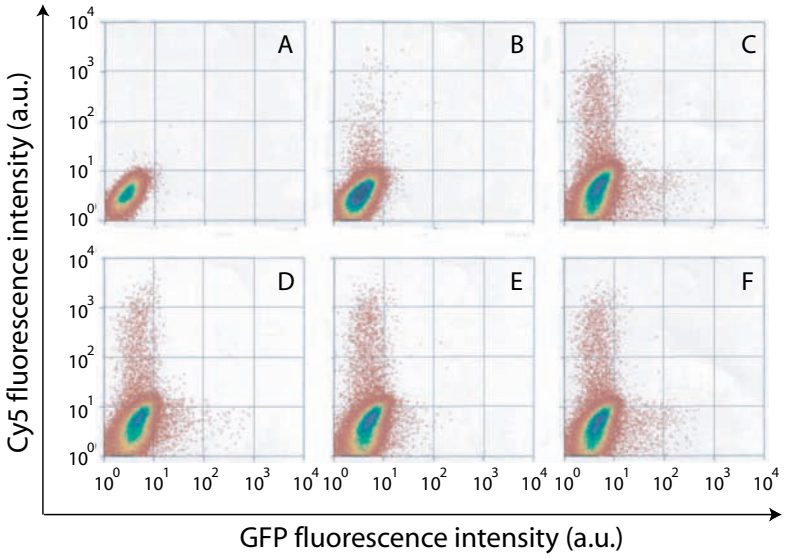

Figure 3.10: FACS analysis of HEK293 cells expressing the ACP - OR17-40 - GFP construct with or without the accessory proteins. *Cell surface expression (CoA-Cy5 intensity) versus total cellular expression (GFP intensity) of individual cells. (*A*) Untransfected HEK293 cells. (*B*) Untransfected HEK293 cells labelled with CoA-Cy5. (*C-F*) HEK293 cells expressing ACP - OR17-40 - GFP (*C*); with ODR-4 (*D*); with β_2-AR (*E*); and with RTP1 and RTP2 (*F*). Analysis was performed on 75,000 cells for each condition (50,000 for* A*).*

As shown in Figure 3.10, none of the different helper proteins enhanced OR17-40 cell surface expression: There is no significant increase in Cy5 fluorescence

intensity as compared with cells expressing the ACP - OR17-40 - GFP construct alone. It can however be noticed that cells with a low or even non-detectable GFP signal and reflecting an overall low receptor expression level have a higher Cy5 intensity, corresponding to a higher cell surface staining. These results confirm the observations on individual cells obtained by fluorescence confocal microscopy.

3.4 Conclusions

To study the expression and subcellular localization of the human odorant receptor OR17-40 in heterologous cells, we constructed different OR17-40 fusion proteins which enabled us to follow receptor biogenesis and trafficking: (i) The enhanced green fluorescent protein (EGFP) allowed a continuous labelling of all translated receptors, (ii) a *c-myc* tag enabled the selective labelling of cell surface receptors on fixed cells, and (iii) the fusion to the acyl carrier protein (ACP) provided a tool to selectively visualize plasma membrane receptors in living cells. We transiently expressed these constructs in HEK293 cells, a cell line which is well suited for GPCR expression [74, 75, 80] and in *odora* cells, a cell line derived from the rat olfactory epithelium [81]. Both cell lines exhibited low cell surface expression of ORs. Our labelling experiments indicated that the majority of the translated receptors were trapped in intracellular compartments, with a better plasma membrane localization of OR17-40 in low expressing cells. Since HEK293 cells are easier to handle than *odora* cells, and since OR membrane localization in *odora* cells was not improved as compared to the one in HEK293 cells, we decided to use HEK293 cells for further experiments.

Although a number of accessory proteins (ODR-4, the β_2-adrenergic receptor, or the RTP proteins) were shown to promote translocation of some ORs to the plasma membrane of heterologous cells, we did not achieve a better cell surface trafficking of OR17-40 by the co-expression of these proteins, as indicated by FACS analysis. It is possible that different ORs require different helper proteins to enhance cell surface expression and that the accessory protein specific to OR17-40 remains to be discovered. On the other hand, as the co-expression of the RTP proteins, which are proteins derived from mouse, induced a significantly lower enhancement of cell surface expression of the rat I7 receptor than of three different mouse ORs [89], it is likely that such accessory proteins are species-specific. Recently, a full-length human cDNA that is homologous to the *C. elegans odr*-4 gene at the protein level across nearly the entire gene was isolated [110]. The protein has not been tested so far for complementation of OR trafficking activity in heterologous cells, but it is possible that this human ODR-4 could increase cell surface

targeting of human odorant receptors, such as OR17-40.

Chapter 4

Biogenesis and Trafficking of the Human Odorant Receptor OR17-40 in HEK293 Cells

4.1 Introduction

In order to establish efficient cell-based assays in which large collections of odorant molecules can be screened and which are generally applicable for all members of the OR super-family, it is necessary to devise a system in which the receptors are efficiently transported to the cell surface. A first step in this direction is the investigation of cellular mechanisms responsible for inefficient OR surface expression. Monitoring the different stages of OR expression and trafficking, from its biosynthesis to its insertion in the plasma membrane, can thus provide valuable information for manipulating these processes *in vivo*.

The subcellular localization of ORs is classically assessed by immnocytochemistry, using fluorescent antibodies generated either against specific ORs [111–113] or against an epitope tag fused to the OR extracellular part [75, 80, 104, 114]. However, antibody labelling in living cells can lead to receptor cross-linking [108, 109], which might induce an artifactual behavior in receptor mobility. Other side effects might be caused by the size of the antibodies, which are often larger than the receptor itself and can therefore prevent the investigation of several processes, such as receptor endocytosis.

Alternatively, OR subcellular localization in living cells can be monitored using a genetic fusion of the receptor to the green fluorescent protein (GFP) [105, 114]. This approach allows the continuous visualization of all receptors in real time. However, since GFP labels all intracellular and membrane-inserted receptors

in the same color, the selective analysis of cell surface receptors can be impeded by a strong intracellular fluorescent background.

In this chapter, we took advantage of a double-tagged OR17-40 receptor construct, where the extracellular N-terminal part was fused to the ACP protein and the intracellular C-terminus was fused to GFP, to resolve for the first time sequential stages in the life cycle of an odorant receptor. This combination of tags did not interfere with the biological function of the odorant receptor and enabled not only to visualize the receptor right after its biosynthesis in intracellular compartments, but also to optically distinguish and quantitatively compare surface (Cy5-labelled) and total (GFP-tagged) receptor pools at any time in living cells. Moreover, as the small fluorophore added by ACP labelling [99] does not prevent receptor endocytosis, this method allowed us to reveal unexpected constitutive internalization in the absence of an agonist.

4.2 Experimental Procedures

4.2.1 Materials

The plasmids pECFP-ER and pECFP-Golgi were purchased from Clontech (Palo Alto, CA, USA). Lipofectamine2000 was from Invitrogen (Breda, NL). Transferrin-alexa488 was from Molecular Probes (Eugene, OR, USA). Sucrose was from Sigma (Buchs, CH). CoA-CypHer was kindly synthesized by A. Peer (LCAN-ISIC, EPFL, CH). Helional and α-methyl-cinnamaldeyde were kindly provided by Dr C. Margot (Firmenich SA, Geneva, CH).

4.2.2 Fluorescence Confocal Microscopy of OR17-40 Biogenesis and Trafficking in HEK293 Cells

HEK293 cells grown on 25 mm diameter glass coverslips in 6-well plates were transfected with ACP - OR17-40 - GFP cDNA together with either pECFP-ER or pECFP-Golgi at a 4:1 ratio using the Lipofectamine2000 reagent according to the manufacturer's protocol. At different time points after the onset of transfection, samples were visualized by laser-scanning confocal microscopy. Detection and distinction of both the receptor (GFP fluorescence) and the ER or Golgi marker was achieved by appropriate filter sets (see Chapter 2) using a multitracking mode.

4.2.3 Receptor Internalization Studies by Fluorescence Microscopy

The clathrin internalization pathway of HEK293 cells was blocked by 10 min incubation at 37 °C in D-PBS containing 0.45 M sucrose [115]. Cells transiently or stably expressing the ACP - OR17-40 fusion protein were labelled with the pH-sensitive dye CoA-CypHer (5 μM CoA-CypHer, 1 μM AcpS and 10 mM $MgCl_2$ in D-PBS containing 0.45 M sucrose) for 30 min at 37 °C. Cells were then washed 3 times with D-PBS containing 0.45 M sucrose. CypHer fluorescence was visualized on a home-built fluorescence microscope as described in Chapter 5 (Excitation: 632.8 nm HeNe; Q645LP dichroic mirror; HQ710/120 filter).

For subcellular co-localization studies with fluorescently labelled transferrin, 50 μg/ml Tf-alexa488 was added to the cells during the ACP labelling with 5 μM CoA-Cy5. Cells were visualized by fluorescence confocal microscopy. Detection and distinction of Tf-alexa488 and the Cy5-labelled receptors was achieved by appropriate filter sets (see Chapter 2) using a multitracking mode.

To quantify the effect of agonist or antagonist binding on the receptor internalization, cells transiently expressing the ACP - OR17-40 - GFP double-tagged construct were incubated at 37 °C either overnight with 300 μM α-methyl-cinnamaldehyde, or 15 min and 1 h with 200 μM helional, and labelled with CoA-Cy5 according to the protocol described in Chapter 2 (for the sample with antagonist, ACP labelling was performed in presence of 300 μM α-methyl-cinnamaldehyde). Cells were then analyzed by FACS.

Cell culturing and preparation, calcium imaging, confocal microscopy and FACS analysis were performed as described in Chapter 2. Cloning steps for the ACP - OR17-40 and ACP - OR17-40 - GFP fusion constructs are detailed in Chapter 3.

4.3 Results and Discussion

4.3.1 Functionality of ACP - OR17-40 and ACP - OR17-40 - GFP

In order to investigate if the fusion of the different peptide tags would interfere with the biological function of OR17-40, we performed calcium imaging on cells stably expressing ACP - OR17-40 or ACP - OR17-40 - GFP together with $G_{\alpha q}$. As shown in Figure 4.1, both cell lines responded to the cognate ligand helional in a dose-dependent manner, with an EC_{50} of 108.0 $\pm$ 4.2 μM for ACP - OR17-

40 and of 90.7 ± 7.9 μM for ACP - OR17-40 - GFP, which are comparable to the EC_{50} measured for the wild-type receptor (98.7 ± 4.7 μM). Furthermore, even Cy5-labelled ORs retained their full activity (Figure 4.1).

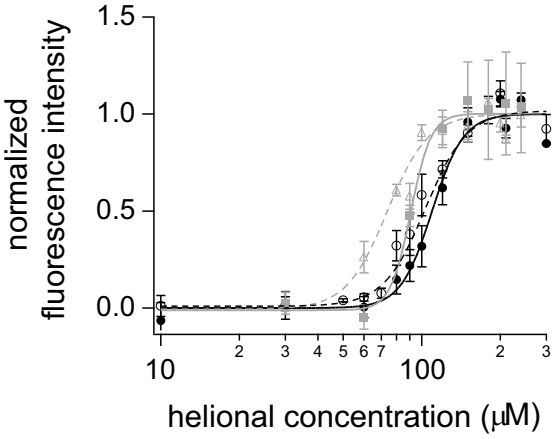

Figure 4.1: Functional expression of ACP - OR17-40 and ACP - OR17-40 - GFP. *Concentration-response relations of the cognate ligand helional on calcium ion release in HEK293 cells stably expressing ACP - OR17-40 (filled circles, black solid line) or ACP-OR17-40-GFP (filled squares, grey solid line) together with $G_{\alpha q}$. The EC_{50} of 108.0 ± 4.2 μM for ACP - OR17-40 and of 90.7 ± 7.9 μM for ACP - OR17-40 - GFP are comparable to the EC_{50} value of 98.7 ± 4.7 μM obtained for the wild-type receptor (open circles, black dashed line). Labelling of the ACP - OR17-40 fusion construct with a saturating (5 μM) concentration of CoA-Cy5 does not impair the receptor activity (open triangles, grey dashed line). Data, normalized to the highest response, are means ± SE of at least 3 independent FLEXstation experiments.*

4.3.2 Trafficking of OR17-40 in HEK293 Cells

We investigated the time course of OR17-40 biogenesis and translocation to the plasma membrane of HEK293 cells either on individual cells using fluorescence confocal microscopy, or on large cell populations using FACS analysis.

ACP - OR17-40 - GFP Biogenesis and Membrane Trafficking studied by Confocal Microscopy — We found that the first GFP signals of the ACP - OR17-40 - GFP double-tagged receptor were detectable in the endoplasmic reticulum typically 4 h after the onset of transfection. The subcellular localization of OR17-40 was confirmed by overlapping the fluorescence signal of the receptor with a spectrally distinguishable enhanced cyan ER marker (Figure 4.2, *A-C*), which

was co-transfected together with the receptor construct. In parallel experiments, we were able to overlap fluorescence images arising from the receptor with ECFP targeted to the Golgi apparatus at $\sim$ 4 h 30 to 5 h after transfection (Figure 4.2, *D-F*). Interestingly, the receptor translocation from the ER to the Golgi apparatus was only seen in low expressing cells. At high expression levels, the receptors accumulated in the ER and did not translocate to the plasma membrane (Figure 4.2, *G-I*). This effect was still visible 12 or even 24 h after transfection.

7 to 8 h after the onset of transfection, the double-tagged receptor could be detected at the cell surface of low expressing cells after labelling with CoA-Cy5 (Figure 4.2, *J-L*). The punctate pattern of Cy5 labelling is similar to the one reported for other ORs stained with antibodies [82, 89], and suggests the aggregation of the receptor into clusters. The reason for an aggregation of the OR is not known, but, as homotypic OR interactions seem to mediate OSN axonal targeting to specific glomeruli in the olfactory bulb [14, 116], OR clustering or aggregation might arise from the natural tendency of the odorant receptors to self-associate [67]. However, whether the clustering behavior of OR17-40 is influenced by receptor-receptor interactions or by cell-specific factors should be investigated by comparative studies of receptor expression in the natural cell background of olfactory sensory neurons.

In a recent paper, Lu *et al.* reported that, when expressed in heterologous cells, ORs are not selected for export from the ER and that ER-retained receptors are degraded by the ubiquitin-proteasome system or are sequestered in ER aggregates that are degraded by autophagy [67]. Furthermore, it was suggested that intramolecular interactions affect OR trafficking [117]. Indeed, truncation prior to the sixth transmembrane domain promoted the translocation of an odorant receptor to the plasma membrane of HEK293 cells, whereas co-expression of the sixth and seventh transmembrane domains prevented cell surface expression of the truncated protein [117].

Our results indicate that ORs are retained in the ER mainly in highly expressing cells, probably because of aggregation of the receptor due to over-expression. Nevertheless, as shown by the co-localization of ACP - OR17-40 - GFP with a Golgi marker, ORs exit the ER of low expressing cells and can be translocated to the plasma membrane (Figure 4.2). Part of the receptors are thus efficiently folded in these cells, suggesting that the poor plasma membrane targeting of odorant receptors in heterologous cells is rather due to OR self-aggregation in the ER than to receptor misfolding. However, even one or two days after transfection, part of the GFP fluorescence could still be detected in the ER of low expressing cells. This signal can arise either from newly synthesized receptors or from a fraction of

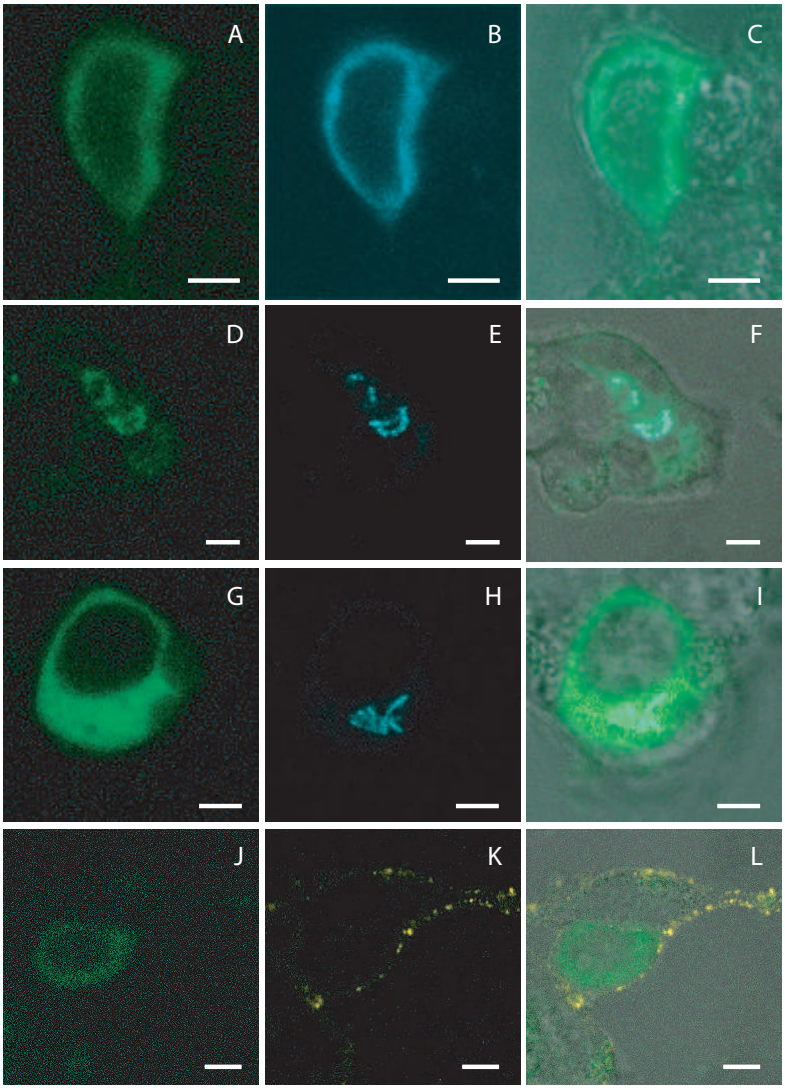

Figure 4.2: Biogenesis and membrane trafficking of ACP - OR17-40 - GFP. *Confocal fluorescence micrographs showing HEK293 cells at different time points after transfection with ACP - OR17-40 - GFP cDNA. 4 to 5 h after the onset of transfection, the receptor is visible in the ER (*A-C*); about 30 min later it can be seen in the Golgi apparatus of low expressing cells (*D-F*), but not of highly expressing cells (*G-I*, images taken 8 h after transfection). 7 to 8 h after transfection, part of the receptors are inserted in the plasma membrane (*J-L*). 1st column, ACP - OR17-40 - GFP (GFP channel); 2nd column, ER (*B*) or Golgi (*E,H*) marker, or CoA-Cy5 (*K*); 3rd column, transmission image of the same area, with fluorescence images of the two first columns superimposed. Scale bar indicates 5 μm.*

the receptors which would be misfolded. This could be addressed by chemically blocking new protein synthesis.

Studies on OR trafficking in *odora* cells supported a model comporting two regulatory checkpoints [82]. The first checkpoint corresponds to the exit from the ER, which is crucial in heterologous cells. Because ORs expressed in undifferentiated *odora* cells are present in the Golgi but not at the plasma membrane, a second checkpoint might occur at a post-Golgi compartment [82]. Our results do not indicate that OR17-40 should be stuck at this second checkpoint, as the receptor was visible at the cell surface a few hours after being present in the Golgi apparatus.

ACP - OR17-40 Expression Time Course — For a more quantitative analysis of the receptor expression in large cell populations over time, we performed FACS analysis on cells expressing the ACP - OR17-40 -GFP construct at different time points after the onset of transfection. Labelling the cells with CoA-Cy5 allowed the monitoring of the receptors reaching the plasma membrane, whereas recording the GFP fluorescence intensity enabled the quantification of the total amount of translated receptors. As shown in Figure 4.3, the total number of expressed receptors reached a plateau $\sim$ 12 h after transfection. The time course of receptor membrane insertion was delayed by 4 to 5 h.

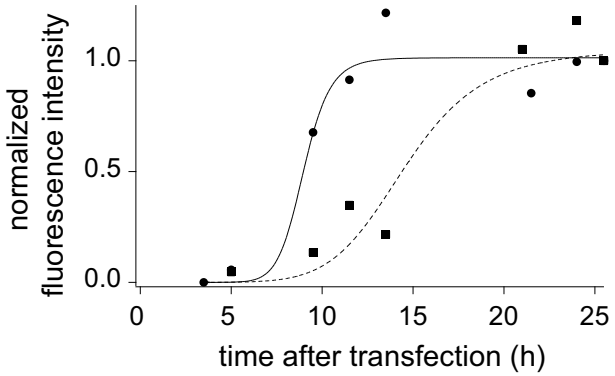

Figure 4.3: Time-lapse analysis of ACP - OR17-40 - GFP expression by FACS. *The total expression of receptors at different time points after transfection onset was measured by monitoring the GFP fluorescence intensity (circles, solid line), while the time course of receptors reaching the plasma membrane was followed by recording the Cy5 fluorescence intensity (squares, dashed line). Data are normalized to the fluorescence intensity after 25 h for each fluorophore.*

4.3.3 Constitutive Receptor Internalization

Cy5-labelled ACP - OR17-40 receptors exhibited a subcellular localization distributed between the plasma membrane and intracellular vesicles. As the ACP technique only labels cell surface receptors, the intracellular fluorescent signals must arise from internalized receptors. Although constitutive internalization in absence of a ligand has been reported for several GPCRs, such as the human α_{1a}-adrenergic receptor [118], the M2 muscarinic receptor [119], the chemokine CXCRa receptor [120], the CB1 cannabinoid receptor [121], the thrombin receptor [122], and the thromboxane A2 receptor [123], to our knowledge, no indication of this phenomenon has ever been provided for odorant receptors.

To verify that the internalization was not caused by the ACP labelling, we performed the same experiment with another GPCR, the neurokinin 1 receptor (NK1R), which was also fused to ACP. Cells expressing the Cy5-labelled NK1R showed a strong fluorescence staining at the cell membrane, with almost no fluorescence inside the cells.

Blocking the Clathrin-Mediated Internalization Pathway by Hypertonic Sucrose — To characterize the pathway by which the constitutive internalization of OR17-40 occurs, we tested the effect of hypertonic sucrose, which selectively inhibits clathrin-mediated endocytosis by inducing abnormal clathrin polymerization, thereby reducing the number of clathrin-coated pits [115]. The ACP - OR17-40 fusion construct was labelled with CoA-CypHer, a pH-sensitive fluorescent dye, which is non-fluorescent at neutral pH, and becomes highly fluorescent when it is protonated [124]. This dye is a valuable tool for studying receptor internalization into acidic vesicles [124]. When the cells expressing the ACP - OR17-40 fusion construct were incubated in 0.45 M sucrose 10 min prior to and during labelling with CoA-CypHer, the fluorescence of the cells was low and detectable at the cell membrane. In contrast, in non-sucrose-treated control cells, the fluorescence intensity was high and concentrated in vesicles that were moving below the plasma membrane, indicating that the receptor was internalized (Figure 4.4). After sucrose removal, apparition of fast moving intracellular vesicles in cells previously incubated in hypertonic sucrose occurred in a time range of minutes.

The addition of 100 μM or 200 μM helional on cells expressing the ACP - OR17-40 fusion construct and incubated in 0.45 M sucrose did not induce any detectable receptor internalization, suggesting that both constitutive and agonist-induced internalization occur along the clathrin-mediated pathway.

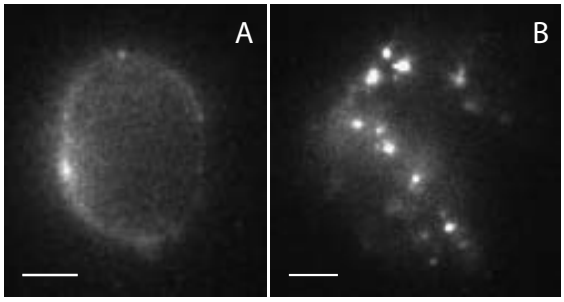

Figure 4.4: The constitutive internalization of ACP - OR17-40 is blocked by hypertonic sucrose. *Fluorescence micrographs showing CypHer-labelled ACP - OR17-40 fusion receptors after ACP labelling performed in the presence (*A*) or absence (*B*) of 0.45 M sucrose. Cells incubated with sucrose exhibit a faint and rather homogenous membrane staining (*A*), while non-sucrose-treated cells contain highly fluorescent mobile intracellular vesicles located just below the plasma membrane (*B*). Scale bar indicates 5 µm.*

Co-Localization with Transferrin Receptor — In order to identify the organelles containing the internalized ACP - OR17-40 fusion receptor, we labelled the cells with transferrin-alexa488 (Tf-alexa488). The transferrin receptor (TfR), which is constitutively endocytosed to early endosomes and efficiently recycles to the plasma membrane, is a commonly used marker for endosomes involved in protein sorting and recycling [118,125–127]. As shown in Figure 4.5, Cy5-labelled ORs were mostly present in vesicles containing TfR after 30 min to 1 h incubation at 37 °C, indicating that OR17-40 was localized in early or recycling endosomes after that time. The overlapping of the two signals increased over time. Cells incubated with 200 µM helional for up to 1 h showed a similar distribution of intracellular vesicles containing both OR and TfR (data not shown). A similar localization of an odorant receptor in TfR-positive endosomes has previously been reported for the U131 receptor in undifferentiated *odora* cells [82], indicating that constitutive OR endocytosis is not specific to HEK293 cells.

Influence of Agonist or Antagonist Binding on Receptor Internalization — The influence of agonist or antagonist binding on receptor internalization was investigated on cells transiently expressing ACP - OR17-40 - GFP. 200 µM helional was added to the cells for 15 min or for 1 h, whereas parallel cell samples were treated overnight with 300 µM α-methyl-cinnamaldehyde (antagonist, see Chapter 6). The subsequent labelling with CoA-Cy5 allowed the quantification of cell surface receptors using FACS analysis. As shown in Figure 4.6, there was no significant variation in the amount of labelled receptors after the different

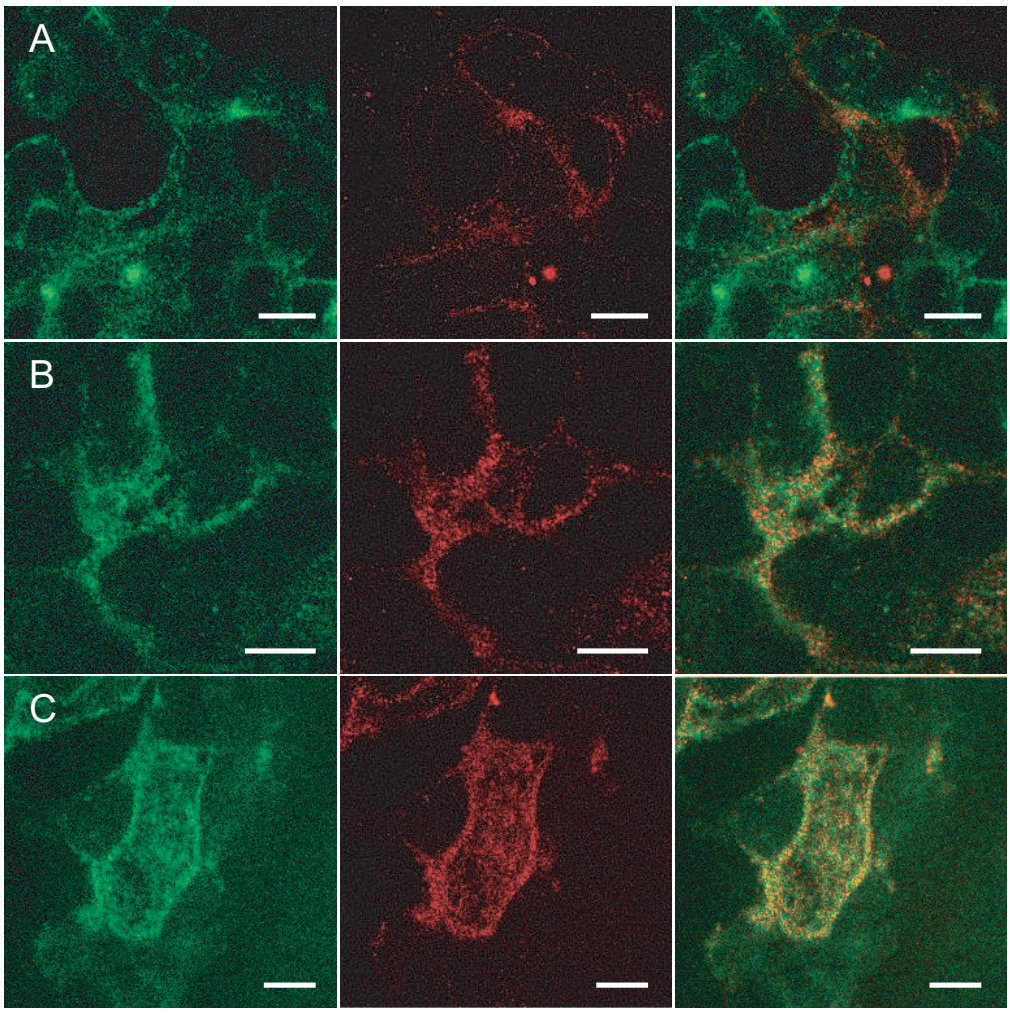

Figure 4.5: Co-localization of Cy5-labelled ACP - OR17-40 and transferrin receptor. *Confocal fluorescence micrographs showing the localization of transferrin receptor (green) and Cy5-labelled ACP - OR17-40 (red) in HEK293 cells. The co-localization of the two receptors is shown in yellow in the third column, which corresponds to the merging of the micrographs in the first two columns. 50 µg/ml Tf-alexa488 was added to the cells during the ACP labelling, which was performed at room temperature. Cells were then washed 3 times with D-PBS and incubated at 37°C for 10 min (*A*), 30 min (*B*) or 1 h (*C*). Scale bar indicates 5 µm.*

treatments. Similar results were found for the human α_{1a}-adrenergic receptor, for which very little variation in the level of constitutive internalization was observed upon addition of both an agonist or an inverse agonist [118]. As the receptors are localized in recycling endosomes trafficking to and from the cell surface in absence of ligand, it is likely that the surface receptor density is maintained constant by recycling, even in presence of an agonist, so that the cells are not desensitized to further ligand exposure [118, 126, 128]. In this respect, constitutive endocytosis of the odorant receptor would help to maintain odor sensitivity over prolonged receptor stimulation.

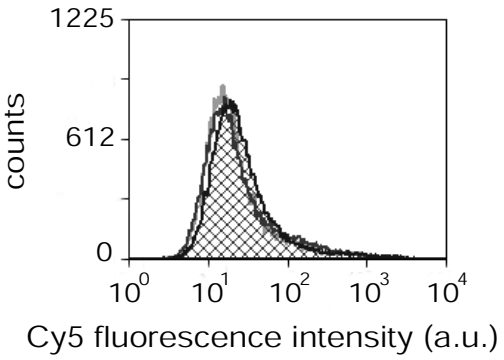

Figure 4.6: Quantification of the amount of cell surface ORs before and after ligand binding. *The Cy5 fluorescence intensity was monitored for 35,000 HEK293 cells expressing the ACP - OR17-40 - GFP fusion construct and labelled with CoA-Cy5 before (patterned) and after incubation with the agonist (black line), or the antagonist (grey line).*

Moreover, the constitutive internalization of OR17-40 is unlikely to be due to the constitutive activation of the receptor or to exogeneous ligands present either in the culture medium or in the air, as it is not blocked by antagonist treatment. This suggests that an endocytic motif might be responsible for targeting the receptor towards internalization. Studies on the thromboxane A_2 receptor indicated that a $YX_{2-3}\phi$ (where X is any amino acid and ϕ is a bulky hydrophobic amino acid) motif in the receptor carboxy-terminal tail was responsible for its constitutive internalization [129]. Although this specific motif is not present in the C-terminal part of OR17-40, it is not impossible that a different motif plays a similar role.

Altogether, these results also indicate that receptor internalization, which, in the classical model of GPCR activation, is normally an agonist-dependent process, can occur without G protein activation. The dissociation of receptor internalization and G protein activation has already been shown for several other GPCRs, such as a mutant of the μ-opioid receptor [130], the human cytomegalovirus-encoded

seven-transmembrane receptor US28 [131], the metabotropic glutamate receptor 1a [127] or the complement factor 5a receptor [132], and suggests that GPCRs can take many more states than usually believed [132].

4.4 Conclusions and Outlook

A functional double-tagged receptor construct enabled the monitoring of OR17-40 expression, trafficking, plasma membrane targeting and endocytosis in real time in living cells. As heterologously expressed odorant receptors are often retained in intracellular compartments, the combination of the intracellular GFP tag and the extracellular fusion to ACP allowed the optical discrimination of cell surface receptors from all translated receptors.

Using this strategy of multicolor labelling, which also involved subcellular markers based on ECFP, we could show that part of the receptors were translocated to the plasma membrane. The amount of these cell surface receptors was higher in low expressing cells than in cells exhibiting high over-expression levels. In highly expressing cells, the ORs did not exit the ER, probably because of receptor self-aggregation caused by over-expression. The use of a weak promoter for OR expression in heterologous cells could thus lead to a better plasma membrane localization of the receptor. However, first attempts in that direction were not conclusive, as the expression of an OR17-40 - GFP fusion protein using the ecdysone-inducible vector pIND (Invitrogen, Breda, NL) led to an unexpectedly homogeneous subcellular localization: The receptor was even present in the nucleus (data not shown).

As the ACP tag at the receptor N-terminus allowed the selective labelling of cell surface receptors in living cells, we were able to follow the fate of OR17-40 after its insertion in the plasma membrane. Interestingly, we could show that OR17-40 undergoes constitutive internalization in the absence of an agonist. This internalization process occurred along the clathrin-dependent pathway, and was not influenced by agonist or antagonist binding. Uncoupling of receptor internalization and G protein activation, two processes usually believed to result from ligand binding, has already been shown for several GPCRs [127, 130–132], and constitutive internalization is believed to be mediated by specific signals on the carboxy-terminal tail of the receptors [122, 129, 131]. Moreover, since constitutive endocytosis of several GPCRs seems to prevent receptor desensitization to further exposure to an agonist [118, 126, 128], it is possible that OR constitutive internalization, as demonstrated for the human OR17-40, helps to prolong odor sensitivity. It would thus be interesting to investigate whether the constitutive endocytosis of

odorant receptors also occurs in olfactory sensory neurons.

Chapter 5

Lateral Diffusion of an Odorant Receptor in HEK293 Cell Membranes

5.1 Introduction

The lateral motion of integral membrane proteins plays an important role in many biological phenomena by promoting for instance collisions of receptors and effectors in the plasma membrane. For GPCRs in particular, there is evidence for a non-random distribution of the receptors, G proteins, and effectors [133–135]. A compartmentalization of the receptors and other partners could also explain the rapidity and specificity of G protein-mediated signalling [136, 137].

According to the fluid-mosaic model proposed by Singer and Jacobson more than 30 years ago [138], the plasma membrane was until recently considered as a two-dimensional solvent in which membrane proteins are homogeneously distributed and free to move. However, the plasma membrane of various mammalian cells is now known to be heterogeneous and to contain various types of domains [139–143]. A first type of domain is referred to as lipid raft or caveola. Lipid rafts are enriched in cholesterol, sphingolipids and glycosylphosphatidyl inositol (GPI)-anchored proteins, and are thought to exist as liquid-ordered microdomains while the rest of the cell membrane would be liquid-disordered [144–146]. Reports about their size vary from 5-10 to 700 nm [144–147]. Very similar to rafts, the caveola consists of a small flask-shaped plasma membrane invagination, 70-100 nm in diameter, that is coated with caveolin and contains the same lipid components as rafts [143]. A second type of compartmentalization found in cell membranes is caused by the membrane-associated cytoskeleton, which provides a barrier to the free diffusion of membrane proteins due to the steric hindrance of

the protein intracellular part [140, 148, 149]. Such domains can have a diameter of 350-750 nm [146]. Due to the dynamical properties of the membrane skeleton, proteins which are confined inside one compartment can eventually escape (hop) to the next one [148]. Moreover, this type of confinement is not restricted to molecules possessing an intracellular part [150]. For instance, the diffusion of a lipid located in the outer leaflet of the plasma membrane and which was therefore not directly interacting with the membrane skeleton, was shown to also sense the membrane compartmentalization [151]. It was proposed that, as many membrane proteins are linked to the cytoskeleton, forming fences for molecules diffusing in the plasma membrane, the membrane skeleton influences the lipid diffusional behavior via transmembrane proteins immobilized to the cytoskeleton ("anchored-protein picket" model) [151,152]. Finally, a third type of protein confinement might arise from long-range attractions between membrane proteins. Such a confinement would not involve the presence of physical fences and was recently proposed for opioid receptors [153].

Compartmentalization and membrane heterogeneity can be revealed by measuring the diffusion of molecules in the membrane. The classical way to measure protein mobility in cell membranes is by fluorescence recovery after photobleaching (FRAP). Briefly, dye molecules are bleached by means of a very intense illumination focused to a region of typically 1-10 μm in diameter. The subsequent recovery of the fluorescence signal due to the diffusion of unbleached molecules into the bleached area is recorded. For most systems, an incomplete recovery of typically 25-80 % [154] has been observed and interpreted within a two-component model including a mobile and an immobile fraction of the species studied. However, because conventional FRAP gives ensemble-averaged recovery times, the behavior of individual particles is masked. Furthermore, FRAP is not a feasible tool for studying sparsely distributed receptors, because it requires a high density of labels to generate a sufficient number of photons for proper photon statistics [155].

Recent advances in single-molecule microscopy (SMM) and spectroscopy (SMS) at room temperature by laser-induced fluorescence offer new tools for observing the movements of individual proteins or lipids in the cell membrane [154–156]. Such methods allow the examination of individual members of a heterogeneous population and the identification and quantitative comparison of different subpopulations. Single-particle tracking (SPT) studies have been carried out using video-enhanced imaging systems and either nanometer-sized gold particles [157] or highly fluorescent molecules [155].

Plasma membrane receptors are usually labelled using fluorescent ligands or antibodies, or genetic fusions to autofluorescent proteins. However, fluorescent

ligands doe not allow the study of unliganded receptors, antibodies are often larger than the receptor itself and may interfere with its mobility and functionality, and autofluorescent proteins are not very photostable and have excitation spectra in the same range as autofluorescent cellular compounds. Here, we take advantage of the newly developed ACP labelling technique, which enables the covalent attachment of a long-wavelength fluorophore (Cy5), with high absorption cross-section, high quantum yield and high photo-stability, to the human odorant receptor OR17-40.

In this chapter, we present the study of lateral diffusion of Cy5-labelled OR17-40 in the plasma membrane of HEK293 cells. The principal objective was, first, to characterize the movements of the receptor and identify a potential compartmentalization of the membrane, and, second, to monitor the receptor diffusional behavior in presence of an agonist or antagonist.

5.2 Experimental procedures

5.2.1 Materials

CoA-Cy5 and AcpS were a kind gift from N. George and K. Johnsson (LIP-ISIC, EPFL, CH). Helional, α-methyl-cinnamaldeyde and piperonal were kindly provided by Dr C. Margot (Firmenich SA, Geneva, CH). Sucrose was purchased from Sigma (Buchs, CH).

Cell culturing and preparation, as well as production of the cell line stably expressing ACP - OR17-40 and $G_{\alpha q}$ were performed as described in Chapter 2. The functionality of the ACP - OR17-40 fusion construct was shown in Chapter 4.

5.2.2 Experimental Set-Up

Experiments were performed on a modified epiluminescence wide-field microscope. An intensified CCD camera allowed a sensitive detection of the light emitted by a single fluorophore. A schematic view of the set-up is shown in Figure 5.1.

Cells grown on 8-well chambered coverglass slides were mounted on an epiluminescence wide-field microscope (Axiovert 200, Zeiss). Circularly polarized light of a 632.8 nm HeNe laser (Coherent, Auburn, CA, USA) was directed by a dichroic mirror (Q645LP, Chroma Corp., Rockingham, VT, USA) into a microscope objective (C-Apochromat 63x water-corrected, 1.2 NA, Zeiss) to illuminate a 22 μm diameter region of the sample. Fluorescence was collected by the same objective, passed through an adequate filter (HQ710/120, Chroma Corp., Rockingham, VT, USA), and imaged on an intensified CCD camera (I-Pentamax 512 EFT, Roper

Scientific, USA). To minimize photobleaching, cells were only illuminated for 50 ms per image using a shutter (LS3T2, Vincent Associates, Rochester, USA).

5.2.3 Principle of Single-Molecule Microscopy

The observation of single molecules requires the use of fluorophores with high quantum yield and high photostability, which emit light at a wavelength where the background autofluorescence of the cell is low and where the detection efficiency of the recording system is high. A dye that emits in the far red, like Cy5 (excitation: 650 nm; emission: 670 nm), is very well suited. The ACP labelling technique enables the covalent attachment of only one Cy5 fluorophore per receptor, thus avoiding artifactual diffusional behaviors caused by receptor cross-linking. Moreover, receptors not properly inserted in the plasma membrane are not labelled and therefore do not contribute to out-of-focus fluorescence. For single-molecule detection, the concentration of labelled molecules has to be low enough that single molecules can be separated. By varying the concentration of CoA-Cy5 substrate added to the cells, it is possible to achieve an optimal amount of labelled receptors to distinguish single molecules (5-20 labels per focal area). On the other hand, non-specific binding of the label on the plasma membrane, which is a very crucial obstacle for single-molecule tracking, is very low in our case because the CoA-moiety is negatively charged.

The principle of single-molecule microscopy is illustrated in Figure 5.2*A*. The wide-field epi-illumination together with the CCD camera allows the simultaneous observation and localization of several single molecules.

A typical image of single receptor molecules is shown in Figure 5.2*B*. Each receptor is labelled with only one fluorophore and the fluorescence is monitored over time. After usually 2-50 images, the fluorophore is bleached, resulting in a one-step decrease of fluorescence intensity (Figure 5.2*C*). The question whether each bright spot corresponds to a single receptor has to be addressed by three different criteria: (i) The intensity is typical for single dye molecules, (ii) it exhibits blinking and/or drops to background level in a single sharp step, and (iii) the size and shape of the spot is diffraction limited.

5.2.4 Single-Molecule Experiments

Experiments were carried out on HEK293 cells stably expressing the ACP - OR17-40 fusion construct together with $G_{\alpha q}$. 24 to 36 h before the measurement, cells were seeded in 8-well chambered coverglass slides and grown at 37^{o}C in D-MEM medium containing 10 % FCS. On the day of measurement, cells were washed with

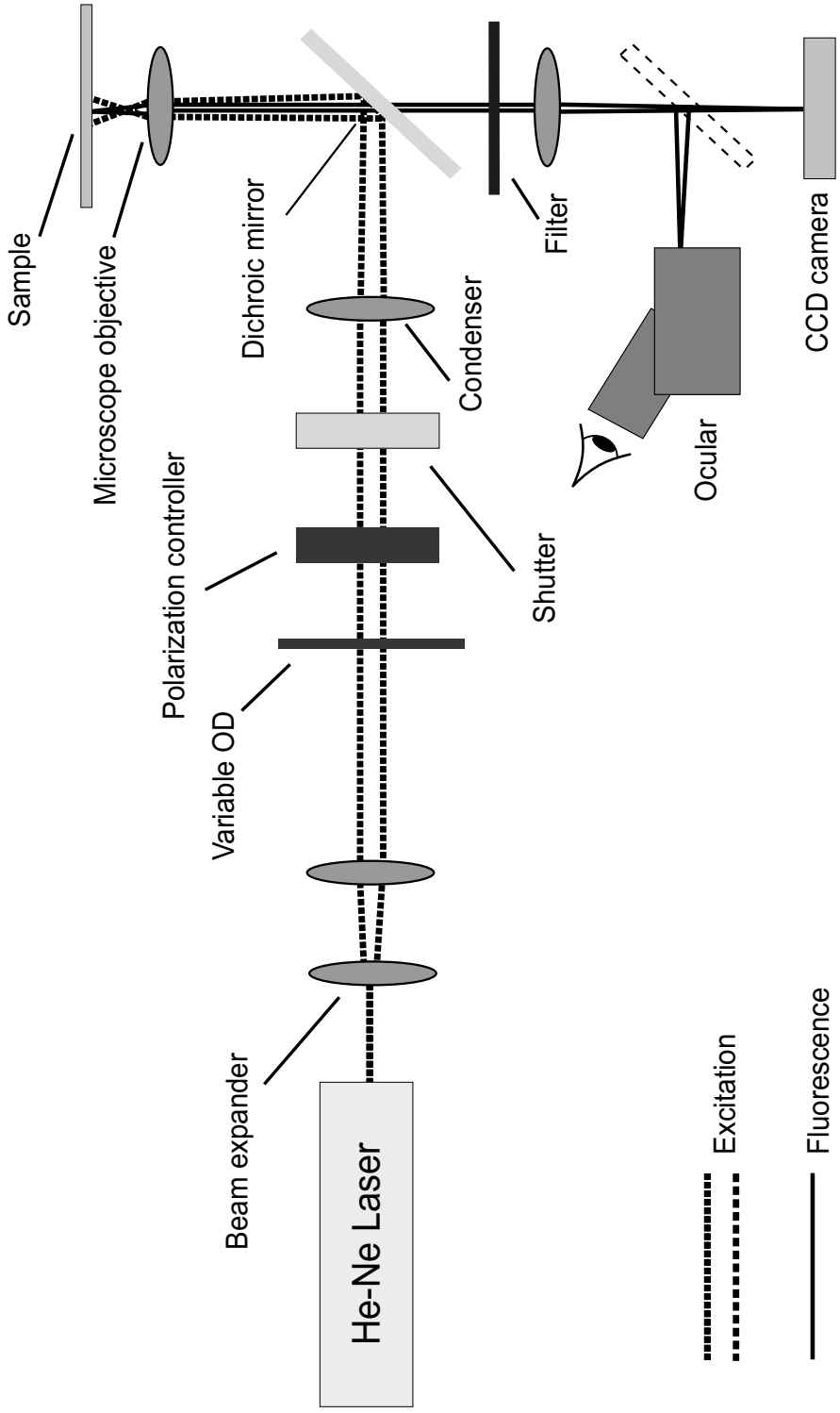

Figure 5.1: Schematic view of the single-molecule fluorescence imaging microscope.

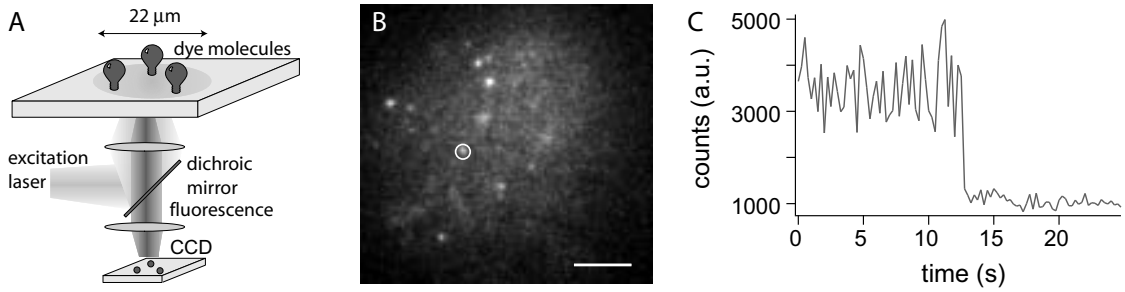

Figure 5.2: Single-molecule imaging of OR17-40. *(*A*) Principle of single-molecule imaging. A 22 µm spot is illuminated with laser light and the fluorescence of single molecules is recorded with a high-sensitivity CCD camera. (*B*) Fluorescence image of a single HEK293 cell containing Cy5-labelled ACP - OR17-40 receptors. Each diffraction-limited spot corresponds to a single receptor. The scale bar indicates 5 µm. (*C*) Fluorescence intensity recorded inside the marked ring in* B*, for a series of images taken at 4 Hz sampling frequency. The one-step photobleaching is the signature of a single fluorophore.*

D-PBS and labelled with Cy5 (50 or 500 nM CoA-Cy5, 1 μM AcpS and 10 mM $MgCl_2$ in D-PBS) for 30 min at room temperature. Cells were then carefully washed three to five times with D-PBS and mounted on a wide-field fluorescence microscope. Series of 100 images were recorded at a sampling frequency of 4 Hz with an integration time of 50 ms and an excitation light intensity of 0.5 kW/cm^2. Images were focused on the upper cell membrane and care was taken to measure on flat cells. All measurements were performed at room temperature.

To investigate the effect of agonist binding on the receptor diffusional behavior, measurements were performed after the addition of 200 μM helional. To study the influence of an antagonist, cells were pre-incubated overnight in 300 μM α-methyl-cinnamaldehyde, and ACP labelling and measurements were performed in presence of the antagonist. Control measurements were performed after the addition of 300 μM piperonal. All three substances were freshly diluted in PBS from a stock solution of 1 M in DMSO, ensuring that the final DMSO concentration was similar for the three compounds.

To block receptor endocytosis, cells were incubated in D-PBS containing 0.45 M sucrose for 10 to 15 min at 37°C prior to ACP labelling. Labelling and measurements were performed in 0.45 M sucrose.

5.2.5 Data Evaluation

The diffusion of single receptors was analyzed with the help of a custom-made computer program based on Igor Pro (WaveMetrics), that has been developed in our laboratory to localize and track single fluorescent molecules, similarly to [149,156,158]. The first step is the identification of real single molecules out of the recorded image series. This is done by addressing the three above-cited criteria, i.e. by the size of the fluorescent spot, its intensity and single-step photobleaching. The computer program first locates bright spots, which clearly exceed the background level. These candidates are then fitted with a two-dimensional Gaussian [158] (Figure 5.3).

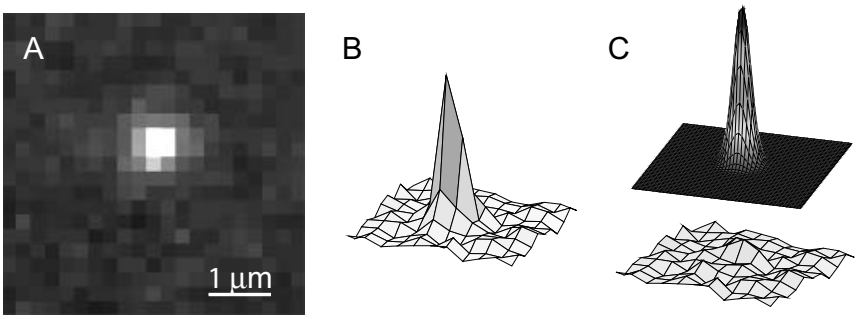

Figure 5.3: Determination of the position of a single fluorophore. *(*A*) The spot of a single fluorescent molecule is diffraction-limited and appears therefore spread over several pixels (pixel size: 225 nm). (*B*) The same image as surface plot, showing the typical signal-to-noise ratio in the third dimension. (*C*) The signal is fitted with a 2-D Gaussian to obtain the exact position of the fluorophore (upper panel). Substracting the fitted Gaussian from the original image leaves the background noise (lower panel).*

The width of the peak in both dimensions and the signal-to-noise ratio are taken as criteria to identify single receptor molecules. This allows the discrimination from artefacts caused by camera noise (too narrow) and from vesicles or autofluorescence of the cell (too large). A successful fit gives the position of a molecule with an accuracy much higher than the actual size corresponding to one pixel. With ideal signal-to-noise ratios on solid substrates, an accuracy of 1 nm is possible [159, 160]. By measuring the position of CoA-Cy5 molecules immobilized on a glass surface, a spatial accuracy of 34 nm was derived for our experimental set-up. Although the positional accuracy is high, the optical resolution of the image is only around 350 nm, and molecules have to be at least half the resolution apart to be distinguishable.

The positions of identified single molecules in individual images are linked within an image series to obtain trajectories. This is done by calculating for all images of a series the distances between all fitted molecules in image i to all fitted molecules in image $i+1$. If their concentration is low enough and the sampling frequency high compared to their mobility, molecules can be tracked. The molecule in image $i+1$ that is closest to a molecule in image i is considered to be the same molecule if the distance between them is within a certain threshold value. Both molecules are then added to the same track and evaluation is continued with image $i+2$. Blinking, crossing of two molecules, and unsuccessful fits interrupt a track, so that traces of single molecules need to be visually checked and interrupted tracks manually linked. Furthermore, care should be taken that only traces which end in a one-step photobleaching are evaluated. Once the traces are computed, square displacements r^2 are calculated between all points of a trace to yield maximal statistics. The average r^2 at each image interval, called mean square displacements (MSD(t_{lag})), depend on the time interval between two images. The MSD for a given time lag can be defined as the average over all independent pairs of points with that time lag, and this averaging reduces the noise in an experimental trajectory [154].

The plot of MSD versus time lag can serve as a basis for the classification of trajectories into different diffusion modes:

For free Brownian diffusion on a two-dimensional plane, the MSD increases linearly with t_{lag}:

$$MSD(t_{\mathrm{lag}}) = 4Dt_{\mathrm{lag}}, \tag{5.1}$$

where D is the diffusion constant.

If the diffusion is confined within certain barriers, the diffusion inside the compartment is free for short t_{lag}, corresponding to MSDs much smaller than the compartment size, and, at larger t_{lag}, the MSD does not exceed the compartment size but reaches a constant value. Such behavior is described for square compartments by [149]

$$MSD(t_{\mathrm{lag}}) = \frac{L^2}{3} \cdot \Big[1 - \exp\Big(- \frac{12Dt_{\mathrm{lag}}}{L^2}\Big)\Big], \tag{5.2}$$

where L is the averaged length of the domain, and D the diffusion constant.

For immobile molecules, MSDs stay constant over time.

In addition, directed diffusion might occur, when molecules are transported or influenced by other forces. In this case, the MSD increases more than linearly with t_{lag}:

$$MSD(t_{\mathrm{lag}}) = v^2t^2, \tag{5.3}$$

where v is the drift velocity.

Finally, anomalous subdiffusion, which occurs in presence of obstacles or traps in the cell membrane, leads to

$$MSD(t_{\mathrm{lag}}) = \Gamma t^{\alpha}{}_{\mathrm{lag}}, \tag{5.4}$$

with $\alpha < 1$.

Cumulative distribution function — Traces of individual molecules are often too short for the determination of MSDs(t_{lag}) with sufficient accuracy. Therefore the data of individual molecules are combined to improve statistics, but by doing this, differences between all diffusion modes are averaged out. To detect any heterogeneity in the diffusion of different populations, MSDs can be evaluated following the method proposed by Schütz and Schmidt [146, 156]: The cumulative probability distribution P to find a molecule after a certain time t_{lag} inside a radius r is plotted versus r^2.

For a single population of molecules, this distribution is described by a single exponential:

$$P(r^2, t_{\mathrm{lag}}) = 1 - \exp\Big(- \frac{r^2}{MSD(t_{\mathrm{lag}})}\Big) \tag{5.5}$$

If two populations of molecules are present with different diffusion modes or diffusion constants, P reads

$$P(r^2, t_{\mathrm{lag}}) = 1 - \Big[f \cdot \exp\Big(- \frac{r^2}{MSD_{\mathrm{fast}}(t_{\mathrm{lag}})}\Big) + (1-f) \cdot \exp\Big(- \frac{r^2}{MSD_{\mathrm{slow}}(t_{\mathrm{lag}})}\Big)\Big], \tag{5.6}$$

where f is the fraction of fast diffusing molecules and MSD_{fast} and MSD_{slow} are the mean square displacements for the fast and slow moving fractions, respectively.

5.3 Results and Discussion

5.3.1 Diffusion of OR17-40 in HEK293 Cell Membranes

The diffusion of Cy5-labelled ACP - OR17-40 receptors was monitored in HEK293 cell membranes. Typical traces, recorded at 4 Hz sampling frequency, were up to 60 images long (Figure 5.4). Data from 230 molecules measured on about 40 different cells were evaluated.

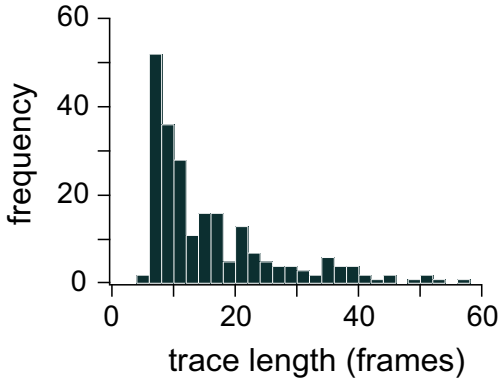

Figure 5.4: Trace length distribution of Cy5-labelled ACP - OR17-40 before photobleaching. *Traces were recorded at 4 Hz sampling frequency, with 50 ms illumination time. The average trace length is around 17 frames, or 4 seconds.*

Mean square displacements of individual receptors — The goal of SMM analysis is to sort trajectories into various diffusion modes and to characterize the diffusion by giving quantities such as the diffusion coefficient, drift velocity, confinement size, or anomalous diffusion exponent. This task is made difficult in case of limited duration or time resolution of the trajectories: The longer the trajectory of a single molecule, the more reliable its classification into one of the different modes or the detection of a change in its diffusion mode during the measurement.

There is no universal method for SMM data analysis. A first method, developed by Kusumi and colleagues [149], consists in the determination of the microscopic diffusion coefficient D for each molecule, by fitting with a straight line its MSDs at time lags $2\delta t$, $3\delta t$, and $4\delta t$. The values of D determined by this method are referred to as $D_{2\text{-}4}$, or "initial diffusion coefficient". $D_{2\text{-}4}$ is convenient because it can be determined independently of the diffusion mode. In order to sort trajectories into different modes of motion, deviations of the individual MSD(t_{lag}) from a straight line with a slope $4D_{2\text{-}4}$ are calculated: Positive and negative variations account for directed and restricted diffusion, respectively [149]. However, one needs long traces in order to classify them according to this method.

A second method is based on the construction of a probability distribution $P(r^2, t_{\text{lag}})$ of many individual molecules in order to improve statistics [156]. This is useful when the traces of the single molecules are short, but the information about individuals is lost. Although this method still allows the distinction between two different subpopulations of molecules (see *Data Analysis*), and gives the mean diffusion coefficient D and the mean compartment size L for each subpopulation, it cannot discriminate classes when the population is more heterogeneous. Moreover,

it is strictly valid only for free diffusion.

Before choosing a method of analysis, we examined the trajectories of individual receptors, and calculated the experimental mean square displacement MSD(t_{lag}) independently for each molecule. Examples of such MSD(t_{lag}) are illustrated in Figure 5.5. Typically, four classes of molecules were observed: molecules undergoing free Brownian diffusion (1), diffusing confined inside large (2), or small (3,4) compartments, and immobile molecules (5).

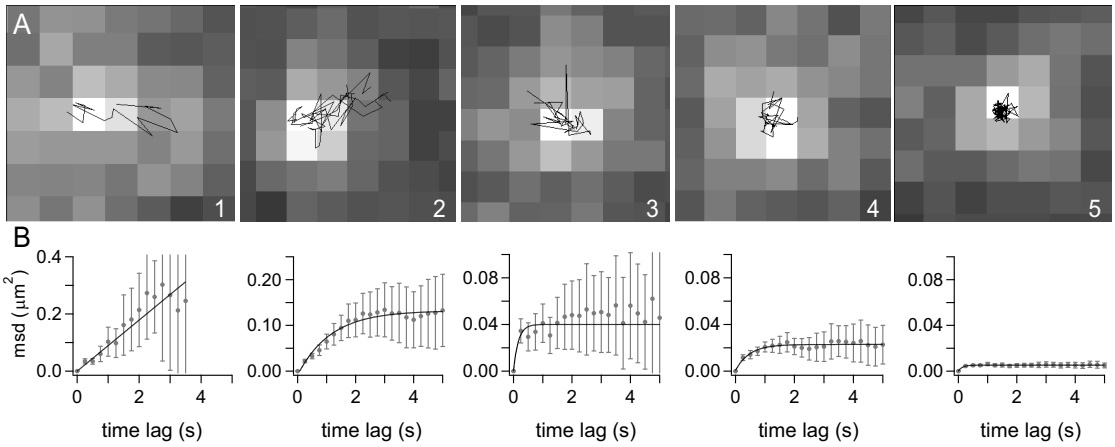

Figure 5.5: Diffusion modes of odorant receptors. *(*A*) The position of Cy5-labelled ACP - OR17-40 was evaluated from 2D Gaussian fits for each image of a series taken at 4 Hz sampling frequency. Trajectories are shown on top of a representative fluorescence image of the respective tracked molecule (pixel size: 225 nm). (*B*) Mean square displacement time courses (broken lines) of the trajectories depicted in* A*. Solid lines represent the fit of the MSD(t_{lag}) according to the analytical formula for free Brownian diffusion (1) and confined diffusion (2-5). Note that the vertical scale is different for the different MSDs. Four different classes of molecules were observed: freely diffusing molecules (1), molecules diffusing inside a large (2) or a small (3, 4) compartment, and immobile molecules (5). Confined molecules can be either fast confined (3), or slow confined (2,4).*

Classification of the receptor trajectories — The observation of the trajectories revealed that, although few receptors diffused freely in HEK293 cell membranes, the movements of most ORs appeared confined within domains of various sizes. The apparent confinement might arise from the presence of microdomains and/or from inter-protein interactions or obstacles in the plasma membrane. In the latter case, the receptors undergo anomalous diffusion and their movements can be described by Equation 5.4, whereas the movements of receptors diffusing confined inside a domain can be described by Equation 5.2. At this stage of the

analysis, it is difficult to decide for one model over the other. We thus fitted the individual MSD(t_{lag}) curves with both Equation 5.4 and Equation 5.2. In general, qualitatively, the MSD(t_{lag}) curves were better fitted by the model for confined diffusion than by the one for anomalous diffusion. Also, Equation 5.4 is intrisically more difficult to fit. For these reasons, the analysis was pursued with the model for confined diffusion.

Fitting the MSD(t_{lag}) curves with Equation 5.2 yields two important parameters: the apparent domain size L, and the microscopic diffusion coefficient D, which characterizes the movement of the molecule in its immediate neighborhood. It should be pointed out that the fit with Equation 5.2 did not converge for all MSD(t_{lag}) curves: For some fast molecules, the first experimental points necessary for determining D were non-reliable. In this case, only the domain size L was extracted.

A scatter plot of the fitted apparent domain sizes and diffusion coefficients for Cy5-labelled ACP - OR17-40, as well as the histograms of these two parameters, are shown in Figure 5.6. For more clarity on the graphs and to distinguish the fast molecules from the others, the values of their diffusion coefficient was set to $0.5\,\mu\mathrm{m}^2/s$. Similarly, molecules with a very large diffusion range (more than 3 μm) had their L arbitrarily set to $3\,\mu$m. If we disregard the points for which D and L were arbitrarily set, the $\log D$ versus $\log L$ values are distributed around a line of slope 2, indicating that $D \propto L^2$. This dependence of the microscopic diffusion coefficient on the domain size was already noticed by Daumas *et al.* for another GPCR, the μ-opioid receptor, and was assumed to arise from protein-protein interactions [161].

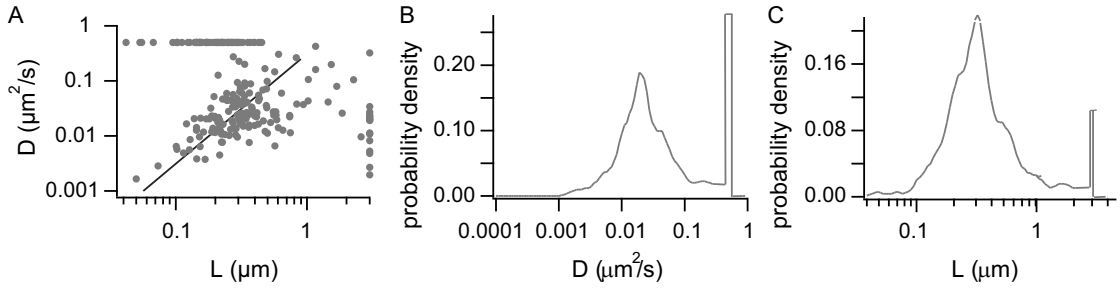

Figure 5.6: Microscopic diffusion coefficients and apparent domain sizes. *(*A*) Log-log plot of the apparent domain size* L *versus the diffusion coefficient* D *determined for each trajectory from the MSD(t_{lag}) fit with Equation 5.2. (*B*) Distribution of the diffusion coefficient* D*. The peak at* D *= 0.5 $\mu m^2/s$ corresponds to the fast molecules. (*C*) Distribution of the apparent domain size* L*. The peak at* L *= 3 μm corresponds to the molecules with a very large diffusion range.*

D is distributed over several orders of magnitude: $1.6 \times 10^{-3} \leq D \leq 4.2 \times 10^{-1}\,\mu\mathrm{m}^2/s$. Diffusion coefficients around 1 x $10^{-1}\,\mu\mathrm{m}^2/s$ measured by FRAP have been reported for several GPCRs, such as the β_2-adrenergic receptor [162], the neurokinin NK2 receptor [163], or the gonadotropin-releasing hormone receptor [164]. The majority of odorant receptors however have a slower microscopic diffusion coefficient, which could result from the binding of the receptor to the cytoskeleton or to clathrin-coated structures. Further discussion of this issue will be given later.

The distribution of the apparent compartment sizes is also broad: $5 \times 10^{-2} \leq L \leq 3\ \mu\mathrm{m}$. If we disregard the molecules for which L was set to $3\,\mu\mathrm{m}$, the histogram shows a continuous distribution of L, with a maximum at $\sim 300\,\mathrm{nm}$ and two shoulders, the first one at $\sim 200\,\mathrm{nm}$ and the second one at $\sim 500\,\mathrm{nm}$. As the comparison of this distribution with the distributions of the domain sizes obtained for the liganded receptor shows a significant difference in the population corresponding to the first shoulder (see below), we assumed that this shoulder corresponds to the population diffusing inside small domains, which increases upon ligand binding. Molecules diffusing more than 1 μm can be considered as freely diffusing molecules, as a large domain size could simply arise from the non-planar geometry of the cell and the molecule going out of focus. Moreover, by measuring the noise on immobile molecules, as well as by comparing this distribution with the distributions of the confinement sizes for the liganded receptor, we could assume that molecules diffusing inside apparent confinement sizes smaller than $0.14\,\mu\mathrm{m}$ are immobile. We thus classified the trajectories according to the apparent domain size determined from their MSD(t_{lag}) fit.

Four classes of molecules were separated: (i) immobile molecules, with $0 < L < 0.14\,\mu\mathrm{m}$; (ii) small-confined molecules, with $0.14 \leq L < 0.25\,\mu\mathrm{m}$; (iii) large-confined molecules, with $0.25 \leq L \leq 1\,\mu\mathrm{m}$; and (iv) freely diffusing molecules, with $L > 1\,\mu\mathrm{m}$. The sorting procedure is summarized in Figure 5.8. It should be noted that it was sometimes very difficult to decide if a molecule was immobile or confined inside a small domain by visual inspection. This is reflected by the large overlap of the population of immobile molecules and of small-confined molecules (Figure 5.6*C*). The different fractions of the molecules classified according to these criteria are illustrated in Figure 5.7.

9 % of Cy5-labelled ACP - OR17-40 are immobile. 12 % are freely diffusing in the cell membrane. 30 % diffuse inside small domains of $195 \pm 10\,\mathrm{nm}$, while 49 % diffuse inside larger domains of $390 \pm 40\,\mathrm{nm}$. The movements of the odorant receptor inside these compartments are random. The molecules stayed usually confined inside one domain during the whole observation time and hopping from one compartment to another was very rarely seen.

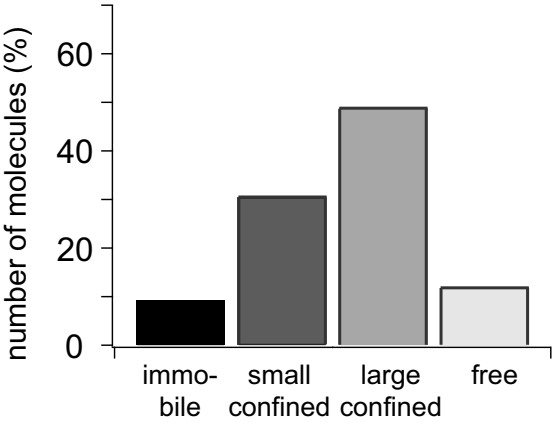

Figure 5.7: Classification of the receptor trajectories into four diffusion modes. *The OR trajectories were separated in four classes according to the value of the apparent domain size* L *calculated from their MSD(t_{lag}) fit with Equation 5.2: (i) the immobile fraction corresponds to* $L < 0.14\,\mu m$*; (ii) the small-confined fraction corresponds to* $0.14 \leq L < 0.25\,\mu m$*; (iii) the large-confined fraction corresponds to* $0.25 \leq L \leq 1\,\mu m$*; and (iv) the free Brownian fraction corresponds to* $L > 1\,\mu m$*.*

Cumulative probability distribution analysis — The analysis using the cumulative probability distribution allows the distinction between one or two subpopulations of molecules in an ensemble. To determine whether the four classes of receptors that were separated contained sub-classes, and also to determine if they are really Brownian, confined or anomalous, cumulative probability distribution functions (PDFs) were calculated for each time lag within one class and fitted either mono- or double-exponentially (Equations 5.5, 5.6). The PDFs of the immobile, small-confined, and large-confined molecules were better fitted with a mono-exponential function, indicating that each of these classes represented only one population. In contrast, the freely diffusing molecules could be separated into two subpopulations diffusing in a Brownian mode (Figure 5.9): 70 $\pm$ 16 % of the freely diffusing receptors diffused fast, with a diffusion coefficient $D_{\text{fast}} = 0.019 \pm 0.002\,\mu\text{m}^2/s$, whereas the second fraction diffused more slowly, with $D_{\text{slow}} = 0.0019 \pm 0.0004\,\mu\text{m}^2/s$ (Figure 5.10, *A-C*).

The MSD(t_{lag}) curves derived from the mono-exponential fit of the PDF for the immobile, small-confined, and large-confined molecules, could be fitted with Equation 5.2, that describes confined motion, yielding the diffusion coefficients and the domain sizes listed in Table 5.1. However, the small-confined fraction could be described as well by the model for anomalous diffusion, with an anomalous coefficient $\alpha = 0.141 \pm 0.003$, suggesting that the apparent confinement could

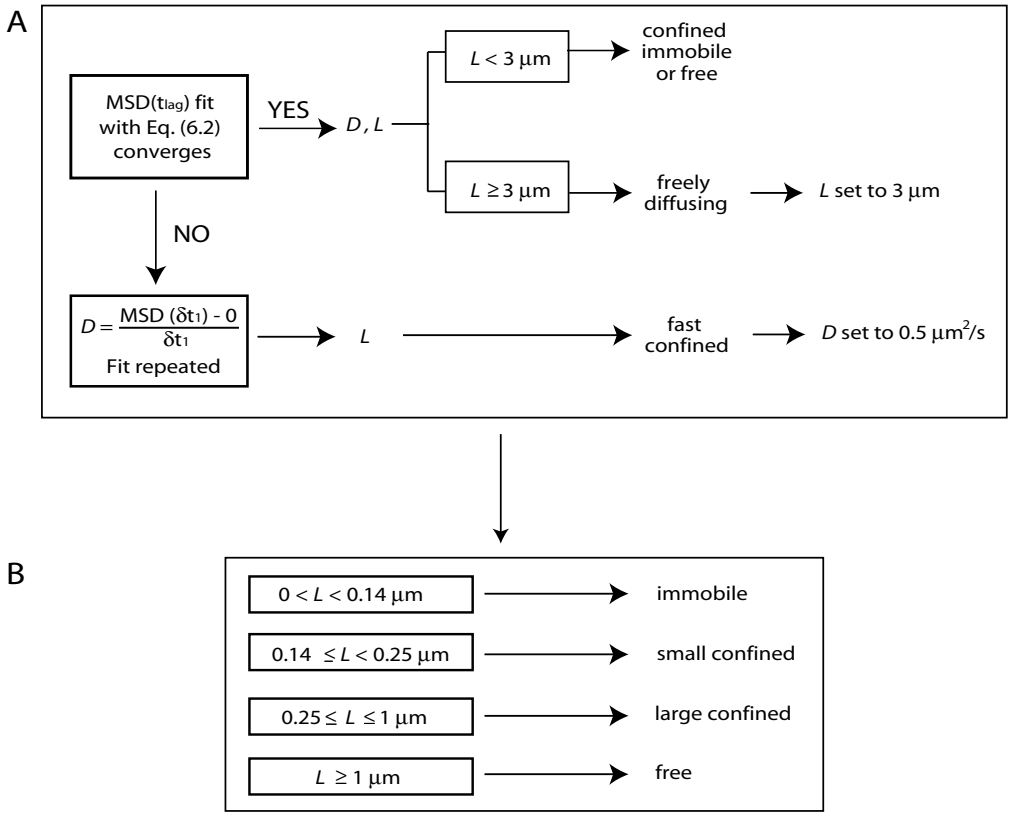

Figure 5.8: Procedure used for sorting the OR trajectories. *(*A*)* D *and* L *were determined from the MSD(t_{lag}) fits. (*B*) The trajectories were classified according to* L*.*

result from protein-protein interactions.

The very small diffusion coefficient calculated for the immobile fraction confirms that these molecules are indeed immobile. Moreover, the domain sizes for the small-confined and large-confined fractions are similar to the ones determined by fitting the individual MSD(t_{lag}) curves. The cumulative probability distribution analysis confirms then the results obtained by the analysis of the individual trajectories.

	D (μm$^2/s$)	L (μm/s)
large-confined	0.0066 ± 0.0006	0.36 ± 0.02
small-confined	0.0082 ± 0.0002	0.195 ± 0.002
immobile	0.000132 ± 0.000008	0.136 ± 0.012

Table 5.1: Diffusion coefficients and confinement sizes for the large-confined, small-confined, and immobile receptors.

The plasma membrane of HEK293 cells thus exhibits two types of compart-

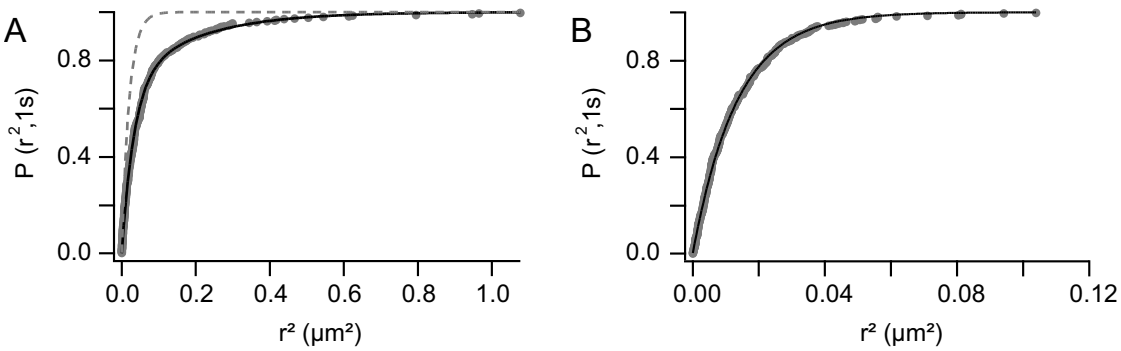

Figure 5.9: Cumulative distribution function of the freely diffusing and small-confined OR17-40 receptors. *(*A*) The P(r², 1s) of the free fraction is well described with Equation 5.6 (solid line), indicating that the freely diffusing receptors can be sub-divided into two populations. In contrast, the fit with Equation 5.5 was not successful (broken line). (*B*) The P(r², 1s) of the small-confined fraction can be described with a mono-exponential function (Equation 5.5), indicating that this fraction represents only one population.*

mentalization: a first one of size $L = 195 \pm 10$ nm and a second one of size $L = 390 \pm 40$ nm. Similar domain sizes have been found for the confinement of the neurokinin NK2 receptor in HEK293 cells [163]: The NK2R was shown to diffuse inside domains of radius = 420 ± 80 nm in absence of ligand, and inside domains of radius = 170 ± 50 nm when bound to neurokinin A (NKA). The larger domains could either arise from the presence of a membrane-skeleton/cytoskeleton fence structure [148,165,166] or from long-range protein interactions [153], whereas the smaller domains are likely to correspond to precursors of clathrin-coated pits [42, 163]. Indeed, as discussed in Chapter 4, OR17-40 is constitutively internalizing when expressed in HEK293 cells. Co-localization of the receptor with the transferrin receptor, a marker of clathrin-coated pits, as well as disruption of receptor endocytosis by hypertonic sucrose indicated that this internalization occurred along the clathrin-dependent pathway. Several GPCRs, such as the β_2-adrenergic receptor [167] or the thyrotropin-releasing hormone receptor [168], have been shown to accumulate in previously formed clathrin-coated domains upon activation, rather than nucleating new coated pits, as was previously believed. It is also believed that the receptors are targeted inside pre-pits that are still flat and which invaginate following clathrin polymerization [169]. Cezanne *et al.* estimated that, since clathrin-coated pits have a radius of 75-100 nm, the radius of the corresponding flat domains should measure between 150 and 200 nm [163], which corresponds to the small domains of confinement found for OR17-40.

The receptors belonging to the immobile fraction are probably in course of

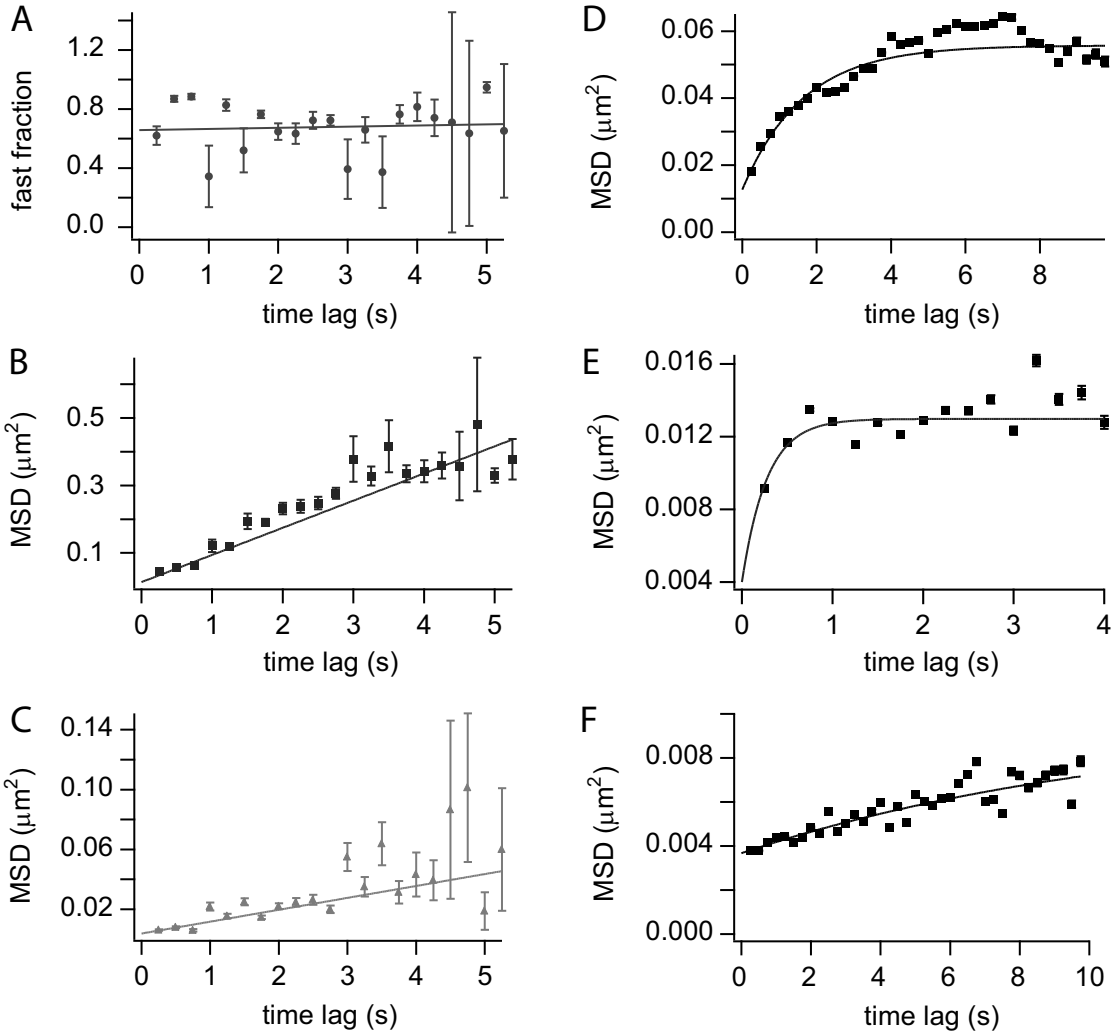

Figure 5.10: Cumulative probability distribution analysis. *(*A-C*) The freely diffusing receptors could be separated into two subpopulations diffusing in a Brownian mode: A fraction of 0.70 ± 0.16 diffused fast (*A*), with a diffusion coefficient* $D_{fast} = 0.019 \pm 0.002\,\mu m^2/s$ *(*B*). The second fraction was diffusing more slowly, with* $D_{slow} = 0.0019 \pm 0.0004\,\mu m^2/s$ *(*C*). (*D*) The large-confined fraction of receptors diffused with* $D = 0.0066 \pm 0.0006\,\mu m^2/s$ *inside a domain of size* $L = 0.36 \pm 0.02\,\mu m$*. (*E*) The small-confined fraction diffused with* $D = 0.0082 \pm 0.0002\,\mu m^2/s$ *inside a domain of size* $L = 0.195 \pm 0.002\,\mu m$*. (*F*) The immobile molecules diffused very slowly (*$D = 0.000132 \pm 0.000008\,\mu m^2/s$*) inside a very small domain (*$L = 0.136 \pm 0.012\,\mu m$*).*

internalization, which is very slow at the experimental temperature [170]. Indeed, receptors located inside clathrin-coated pits are thought to be tightly packed and immobile [148], and, since the formation of coated pits repeatedly occurs at definite sites of the plasma membrane, coated pits themselves are believed to be attached to the membrane skeleton [171]. Moreover, immobile and small-confined molecules often photobleached in a multi-step manner, as shown in Figure 5.11, indicating that several receptors were located very closely one to another, below the resolution limit. These receptors are probably located inside clathrin-coated pits, waiting for internalization.

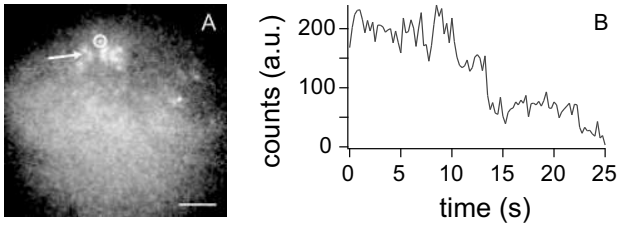

Figure 5.11: Multistep photobleaching. *(*A*) Fluorescence image of Cy5-labelled ORs stably expressed in HEK293 cells. In the region indicated by the arrow, the receptors are organized in clusters. Scale bar indicates 5 μm. (*B*) Fluorescence intensity recorded inside the marked ring in image* A*. Multi-step photobleaching indicates that several receptors are located inside this ring.*

It should be noted that during the examination of individual trajectories, we did not observe any molecule undergoing directed motion, for example towards the clathrin-coated pits. This suggests that the receptors are trapped at the coated pits following random diffusion, and are not targeted towards the pits by lipid flow or by transport by the cytoskeleton [148].

5.3.2 Lateral Diffusion of ACP - OR17-40 with Bound Agonist or Antagonist

To investigate the effect of ligand binding on the lateral diffusion of OR17-40, measurements were performed after addition of 200 μM helional (agonist) or 300 μM α-methyl-cinnamaldehyde (antagonist, see Chapter 6). As a control, the diffusion of Cy5-labelled ACP - OR17-40 was also monitored after addition of 300 μM piperonal, a compound structurally similar to the agonist (Figure 5.12*E*) but that does not bind to the receptor. The trajectories of about 130 molecules for each condition were evaluated. Analysis was performed in the same manner as for the unliganded receptor.

The log-log plots of D versus L for all three compounds and the histograms for the microscopic diffusion coefficients and for the apparent domain sizes are shown in Figure 5.12.

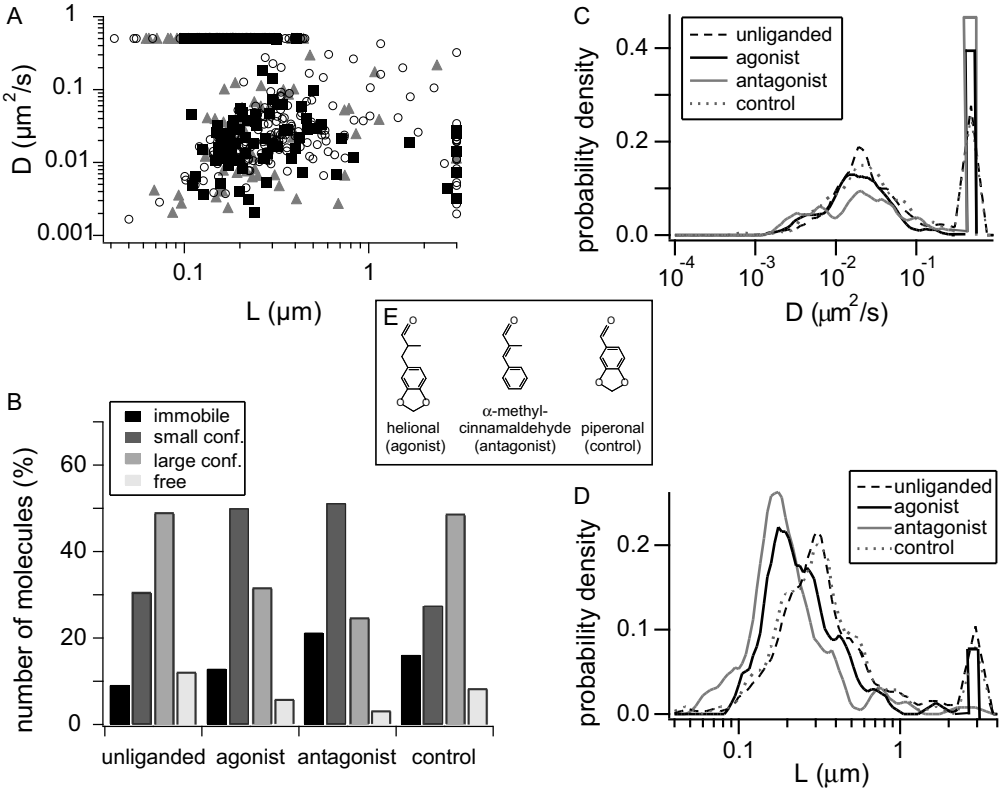

Figure 5.12: Mobility analysis of liganded ORs. *(*A*) Log-log plot of the diffusion coefficient* D *against the apparent domain size* L *for the unliganded receptor (open circles), the receptor bound to an agonist (full squares), and the receptor bound to an antagonist (full triangles). (*B*) Classification of the trajectories into four diffusion modes, according to the domain size determined from their MSD(t_{lag}) fit, for the different conditions. (*C *and* D*) Distribution of the diffusion coefficient* D *(*C*) and of the apparent domain size* L *(*D*). (*E*) Chemical structures of the agonist helional, the antagonist α-methyl-cinnamaldehyde, and the control substance piperonal.*

Although the distribution of the diffusion coefficients after addition of helional, α-methyl-cinnamaldehyde or piperonal does not differ greatly from the one obtained for the unliganded receptor (Figure 5.12*C*), the distribution of the domain sizes changes significantly depending on the added compound. As shown in Figure 5.12*B*, the fraction of small-confined molecules increases from 30 % to 50 % upon agonist addition and to 51 % in presence of the antagonist, whereas the fraction of large-confined molecules decreases from 49 % to 31 % for the agonist

and to 24 % for the antagonist. These two fractions stay constant upon addition of the control substance piperonal (28 % for the small-confined fraction and 48 % for the large-confined fraction). The sizes of the two types of compartments are listed in Table 5.2.

	L_{small} (nm)	L_{large} (nm)
no ligand	195 ± 10	390 ± 40
agonist	190 ± 5	370 ± 40
antagonist	190 ± 5	400 ± 60
control	195 ± 10	420 ± 40

Table 5.2: Domain sizes for the liganded and unliganded receptor. *Data are means ± 95 % confidence interval of the small and large compartment sizes determined from the fit of the MSD(t_{lag}) curves.*

If we consider that the small domains of confinement correspond to precursors of clathrin-coated pits, the fact that the small-confined fraction increases upon agonist binding is expected, as activated receptors are recruited to clathrin-coated pits and subsequently internalized. A similar restriction of receptor diffusion was found for the NK1R [172] and the NK2R [163] after the addition of an agonist. Why this also occurs upon antagonist addition is not clear. The increase in the small-confined fraction is due to specific ligand binding, as the control substance piperonal does not alter the diffusional behavior of the receptor. An antagonist causing internalization was also found for the cholecystokinin receptor [173]. It was postulated that the conformational change in the receptor induced by or stabilized by the antagonist results in the unveiling of a domain that could promote receptor internalization [173]. Similarly, our results suggest that the presence of a ligand inside the receptor binding pocket is sufficient to promote the targeting of the receptor to precursors of clathrin-coated pits, even without receptor activation. We can thus postulate that both agonists and antagonists modulate the continuous recycling of the odorant receptor.

5.3.3 Lateral Diffusion of ACP - OR17-40 in Hypertonic Sucrose

In order to block the constitutive endocytosis of the receptor, cells stably expressing ACP - OR17-40 and $G_{\alpha q}$ were incubated in D-PBS containing 0.45 M sucrose for 10 to 15 min prior to and during labelling with CoA-Cy5. The diffusion of the Cy5-labelled receptors was monitored in 0.45 M sucrose. As shown in Figure 5.13, hypertonic sucrose was found to induce an immobilization of the receptors:

The immobile fraction increased to 30 % and the small-confined fraction to 50 %, whereas the large-confined fraction decreased to 17 %. The immobilization was reversed upon sucrose removal. The sizes of the two types of compartments are listed in Table 5.3.

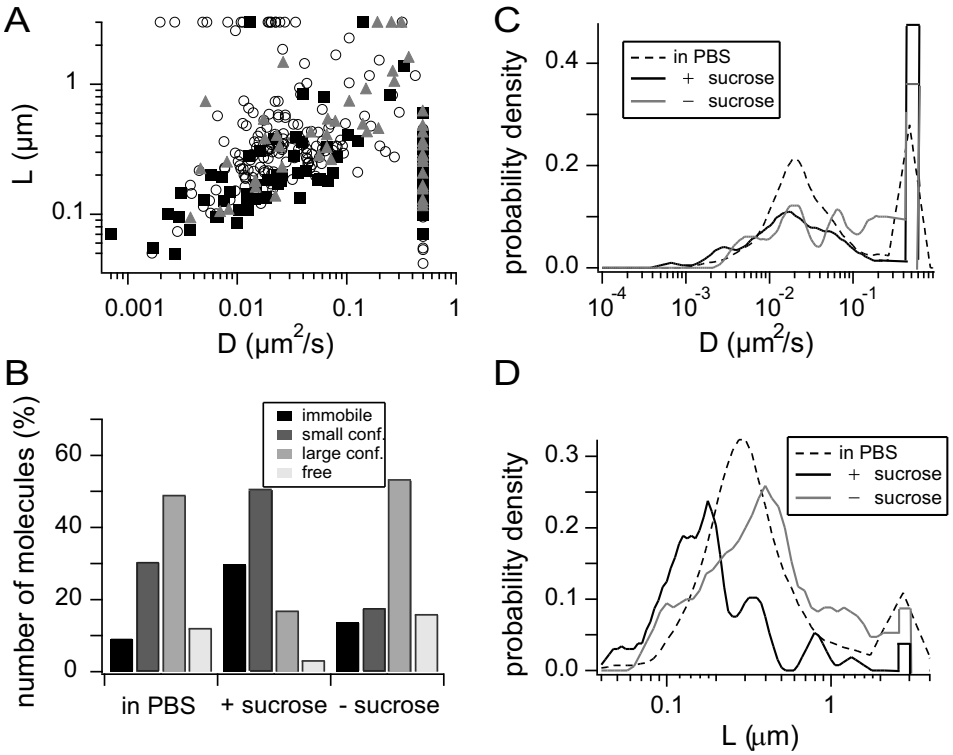

Figure 5.13: OR mobility analysis when the constitutive internalization is blocked. *(*A*) Log-log plot of the diffusion coefficient* D *against the apparent domain size* L *for the receptor when the cells are in PBS (open circles), when the cells are incubated in 0.45 M sucrose (closed squares), and after sucrose removal (closed triangles). (*B*) Classification of the trajectories into four diffusion modes, according to the domain size determined from their MSD(t_{lag}) fit, for the different conditions. (*C *and* D*) Distribution of the diffusion coefficient* D *(*C*) and of the apparent domain size* L *(*D*).*

	L_{small} (nm)	L_{large} (nm)
in PBS	195 ± 10	390 ± 40
in 0.45 M sucrose	180 ± 10	440 ± 100
after sucrose removal	185 ± 20	440 ± 70

Table 5.3: Domain sizes for the receptor in PBS and in hypertonic sucrose. *Data are means ± 95 % confidence interval of the small and large compartment sizes determined from the fit of the MSD(t_{lag}) curves.*

As already discussed, ORs are probably targeted to flat precursors of clathrin-coated pits [163, 169]. Since clathrin polymerization is blocked by hypertonic sucrose, the pre-pits do not invaginate and the receptors do not internalize. It is likely that, in order to maintain a constant cell surface receptor density, the recycling of the receptors from the endosomes is diminished. There would then be a higher density of receptors immobilized inside precursors of clathrin-coated pits than of free receptors. Furthermore, as hypertonic sucrose induces shrinkage of the cells, it is possible that the interactions with the cytoskeleton are tightened, thus accounting for the increased immobilization of the receptor.

5.4 Conclusions and Outlook

In conclusion, we monitored the lateral diffusion of the human odorant receptor OR17-40 in HEK293 cell membranes. While few (12 %) receptors were undergoing normal Brownian diffusion, the movements of most ORs were confined inside two types of domains. A first type of compartment, of size $L = 390 \pm 40\,\text{nm}$, seems to arise from the presence of the membrane-skeleton/cytoskeleton fence structure or from long-range inter-protein interactions, while the smaller compartments ($L = 195 \pm 10\,\text{nm}$) are likely to be precursors of clathrin-coated pits [163].

In agreement with the fact that OR17-40 receptors undergo constitutive endocytosis, as discussed in Chapter 4, 30 % of the unliganded receptors belong to the small-confined fraction. This fraction increases upon addition of both an agonist (51 %) or an antagonist (50 %), whereas the large-confined fraction decreases (49 % to 31 % for the agonist and to 24 % for the antagonist), suggesting that the binding of a ligand can promote the targeting of the odorant receptor to clathrin-coated pre-pits, even without activating the receptor.

Hypertonic sucrose, which blocks the constitutive endocytosis of the receptor, also induces an increase in the small-confined fraction, probably by modifying the equilibrium between the receptors inside clathrin-coated pre-pits and the free receptors. Moreover, the fraction of immobile receptors increases. This immobilization might arise from anchoring of the receptors by clathrin and/or by the actin cytoskeleton [163, 171]. This could be addressed in future experiments by using fluorescent clathrin [171] or by modulating actin dynamics by the over-expression of actin-binding proteins [163].

Chapter 6

Characterization of an Extended Ligand Repertoire of OR17-40 using Calcium Imaging

6.1 Introduction

The chemical interaction of volatile molecules with odorant receptors is the primary step in odor perception and is a central focus of current research activities for unravelling the molecular basis of olfaction, its selectivity, and sensitivity. The pairing of odorant receptors with their ligands, so far achieved for only a limited number of receptors, pointed to either a broad tuning or a high OR selectivity for few or single odorants [74, 75, 79, 174, 175].

In this chapter, we analyzed odorant structure-response relationships on OR17-40, which has been shown to respond to one single compound (helional) out of a mixture of 100 odorants, but not to a closely related molecule (piperonal) [75], and investigated molecular determinants critical for the recognition of the ligand by OR17-40. In order to test a collection of chemically modified derivatives of helional for their ability to activate the receptor, a large-scale functional assay allowing efficient screenings of compounds was developed. This assay is based on the optical detection of intracellular calcium release upon odorant stimulation, which can be achieved by stably expressing the human odorant receptor OR17-40 in HEK293 cells together with the promiscuous G protein $G_{\alpha q}$.

Based on the observation that cells with high OR expression levels have a low cell surface targeting, and that the carboxy-terminal fusion of OR17-40 to the enhanced green fluorescent protein (EGFP) retains full receptor activity, we then explored the use of fluorescence-activated cell sorting (FACS) for the

separation of low OR17-40 - GFP expressing cells, resulting in the enrichment of cells exhibiting OR surface expression and an improved efficiency of OR-mediated calcium signalling.

6.2 Experimental Procedures

6.2.1 Materials

Cytochalasin B was from Sigma (Buchs, CH); 1-palmitoyl-2-oleoyl-sn-glycero-3-(phosphor-rac-(1-glycerol)) (POPG) was from Avanti Polar Lipids (Alabaster, Al, USA); N-(fluorescein-5-thiocarbamoyl)-1,2-dihexadecanoyl-sn-glycero-3-phosphoethanolamine, triethylammonium salt (fluorescein DHPE) was from Molecular Probes (Eugene, OR, USA).

Odorants were kindly provided by Dr C. Margot (Firmenich SA, Geneva, CH).

6.2.2 Flow Cytometry and Sterile Cell Sorting

Cell samples were diluted in DMEM to concentrations between 1-5x10^6 cells per ml. Flow cytometry was performed using a Becton Dickinson FACS Vantage sorter (excitation: 488 nm / emission: 525 nm). Gates were set to exclude cellular debris and to sort cells in two defined fractions of high and low GFP fluorescence intensities. Analysis was performed using the Cell Quest program from BD Sciences. Collected cells were resuspended in DMEM containing 10 % FCS, puromycin (20 μg/ml) and hygromycin (200 μg/ml), and antibiotics selection was continued for 1 to 4 weeks in 25 cm^2 culture flasks in a 37 ^{o}C/5 % CO_2 incubator.

6.2.3 Receptor Quantification

Cell surface concentrations of odorant receptors were estimated by GFP fluorescence intensity measurements on native vesicles derived from the plasma membrane of cells expressing OR17-40 - GFP. Native vesicles were produced by incubating the cells with 10 μg/ml cytochalasin B for 10 to 15 min at 37 ^{o}C. Cell bodies were separated from native vesicles by centrifugation at 500 rpm for 5 min. Vesicles were collected at 2,000 rpm for 20 min and resuspended in 1 ml PBS. The GFP fluorescence intensity (excitation: 488 nm / emission: 510 nm) was measured on selected plasma membrane regions of the vesicles using the Zeiss LSM510 software, and compared with those of unilamellar vesicles comprising a defined amount of fluorescein-labelled lipids. The lipid mixture was composed of

1-palmitoyl-2-oleoyl-sn-glycero-3- (phosphor-rac-(1-glycerol)) (POPG) mixed with 0.05-5 per mille N-(fluorescein-5-thiocarbamoyl)-1,2-dihexadecanoyl-sn-glycero-3-phosphoethanolamine, triethylammonium salt (fluorescein DHPE).

Cell culture, transfection and stable cell lines selection, as well as immunocytochemistry and Ca^{2+} - FLEX assay were performed as described in Chapter 2.

6.3 Results and Discussion

6.3.1 Functional Expression of an OR17-40 - GFP Fusion Construct

The insertion of odorant receptors in the plasma membrane is important for their proper configuration and biological function. We monitored the subcellular localization of OR17-40 in two ways. First, EGFP fused at the receptor C-terminus allowed the subcellular detection of all intracellular and plasma membrane receptors; second, the N-terminal fusion of a *c-myc* epitope provided a tool to selectively visualize OR17-40 receptors on the cell surface (Figure 6.1*B*). As already discussed in Chapters 3 and 4, the receptor translocation to the cell membrane was better in faint green cells, reflecting a lower OR expression level. Furthermore, mainly these weak fluorescent cells evoked helional-mediated calcium responses, as monitored by *in situ* calcium imaging using laser-scanning confocal microscopy.

To quantitatively compare the activation of the two receptor proteins by different ligands, HEK293 cell lines stably expressing either the wild-type OR17-40 or the carboxy-terminal fusion of OR17-40 to EGFP were established by antibiotic selection for 6 to 8 weeks. The stable co-expression of $G_{\alpha q}$ allowed the functional coupling of OR17-40 activation to the inositol 1,4,5-triphosphate (IP_3) pathway, resulting in the opening of intracellular Ca^{2+} ion stores, which can be detected by monitoring the fluorescence intensity of calcium-sensitive indicator dyes. The selection of cell lines stably expressing both the odorant receptor and the G protein allowed for efficient functional screenings in microtiter plates using the high-throughput FLEXstation instrument.

The activation of OR17-40 - GFP by its cognate ligand was first confirmed by the obtention of helional dose-dependent calcium responses. The resulting EC_{50} value of $114.4 \pm 8.6\,\mu$M was comparable to that determined on the wild-type receptor ($98.7 \pm 4.7\,\mu$M) (Figure 6.1*C*), indicating that the human odorant receptor OR17-40 fused to GFP retained its full activity.

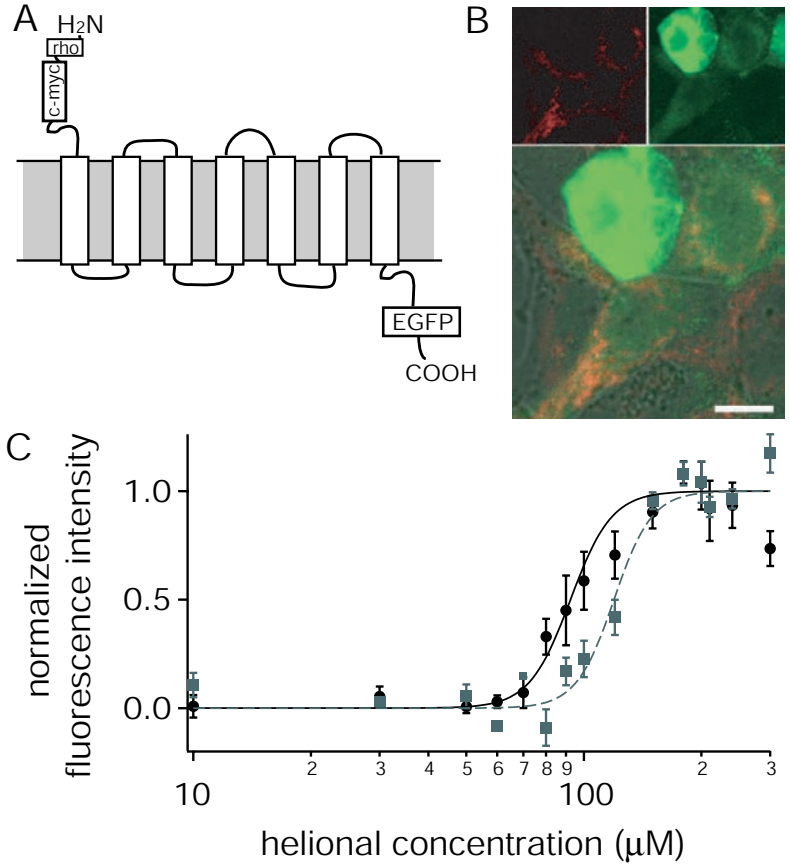

Figure 6.1: Subcellular localization and functional characterization of OR17-40 fused to EGFP. *(*A*) Schematic view of the membrane topology of OR17-40 - GFP showing the position of the inserted EGFP at the C-terminus and of the* c-myc *epitope at the N-terminus, after the rhodopsin membrane import sequence. (*B*) Multi-channel confocal micrograph of a representative HEK293 cell population transiently expressing c-Myc-OR17-40-EGFP labelled with the monoclonal anti-c-myc, Cy3 conjugate antibody. Upper right-hand image (Ex. 488 nm / Em. 505-530 nm) shows cell-to-cell differences of c-Myc-OR17-40-EGFP fluorescence intensities. Upper left-hand image (Ex. 543 nm / Em 560 nm) shows the immuno-localization of Cy3-labelled c-Myc-OR17-40-EGFP in plasma membranes. Lower image shows an overlay of the green, red, and transmission channel indicating that weakly expressing cells (low EGFP fluorescence intensities) exhibit a better translocation of c-Myc-OR17-40-EGFP to the cell surface than strongly expressing cells, as reflected by higher Cy3 fluorescence signals on plasma membranes. Scale bar is 10 µm. (*C*) Concentration-response relation of helional on Ca^{2+} release in HEK293 cells stably expressing OR17-40 and $G_{\alpha q}$ (circles, solid line) or OR17-40 - GFP and $G_{\alpha q}$ (squares, broken line). Data, normalized to the highest response, are means ± S.E. of at least 3 independent FLEXstation experiments.*

6.3.2 Determination of an Extended Ligand Repertoire of OR17-40

Based on the high ligand selectivity of OR17-40 [75], we were interested in analyzing molecular features of helional essential for its recognition by the receptor. In committing this study, we followed two strategies. The first one was based on measurements performed with the HEK293 cell line stably co-expressing the wild-type OR17-40 and $G_{\alpha q}$. The other strategy involved the use of the OR17-40 - GFP fusion construct, which exhibited the same ligand specificity as the wild-type receptor (Table 6.1), but allowed for a more rapid selection of odorant-responsive cells based on fluorescence-activated cell sorting as described below. We tested odorant compounds structurally related to helional for their ability to elicit intracellular calcium responses (Figure 6.2). Seven out of 23 tested compounds activated OR17-40 in a dose-dependent manner. Among these odorants, lilial was the most potent one. We found that agonists lacking a molecular group in the para position on the aromatic ring, such as α-methyl-hydrocinnamaldehyde, methyl-phenyl-pentanal, and trifernal, were less effective (Table 6.1). None of the tested odorants evoked non-specific calcium responses on control cells expressing only the $G_{\alpha q}$ protein without the receptor.

Our results suggest that the aldehyde group of the ligand is essential, as its replacement by other chemical groups (alcohol, acetate, ketone, etc.) yielded odorant molecules that did not bind to the receptor. Furthermore, the length of the carbon chain between the aldehyde and the aromatic ring is of importance, since piperonal and vanillin, which have a shorter carbon chain, failed to induce a calcium response. Removing the methyl group also impaired receptor activation, as shown for hydrocinnamaldehyde and bourgeonal. However, shifting it from the α to the β position on the carbon chain (methyl-phenylpentanal, trifernal) was tolerated. The insertion of a double bond in the case of α-methyl-cinnamaldehyde effectively decreased the ability of the ligand to activate the receptor. Analogous findings on the human testicular receptor OR17-4 [176] revealed inactivation of receptor-specific ligands by introducing additional double bonds in the carbon chain connecting the aldehyde group to an aromatic ring. Finally, the modification of functional groups at the aromatic ring structure did not significantly influence the interaction with OR17-40.

Since previous reports on a number of ORs have demonstrated that slight modifications of activating ligands could give rise to antagonistic effects [175–178], we tested whether the non-activating compounds of our collection had inhibitory properties. We found that pre-incubation of cells expressing OR17-40 with three different odorants (α-methyl-cinnamaldehyde, hydrocinnamaldehyde, and bour-

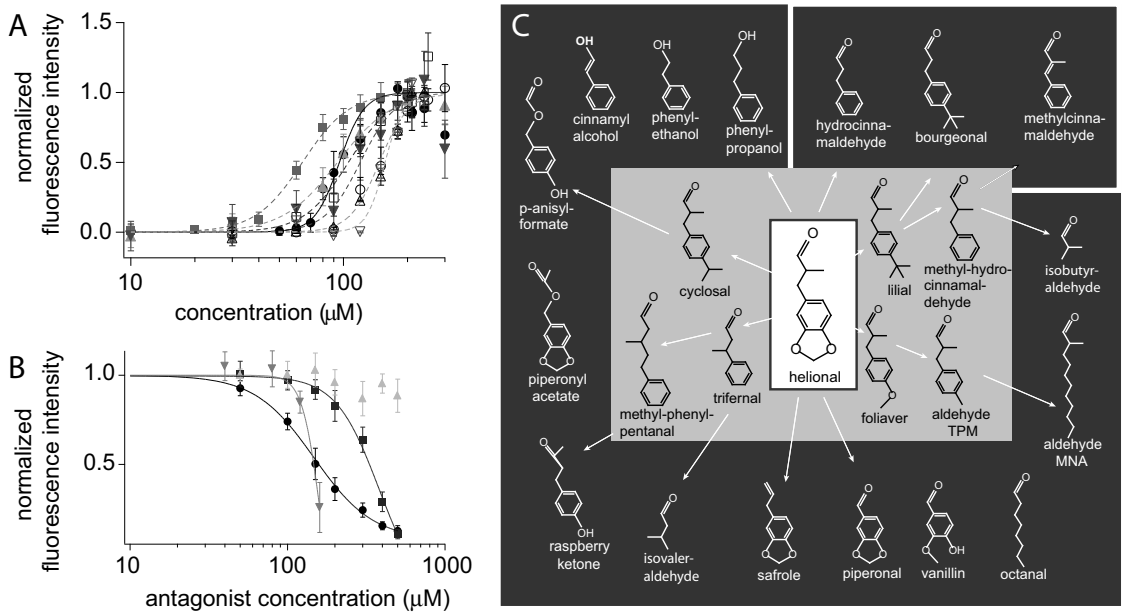

Figure 6.2: Odorant specificity of wild-type OR17-40. *(*A*) Dose-response curves of OR17-40 agonists: helional (closed circles); lilial (closed squares); foliaver (closed triangles); cyclosal (closed inverted triangles); trifernal (open circles); aldehyde TPM (open squares); methyl-phenylpentanal (open triangles); and methylhydrocinnamaldehyde (open inverted triangles). HEK293 cell populations stably expressing OR17-40 and $G_{\alpha q}$ were stimulated with increasing concentrations of the indicated odorants and the fluorescence intensity of a calcium-sensitive indicator dye was measured in a microplate reader. Data, normalized to the highest response for each odorant, are means ± S.E. of at least 3 independent experiments. (*B*) Inhibition of the helional-induced Ca^{2+} ion response by α-methyl-cinnamaldehyde (circles); hydrocinnamaldehyde (squares); and bourgeonal (inverted triangles). Cinnamyl alcohol (triangles) is shown as a control substance. Increasing concentrations of the antagonists were added 100 s prior to the addition of 200 μM helional. At the end of each measurement, ATP (100 μM) was applied to verify cell viability. Data, normalized to the helional response in absence of antagonist, are means ± S.E. of 2 independent experiments. (*C*) Structural comparison of the different substances used in this study. The cognate ligand helional is shown in the middle. The activating substances are depicted in the light grey area and the non-activating ones in the dark grey area. Antagonists are separated by white lines in the upper right-hand corner.*

geonal) blocked the activation of the receptor by helional in a dose-dependent manner (IC_{50}: α-methyl-cinnamaldehyde: $154.7 \pm 17.5\,\mu$M; hydrocinnamaldehyde: $341 \pm 33.2\,\mu$M; bourgeonal: $133.1 \pm 7.3\,\mu$M). The molecular structures of these compounds indicate that removing the methyl group or inserting an additional double bond at the α position of the propanal chain leads to antagonistic effects. All antagonists were tested at concentrations that did not affect the cell viability (for bourgeonal, concentrations higher that $200\,\mu$M were harmful for the cells, since a subsequent stimulation by ATP evoked a reduced or even no intracellular calcium response).

Odorant	OR17-40 [μM]	OR17-40 - GFP [μM]
helional	98.7 ± 4.7	114.4 ± 8.6
lilial	63.9 ± 2.0	124.1 ± 7.1
foliaver	96.7 ± 4.1	145.4 ± 10.1
cyclosal	112.3 ± 16.0	142.9 ± 6.2
aldehyde TPM	113.3 ± 4.2	139.5 ± 3.4
methyl-hydro-cinnamaldehyde	163.2 ± 10.0	168.0 ± 12.3
methyl-phenyl-pentanal	157.0 ± 7.5	158.5 ± 25.8
trifernal	154.6 ± 17.4	120.3 ± 6.6

Table 6.1: Ligand activity profiles for wild-type OR17-40 and for OR17-40 - GFP. *EC_{50} values are means ± S.E. of at least 3 independent experiments.*

6.3.3 Enrichment of Odorant-Responsive Cells

Based on our observation that mainly HEK293 cells with low GFP fluorescence intensities exhibited functionally active OR17-40 - GFP at the plasma membrane which induced sufficiently strong calcium ion signalling amplitudes, we explored the possibility of selecting those cells from a transiently transfected HEK293 cell population.

We used fluorescence-activated cell sorting (FACS) to separate cells expressing OR17-40 - GFP and $G_{\alpha q}$ in two fractions of defined GFP fluorescence intensities (Figure 6.3*A*), which were individually analyzed for their ability to elicit calcium signals in response to helional. Ligand-induced intracellular calcium ion responses were significantly stronger in the cell fraction exhibiting a low GFP fluorescence intensity than in the strong fluorescent one (Figure 6.3*C*). In support of this finding, we obtained in a parallel selection of 20 transfected cell samples only one stable OR17-40 - GFP cell line exhibiting overall low and relatively homogenous GFP fluorescence intensities (Figure 6.3*D*). A flow cytometry analysis

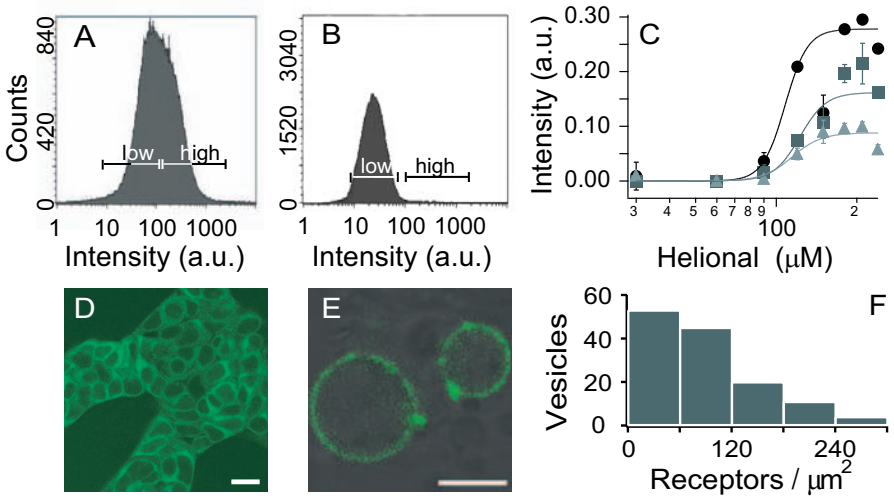

Figure 6.3: Flow cytometry and cell sorting of OR17-40 - GFP. *(*A*) EGFP fluorescence intensity distribution of HEK293 cell populations transiently expressing OR17-40 - GFP and $G_{\alpha q}$. The cells were sorted in two fractions of low and high intensity. (*B*) EGFP fluorescence intensity distribution of a helional-responsive clone stably expressing OR17-40 - GFP and $G_{\alpha q}$. The cells were sorted in two fractions of low and high intensity. (*C*) Concentration-response relation of helional on Ca^{2+} release in the cell fractions sorted in* A *and* B*: cell line stably expressing OR17-40 - GFP (black circles); low fluorescent cell fraction transiently expressing OR17-40 - GFP (grey squares); high fluorescent cell fraction transiently expressing OR17-40 - GFP (light grey triangles). (*D*) Confocal fluorescence micrograph of the low fluorescent cell fraction stably expressing OR17-40 - GFP. Scale bar indicates 20 µm. (*E*) Confocal fluorescence micrograph of native vesicles derived from cells in* D*. Scale bar indicates 2 µm. (*F*) Distribution of OR17-40 - GFP in the membrane of native vesicles. The receptor density was determined by comparing the GFP intensity in the vesicle membranes to the intensity in the membrane of artificial vesicles containing known concentrations of fluorescein.*

of this clone indicated a fluorescence intensity similar to the odorant-responsive fraction derived from transiently transfected cells (Figure 6.3*C*). We conclude that an efficient translocation of OR17-40 to the cell surface and, in turn, a strong odorant-evoked calcium signalling, correlates with defined low levels of intracellular receptor biosynthesis.

We therefore determined the cell surface density of OR17-40 in the low fluorescent cell fraction. For the selective analysis of GFP fluorescence intensity signals in plasma membranes, we produced native vesicles from cells stably expressing OR17-40 - GFP by chemical treatment with cytochalasin B (Figure 6.3*E*). Such

native vesicles were shown to retain the orientation and functionality of surface receptors [179]. By comparison with reference fluorescent lipid membranes of giant unilamellar vesicles, we could estimate a receptor density distribution between 0 (not detectable) and 300 receptors per square micrometer. This maximal value corresponds to roughly 130,000 receptors per cell, considering a HEK293 cell surface of 450 μm^2 [180]. However, the majority of the cells had less than 100 receptors per square micrometer, or less than 45,000 receptors per cell (Figure 6.3*F*).

6.4 Conclusions

A large-scale functional assay based on the optical read-out of odorant responses by calcium imaging was developed. By screening a library comprising 23 chemical derivatives of the cognate ligand helional, we could determine the molecular determinants necessary for OR17-40 binding and/or activation: An aldehyde group connected to an aromatic ring via a carbon chain of 3-5 carbons appears to be essential for binding to the receptor, while a methyl group in α or β position is necessary for its activation. Moreover, an additional double bond within the carbon chain also leads to antagonistic effects.

Since the carboxy-terminal fusion of OR17-40 to EGFP retained its full activity and since low expressing cells exhibit a better plasma membrane localization of the odorant receptor, we used FACS sorting to enrich odorant-responsive cells out of a population with variable OR expression levels. In the separated low fluorescent fraction, calcium responses were obtained in up to 80 % of the cells, which significantly enhanced the signal-to-noise ratio essential for high-throughput measurements in fluorescence plate readers. Compared to classical antibiotic selection procedures, the FACS selection was significantly less time-consuming and allowed for rapid screenings of odorant molecules within 4-6 days after transfection.

Chapter 7

Towards a Chip-Based Screening of Odorant Molecules: Calcium Imaging in Cell-Derived Vesicles

7.1 Introduction

Odorant molecules, which can influence personal behaviors in many respects, like the choice of food, personal hygiene, household products, and fashion, represent a market of large economic impact. Important industrial branches such as perfume producers and food industry are concerned with the production of odorant substances of constant quality, as well as with the development of new odorous compounds. In this context, there is a need for objective and efficient screening of odorant molecules.

As described in Chapter 6, heterologous expression and functional imaging of recombinant ORs in HEK293 cells has been achieved by forcing the receptors to induce an intracellular Ca^{2+} ion release through the over-expression of promiscuous G proteins that couple to the DAG/IP_3 signalling pathway [74, 75, 79, 80]. This strategy of translating OR activation into an optically detectable signal can lead to large-scale functional screenings. However, odorant molecule analysis is complicated by the combinatorial recognition principles of odor coding [66, 181], as one molecule usually leads to the activation of a set of ORs. It is therefore reasonable to test odors on a collection of odorant receptors to discover patterns of activation which can be used as "fingerprints" for a given odorant.

In this chapter, we present a novel strategy allowing a substantial miniaturization of assays for odorant molecule detection, opening new ways for parallel screenings in an array format. We take advantage of micrometer or submicrometer-

sized mammalian cell-derived native vesicles containing ORs in their membrane and molecular components of the signalling cascade in their lumen. Native vesicles have been shown to be the smallest autonomous containers capable of performing cellular signalling reactions under physiological conditions [179]. They can be prepared in large quantities, frozen and stored for weeks without losing their functional integrity, and are thus extremely useful for the investigation of signalling reactions in a parallel format [179].

As a proof of principle, we develop this assay with two ORs, the human helional receptor OR17-40 and the nematode ODR-10 receptor, which specifically responds to diacetyl [68, 69, 80]. Both receptors can be functionally expressed in HEK293 cells and coupled to the phosphoinositol pathway, allowing an optical read-out of receptor activation by calcium imaging [75, 80].

7.2 Experimental Procedures

7.2.1 Materials

ODR-10 cDNA was a kind gift from H. Hatt (Ruhr-Universität, Bochum, D). The Venus variant of GFP was kindly provided by A. Miyawaki (Saitama, Japan) [182]. The pECFP-N1 plasmid was from Clontech (Palo Alto, CA, USA). $G_{\alpha q}$ - CFP was a kind gift from B. Meyer (LCPPM-ISIC, EPFL, CH).

Cytochalasin B was from Sigma (Buchs, CH). FuraRed was from Molecular Probes (Eugene, OR, USA).

Helional was kindly provided by Dr C. Margot (Firmenich SA, Geneva, CH). Diacetyl was purchased at Sigma (Buchs, CH).

7.2.2 Fluorescence Labelling of Odorant Receptors with Spectrally Distinguishable GFP Variants

pOR17-40 - YFP was obtained by replacing the GFP coding sequence of pEAK8:: OR17-40 - GFP by YFP. The YFP coding sequence was first amplified from Venus by PCR using the following primers: YFP-fo: `5'- CGC GGA TCC ATG GTG AGC AAG GGC GAG GAG CTG -3'`; YFP-rev: `5'- CGC GAT CGA TGC GGC CGC TTA CTT GTA CAG CTC GTC CAT GCC -3'`; and the resulting 750 bp *Bam*HI - *Not*I fragment was subcloned into pBS::OR17-40 - GFP (see Chapter 3) digested with *Bam*HI and *Not*I. OR17-40 - YFP was cut out with *Eco*RV and *Not*I and subcloned into pEAK8.

Cloning of the ODR-10 - CFP fusion construct was obtained by the following strategy: For a better plasma membrane localization, the 20 first amino acids of

the bovine rhodopsin [74] followed by a *Nde*I site were added at the N-terminus of ODR-10 by PCR using the following primers: ODR-10-fo: `5'- TCT GAT ATC GC ACC ATG AAC GGG ACC GAG GGC CCA AAC TTC TAC GTG CCT TTC TCC AAC AAG ACG GGC GTG GTG CAT ATG TCG GGA GAA TTG TGG ATT ACC CTA GTT GAC ACA GCG G -3'`; ODR-10-rev: `5'- CGC GAT CGA TGC GGC CGC TCA CGT CGG AAC TT G AGA CAA ATT GGC -3'`; and the resulting 1.1 kb *Eco*RV - *Not*I fragment was subcloned both into the cloning vector pBluescript II KS+ and into the mammalian expression vector pEAK8, yielding pBS::ODR-10 and pEAK8::ODR-10. The stop codon of ODR-10 was replaced by a *Bam*HI site using site-directed mutagenesis on pBS::ODR-10. CFP was amplified by PCR from pECFP-N1 using the following primers: CFP-fo: `5'- CGC GGA TCC ATG GTG AGC AAG GGC GAG GAG CTG -3'`; CFP-rev: `5'- CGC GAT CGA TGC GGC CGC TTA CTT GTA CAG CTC GTC CAT GCC -3'`; and the resulting 750 bp *Bam*HI - *Not*I fragment was subcloned into pBS::ODR-10. ODR-10 - CFP was cut out with *Eco*RV and *Not*I and subcloned into pEAK8.

All plasmids were verified by restriction analysis and DNA sequencing.

7.2.3 Single-Cell Calcium Imaging

HEK293 cells exponentially growing in 6-well plates were transfected with pOR17-40 - YFP or pODR-10 - CFP together with $pG_{\alpha q}$ DNA using the calcium phosphate precipitation method [76]. Twenty-four hours after transfection, cells expressing the blue or the yellow receptor construct were shortly trypsinized, mixed in the same tube, centrifuged for 4 min at 1,200 rpm, resuspended in DMEM containing 2.2 % FCS, and seeded on 25 mm glass cover slides placed in 6-well plates. After incubation for 24 h at 37 °C in a humidified 5 % CO_2 atmosphere, cells were loaded with 5 μM FuraRed-AM in serum-free DMEM for 30 min at 37 °C. The dye loading medium was then exchanged against DMEM containing 10 % FCS and the cells were placed in the incubator for another 30 min in order to allow for cleavage of the ester. Odorant-mediated calcium ion responses were recorded using laser-scanning confocal microscopy. Detection and distinction of YFP and CFP, and of the FuraRed dye, was achieved by appropriate filter sets (see Chapter 2) using a multitracking mode.

7.2.4 Native Vesicle Production

Native vesicles were produced from cells stably expressing the OR17-40 - GFP fusion construct together with $G_{\alpha q}$ by a 10-20 min incubation at 37 °C with cytochalasin B (10 μg/ml). Cells were first separated from vesicles by centrifugation

at 500 rpm for 5 min in an Eppendorf centrifuge. Vesicles were then collected by centrifugation at 2000 rpm for 20 min and resuspended in D-PBS.

7.2.5 Calcium Imaging of Odor Responses in Native Vesicles

Cells were loaded at 37 ^{o}C for 30 min with 5 μM FuraRed-AM in serum-free DMEM and were then washed and incubated in DMEM containing 10 % FCS for 30 min. Subsequently, cells were treated with cytochalasin B as described above.

Vesicles containing FuraRed were transferred to 8-well chambered coverglass slides pre-coated with 0.1 mg/l poly-L-Lysine to ensure electrostatic binding of the vesicles to the glass surface, and were investigated by confocal fluorescence microscopy. The excitation was at 488 nm (Ar+ laser); 505-530 nm band-pass or 560 nm long pass filters were used to image the GFP-tagged receptor or FuraRed, respectively. Individual responses to 100 μM helional were recorded for 120 s.

7.3 Results and Discussion

7.3.1 Functionality of the Fluorescent Odorant Receptors

For the direct visualization and optical discrimination of two different odorant receptors inside living cells, and, subsequently, to be able to address odorant-mediated responses in vesicles to specific receptors, we genetically fused Venus to the human OR17-40, and CFP to the nematode ODR-10. Figure 7.1 shows that the two receptors can be distinguished in mixed cell cultures of OR17-40 - YFP and ODR10 - CFP expressing cells. Ligand-specific receptor activation was observed by laser-scanning confocal microscopy. Helional specifically activated OR17-40 - expressing cells and diacetyl ODR-10 - expressing cells, indicating the functional expression of these receptors. Cells highly expressing any of the two receptor constructs did not respond upon addition of the odorants, probably because of an inefficient membrane trafficking of the receptors, as already discussed in Chapters 4 and 6.

7.3.2 Receptor and G Proteins are Present in Native Vesicles

Native vesicles derived from the plasma membrane of cells expressing OR17-40 fused to GFP were tested for their ability to be activated by the OR17-40-specific agonist helional. As shown in Figure 7.2*A*, vesicles produced using cytochalasin

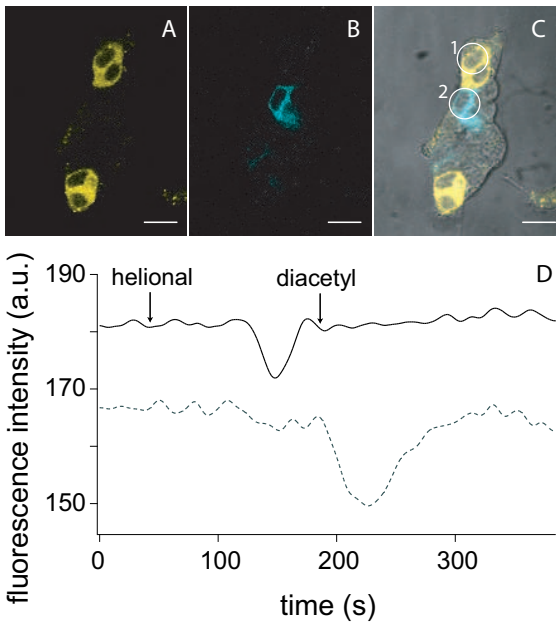

Figure 7.1: Ligand-specific activation of two differently labelled odorant receptors. *(*A *and* B*) Confocal fluorescence micrographs of HEK293 cells transiently expressing OR17-40 - YFP (*A*) or ODR-10 - CFP (*B*) together with* $G_{\alpha q}$*. (*C*) Transmission image of the same area with the fluorescence micrographs* A *and* B *superimposed. Scale bar indicates 20* μ*m. (*D*) Simultaneous recordings in response to helional (100* μ*M) and diacetyl (100* μ*M) measured by laser-scanning confocal microscopy using FuraRed as a calcium indicator dye. The OR17-40 - YFP fusion construct (solid line, response corresponding to cell #1 on image* C*) responds specifically to helional and the ODR-10 - CFP fusion construct (dashed line, response corresponding to cell #2 on image* C*) specifically to diacetyl. Arrows indicate the time points of odorant stimulation.*

B contained the receptor in the vesicle membrane. To allow the detection of odorant receptor activation by calcium signalling, it is necessary that the native vesicles contain G proteins and the other molecular components of the transduction cascade. The presence of G proteins in native vesicles could be confirmed by treating cells expressing $G_{\alpha q}$ - CFP with cytochalasin B (Figure 7.2*B*).

7.3.3 Odorant-Induced Calcium Signalling in Native Vesicles

Native vesicles were prepared from HEK293 cells transiently or stably expressing OR17-40 - GFP together with the promiscuous $G_{\alpha q}$ protein. The number of native vesicles containing the odorant receptor was rather low (5 to 10 %) when vesicles

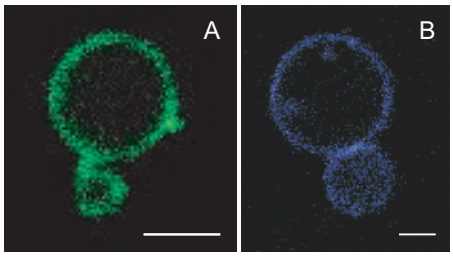

Figure 7.2: Localization of the odorant receptor and of the G protein in native vesicles. *Fluorescence confocal micrographs showing OR17-40 - GFP fusion construct (*A*) and $G_{\alpha q}$ fused to CFP (*B*) inside cell-derived native vesicles. Scale bar indicates 2 µm.*

were prepared from transiently transfected cells. In contrast, when derived from a cell line stably expressing OR17-40 - GFP together with $G_{\alpha q}$ (see Chapter 6), almost all vesicles contained the OR. For this reason, we performed calcium imaging experiments on native vesicles prepared from this stable cell line, which was loaded with FuraRed before treatment with cytochalasin B.

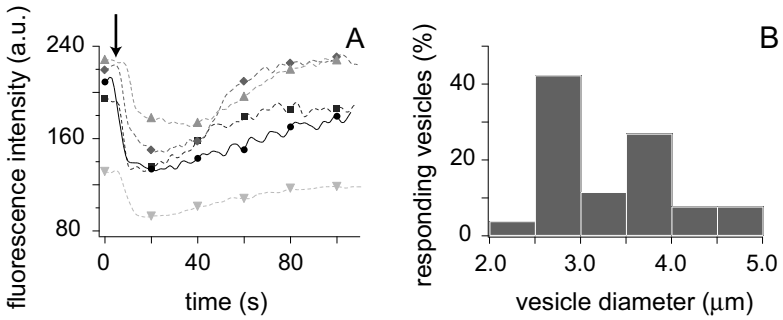

Figure 7.3: Imaging odor responses in cell-derived vesicles. *(*A*) Ligand-induced calcium release inside native vesicles derived from cells stably expressing the OR17-40 - GFP fusion construct together with $G_{\alpha q}$. Vesicles were loaded with the calcium ion indicator dye Fura-Red and stimulated with helional. Changes in fluorescence intensities were recorded for 100 s using laser-scanning confocal microscopy. The addition of 100 µM helional (arrow) induced a transient calcium increase inside vesicles of different diameters: 2.26 µm (circles); 2.76 µm (squares); 2.99 µm (diamonds); 3.57 µm (triangles); and 5.05 µm (inverted triangles). (*B*) Size distribution of the vesicles which responded to 100 µM helional addition.*

Upon helional addition, a transient calcium increase was monitored inside native vesicles (Figure 7.3*A*), indicating that the orientation and functional activity of odorant receptors and of cytosolic proteins were preserved. However, only vesicles of a diameter larger than 2 µm responded upon ligand application (Figure

7.3*B*), probably because the endoplasmic reticulum, which is needed as a cellular ion store, is only present in bigger vesicles. This limitation could be overcome by using the natural olfactory signalling pathway found in OSNs: In these cells, the binding of an odorant molecule to the receptor induces an increase in the intracellular concentration of cAMP, which is mediated by an olfactory-specific G protein subunit, $G_{\alpha olf}$. cAMP binds to cyclic nucleotide-gated (CNG) ion channels, leading to an influx of Na^+ and Ca^{2+} from the outside. In HEK293 cells co-expressing an OR and $G_{\alpha olf}$, ligand binding can induce cAMP signalling [79, 89]. Moreover, calcium imaging allowed the monitoring of odorant-induced Ca^{2+} influx through CNG channels in HeLa cells stably co-expressing an odorant receptor, $G_{\alpha olf}$ and a CNG channel [175]. It should thus be possible to perform calcium imaging on native vesicles derived from HEK293 cells stably co-expressing these three components (an OR, $G_{\alpha olf}$ and the CNG channel). This strategy should allow the monitoring of OR activation in nanometer-sized vesicles.

7.4 Conclusions and Outlook

Native vesicles were produced from HEK293 cells co-expressing OR17-40 - GFP and the G protein $G_{\alpha q}$. The OR, as well as the other components of the signal transduction machinery were present inside vesicles in their correct configuration. We provided evidence for the localization of a fluorescently labelled $G_{\alpha q}$ at the inner side of the vesicle membrane.

As a proof of principle, we could show that native vesicles are capable of responding to exogenously added odorant compounds by transient calcium signalling, thus allowing the miniaturization of functional assays for the screening of odorant molecules in small volumes. Monitoring odorant receptor activation in native vesicles represents an important finding which opens new ways for assay miniaturization and the development of micro-arrays for the screening of odorant molecules: Collections of native vesicles representing large libraries of different odorant receptors can be modified by proper tags at the vesicle surface (biotin, polyhistidine, oligonucleotides, lectins, antigens, etc.) provided by labelled lipids [183, 184] or proteins [98, 100, 185] and enabling the formation of microarrays of vesicles by self-assembly on complementary micropatterned sensor surfaces [186, 187].

As a first step towards such parallel screenings, we have labelled two OR subtypes, the human helional receptor OR17-40 and the nematode diacetyl receptor ODR-10 with spectrally distinguishable GFP variants, and demonstrated that these fusion proteins retained full receptor activity. We propose the fluorescent labelling of the ORs in order to address odorant-mediated simultaneous responses

in vesicles to a specific OR subtype. This strategy allows screenings on different ORs. It is however obvious that labelling with available GFP variants will deliver only a limited set of optically distinguishable ORs. Post-translational *in vivo* labelling methods, where a fluorescent label is covalently or non-covalently attached to a fusion tag or fusion protein [97–102], should increase the diversity and allow the specific and distinguishable labelling of a set of 10-20 OR subtypes. Such a collection might already be sufficient to obtain reliable "fingerprints" of calcium signalling profiles for a specific odorant molecule.

Chapter 8

Summary and Outlook

The discovery fourteen years ago of a multigene family encoding odorant receptors [1] provided a molecular basis for initiating studies on the sensitivity and selectivity of these receptors, and on biochemical processes involved in olfaction. However, due to the great difficulty of functionally expressing odorant receptors in the plasma membrane of heterologous cells, only little progress has so far been achieved in matching odorant molecules to specific receptors and in establishing efficient screenings of large compound collections.

In order to analyze the problem of inefficient OR surface expression in more detail, we focused on the sequential stages in the life cycle of the human odorant receptor OR17-40, analyzing its intracellular biosynthesis, its membrane trafficking, and its internalization back into the cytoplasm. For this purpose, OR17-40 was modified by different tags, which enabled the direct visualization of the receptor expression and subcellular localization in living cells. Using multi-color labelling of OR17-40 and subcellular markers, we could show that high receptor expression led to the accumulation of the receptor in the endoplasmic reticulum of HEK293 cells, probably because of receptor self-aggregation caused by over-expression. Co-expression of various accessory proteins did not enhance its cell surface expression. The use of a double-tagged receptor construct, which allowed the discrimination of membrane-inserted receptors from the whole population of translated receptors, revealed that the translocation of the receptor to the plasma membrane was better in low expressing cells.

The selective labelling of membrane-inserted receptors and their observation by confocal microscopy in real time interestingly revealed the constitutive internalization of OR17-40 in HEK293 cells. Co-localization of the receptor with the transferrin receptor, a marker of clathrin-coated pits, as well as disruption of receptor endocytosis by hypertonic sucrose indicated that the internalization process

occurred along the clathrin-dependent pathway. Moreover, the level of receptor endocytosis was not influenced by agonist or antagonist binding, suggesting that activation and internalization of OR17-40 are two independent processes.

In agreement with this finding, we could show that, in absence of ligand, $\sim$ 30 % of the cell surface receptors were confined inside small domains of 195 ± 10 nm, which probably correspond to precursors of clathrin-coated pits. While 12 % of the receptors seemed to diffuse freely in the plasma membrane, 49 % were diffusing within domains of 390 ± 40 nm. This fraction decreased and the proportion of receptors confined inside the smaller domains increased upon binding of an agonist or an antagonist, suggesting that both can direct OR17-40 towards clathrin-coated pre-pits, even without receptor activation.

In order to analyze the structural properties of odorant molecules essential for OR17-40 binding and/or activation, we developed an efficient functional assay based on the optical read-out of odorant responses by calcium imaging. By testing a collection of chemical derivatives of the cognate ligand helional, we could determine that an aldehyde group connected to an aromatic ring via a carbon chain of 3-5 carbons seems essential for binding to the receptor, while a methyl group in α or β position appears to be necessary for its activation. Moreover, the addition of a double bond in the carbon side chain leads to antagonistic effects.

As a first step towards more efficient odorant screenings, we developed a miniaturized assay based on cell-derived native vesicles containing different odorant receptors. By labelling with spectral variants of GFP, we could demonstrate that native vesicles contained the OR in their membrane, and the molecular components necessary for a functional response in their lumen. Furthermore, native vesicles containing OR17-40 fused to GFP together with the G protein $G_{\alpha q}$ responded to helional by a transient calcium increase, indicating the preservation of functional activity of the receptor. The micro- or sub-micrometer size of native vesicles makes them suitable for assays in micro-array format, allowing the parallel and simultaneous screening of many odorant receptors, and yielding a specific pattern of activation which could be used as a fingerprint for a given odor molecule.

Glossary

ACP	Acyl carrier protein
AcpS	Phosphopantetheine transferase from *E. coli*
AOB	Accessory olfactory bulb
ATP	Adenosine triphosphate
β_2-AR	β_2-adrenergic receptor
βARK-1, βARK-1	β-adrenergic receptor kinase 1, 2
βarr1, βarr2	β-arrestin 1, 2
Ca^{2+}	Calcium ion
cAMP	Cyclic adenosine monophosphate
cDNA	Coding DNA
C. elegans	*Caenorhabditis elegans*
CHO cells	Chinese hamster ovary cells
CNG channel	Cyclic nucleotide-gated channel
CoA	Co-enzyme A
C-terminus	Carboxy-terminus
DAG	Diacylglycerol
DMEM	Dulbecco's modified Eagle medium
DNA	Desoxyribonucleotide acid
D-PBS	Dulbecco's phosphate buffered saline
E. coli	*Escherichia coli*
ECFP	Enhanced cyan fluorescent protein
EGFP	Enhanced green fluorescent protein
ER	Endoplasmic reticulum
EYFP	Enhanced yellow fluorescent protein
FACS	Fluorescence-activated cell sorting
FCS	Fetal calf serum
FRAP	Fluorescence recovery after photobleaching
GABA	Gamma aminobutyric acid

GDP	Guanosine diphosphate
GFP	Green fluorescent protein
GPCR	G protein-coupled receptor
GPI	Glycosylphosphatidylinositol
G protein	Heterotrimeric GTP-binding protein
GRK	G protein-coupled receptor kinase
GTP	Guanosine triphosphate
HEK293 cells	Human embryonic kidney cells
IP_3	Inositol triphosphate
MOB	Main olfactory bulb
MOE	Main olfactory epithelium
MSD	Mean square displacement
NK1R	Neurokinin 1 receptor
NK2R	Neurokinin 2 receptor
N-terminus	Amino-terminus
OBP	Odorant binding protein
OR	Odorant receptor
ORF	Open reading frame
ORK	Olfactory receptor kinase
OSN	Olfactory sensory neuron
PBS	Phosphate buffered saline
PCR	Polymerase chain reaction
PDF	Probability distribution function
PKA	Protein kinase A
PKC	Protein kinase C
PLC_β	Phospholipase C type β
PPTase	Phosphopantetheine transferase
REEP1	Receptor expression enhancing protein 1
RGS	Regulator of G-protein signalling
RNA	Ribonucleotide acid
rpm	Round per minute
RTP1, RTP2	Receptor transporting protein 1, 2
SD	Standard deviation
SE	Standard error
SMM	Single-molecules microscopy
SMS	Single-molecule spectroscopy
SPT	Single-particle tracking
T1R, T2R, T3R	Taste 1,2,3 receptor
Tf	Transferrin
TfR	Transferrin receptor

Mathematical Symbols

D	Diffusion coefficient
D_{micro}	Microscopic diffusion coefficient
L	Domain length
r^2	Square displacement
t_{lag}	Time lag
EC_{50}	Molar concentration of an agonist that produces 50 % of the maximal possible effect of that agonist
IC_{50}	Molar concentration of an antagonist required for 50 % inhibition of the response evoked by an agonist

Bibliography

[1] L. Buck and R. Axel. A novel multigene family may encode odorant receptors: A molecular basis for odor recognition. *Cell*, 65(1):175–87, 1991.

[2] L. B. Buck. Unraveling the sense of smell (Nobel lecture). *Angew Chem Int Ed Engl*, 44(38):6128–6140, 2005.

[3] H. Breer. Olfactory receptors: Molecular basis for recognition and discrimination of odors. *Anal Bioanal Chem*, 2003.

[4] P. Mombaerts. Genes and ligands for odorant, vomeronasal and taste receptors. *Nat Rev Neurosci*, 5(4):263–78, 2004.

[5] R. Axel. Scents and sensibility: A molecular logic of olfactory perception (Nobel lecture). *Angew Chem Int Ed Engl*, 44(38):6110–6127, 2005.

[6] P. Mombaerts. Seven-transmembrane proteins as odorant and chemosensory receptors. *Science*, 286(5440):707–11, 1999.

[7] S. Firestein. How the olfactory system makes sense of scents. *Nature*, 413(6852):211–8., 2001.

[8] P. Mombaerts. Molecular biology of odorant receptors in vertebrates. *Annu Rev Neurosci*, 22:487–509, 1999.

[9] G. V. Ronnett and C. Moon. G proteins and olfactory signal transduction. *Annu Rev Physiol*, 64:189–222, 2002.

[10] D. R. Kornack and P. Rakic. The generation, migration, and differentiation of olfactory neurons in the adult primate brain. *Proc Natl Acad Sci U S A*, 98(8):4752–7, 2001.

[11] P. Feinstein, T. Bozza, I. Rodriguez, A. Vassalli, and P. Mombaerts. Axon guidance of mouse olfactory sensory neurons by odorant receptors and the β_2-adrenergic receptor. *Cell*, 117(6):833–46, 2004.

[12] R. Vassar, S. K. Chao, R. Sitcheran, J. M. Nunez, L. B. Vosshall, and R. Axel. Topographic organization of sensory projections to the olfactory bulb. *Cell*, 79(6):981–91, 1994.

[13] S. Zozulya, F. Echeverri, and T. Nguyen. The human olfactory receptor repertoire. *Genome Biol*, 2(6), 2001.

[14] P. Mombaerts. How smell develops. *Nat Neurosci*, 4 Supp 1:1192–1198, 2001.

[15] B. K. Rana, T. Shiina, and P. A. Insel. Genetic variations and polymorphisms of G protein-coupled receptors: Functional and therapeutic implications. *Annu Rev Pharmacol Toxicol*, 41:593–624, 2001.

[16] B. K. Kobilka, T. S. Kobilka, K. Daniel, J. W. Regan, M. G. Caron, and R. J. Lefkowitz. Chimeric α_2-, β_2-adrenergic receptors: Delineation of domains involved in effector coupling and ligand binding specificity. *Science*, 240(4857):1310–6, 1988.

[17] K. Palczewski, T. Kumasaka, T. Hori, C. A. Behnke, H. Motoshima, B. A. Fox, I. Le Trong, D. C. Teller, T. Okada, R. E. Stenkamp, M. Yamamoto, and M. Miyano. Crystal structure of rhodopsin: A G protein-coupled receptor. *Science*, 289(5480):739–45, 2000.

[18] Y. Pilpel and D. Lancet. The variable and conserved interfaces of modeled olfactory receptor proteins. *Protein Sci*, 8(5):969–77, 1999.

[19] E. Hermans. Biochemical and pharmacological control of the multiplicity of coupling at G-protein-coupled receptors. *Pharmacol Ther*, 99(1):25–44, 2003.

[20] S. A. Chasse and H. G. Dohlman. RGS proteins: G protein-coupled receptors meet their match. *Assay Drug Dev Technol*, 1(2):357–64, 2003.

[21] T. Kozasa. Regulation of G protein-mediated signal transduction by RGS proteins. *Life Sci*, 68(19-20):2309–17, 2001.

[22] R. J. Lefkowitz, S. Cotecchia, P. Samama, and T. Costa. Constitutive activity of receptors coupled to guanine nucleotide regulatory proteins. *Trends Pharmacol Sci*, 14(8):303–7, 1993.

[23] J. M. Herz, W. J. Thomsen, and G. G. Yarbrough. Molecular approaches to receptors as targets for drug discovery. *J Recept Signal Transduct Res*, 17(5):671–776, 1997.

[24] W. F. Simonds. G protein regulation of adenylate cyclase. *Trends Pharmacol Sci*, 20(2):66–73, 1999.

[25] M. J. Clark and J. R. Traynor. Assays for G-protein-coupled receptor signaling using RGS-insensitive G_α subunits. Methods in Enzymology. pages 155–169. Academic Press, volume 389 edition, 2004.

[26] V. J. Watts. Molecular mechanisms for heterologous sensitization of adenylate cyclase. *J Pharmacol Exp Ther*, 302(1):1–7, 2002.

[27] P. C. Sternweis and A. V. Smrcka. Regulation of phospholipase C by G proteins. *Trends Biochem Sci*, 17(12):502–6, 1992.

[28] D. Schild and D. Restrepo. Transduction mechanisms in vertebrate olfactory receptor cells. *Physiol Rev*, 78(2):429–66, 1998.

[29] S. Firestein, B. Darrow, and G. M. Shepherd. Activation of the sensory current in salamander olfactory receptor neurons depends on a G protein-mediated cAMP second messenger system. *Neuron*, 6(5):825–35, 1991.

[30] L. J. Brunet, G. H. Gold, and J. Ngai. General anosmia caused by a targeted disruption of the mouse olfactory cyclic nucleotide-gated cation channel. *Neuron*, 17(4):681–93, 1996.

[31] L. Belluscio, G. H. Gold, A. Nemes, and R. Axel. Mice deficient in G_{olf} are anosmic. *Neuron*, 20(1):69–81, 1998.

[32] S. T. Wong, K. Trinh, B. Hacker, G. C. Chan, G. Lowe, A. Gaggar, Z. Xia, G. H. Gold, and D. R. Storm. Disruption of the type III adenylyl cyclase gene leads to peripheral and behavioral anosmia in transgenic mice. *Neuron*, 27(3):487–97, 2000.

[33] K. Touhara. Odor discrimination by G protein-coupled olfactory receptors. *Microsc Res Tech*, 58(3):135–41, 2002.

[34] B. W. Ache and A. Zhainazarov. Dual second-messenger pathways in olfactory transduction. *Curr Opin Neurobiol*, 5(4):461–6, 1995.

[35] I. Boekhoff, W. C. Michel, H. Breer, and B. W. Ache. Single odors differentially stimulate dual second messenger pathways in lobster olfactory receptor cells. *J Neurosci*, 14(5 Pt 2):3304–9, 1994.

[36] D. A. Fadool and B. W. Ache. Plasma membrane inositol 1,4,5-trisphosphate-activated channels mediate signal transduction in lobster olfactory receptor neurons. *Neuron*, 9(5):907–18, 1992.

[37] J. Krieger, M. Mameli, and H. Breer. Elements of the olfactory signaling pathways in insect antennae. *Invert Neurosci*, 3(2-3):137–44, 1997.

[38] A. Sorkin and M. von Zastrow. Signal transduction and endocytosis: Close encounters of many kinds. *Nature Reviews Molecular Cell Biology Nat Rev Mol Cell Biol*, 3(8):600–614, 2002.

[39] S. S. Ferguson. Evolving concepts in G protein-coupled receptor endocytosis: The role in receptor desensitization and signaling. *Pharmacol Rev*, 53(1):1–24, 2001.

[40] P. Tsao, T. Cao, and M. von Zastrow. Role of endocytosis in mediating down-regulation of G-protein-coupled receptors. *Trends Pharmacol Sci*, 22(2):91–6, 2001.

[41] M. von Zastrow. Role of endocytosis in signalling and regulation of G-protein-coupled receptors. *Biochem Soc Trans*, 29(Pt 4):500–4, 2001.

[42] S. A. Mousavi, L. Malerod, T. Berg, and R. Kjeken. Clathrin-dependent endocytosis. *Biochem J*, 377(Pt 1):1–16, 2004.

[43] S. M. Sweitzer and J. E. Hinshaw. Dynamin undergoes a GTP-dependent conformational change causing vesiculation. *Cell*, 93(6):1021–9, 1998.

[44] J. A. Koenig and J. M. Edwardson. Endocytosis and recycling of G protein-coupled receptors. *Trends Pharmacol Sci*, 18(8):276–87, 1997.

[45] R. H. Oakley, S. A. Laporte, J. A. Holt, M. G. Caron, and L. S. Barak. Differential affinities of visual arrestin, β-arrestin1, and β-arrestin2 for G protein-coupled receptors delineate two major classes of receptors. *J Biol Chem*, 275(22):17201–10, 2000.

[46] R. H. Oakley, S. A. Laporte, J. A. Holt, L. S. Barak, and M. G. Caron. Association of β-arrestin with G protein-coupled receptors during clathrin-mediated endocytosis dictates the profile of receptor resensitization. *J Biol Chem*, 274(45):32248–57, 1999.

[47] J. Zhang, S. S. Ferguson, L. S. Barak, L. Menard, and M. G. Caron. Dynamin and β-arrestin reveal distinct mechanisms for G protein-coupled receptor internalization. *J Biol Chem*, 271(31):18302–5, 1996.

[48] A. G. Roseberry and M. M. Hosey. Internalization of the M2 muscarinic acetylcholine receptor proceeds through an atypical pathway in HEK293 cells that is independent of clathrin and caveolae. *J Cell Sci*, 114(Pt 4):739–46, 2001.

[49] R. G. Vickery and M. von Zastrow. Distinct dynamin-dependent and -independent mechanisms target structurally homologous dopamine receptors to different endocytic membranes. *J Cell Biol*, 144(1):31–43, 1999.

[50] B. J. Nichols and J. Lippincott-Schwartz. Endocytosis without clathrin coats. *Trends Cell Biol*, 11(10):406–12, 2001.

[51] N. F. Neel, E. Schutyser, J. Sai, G. H. Fan, and A. Richmond. Chemokine receptor internalization and intracellular trafficking. *Cytokine Growth Factor Rev*, 2005.

[52] C. Le Roy and J. L. Wrana. Clathrin- and non-clathrin-mediated endocytic regulation of cell signalling. *Nat Rev Mol Cell Biol*, 6(2):112–26, 2005.

[53] W. F. de Weerd and L. M. Leeb-Lundberg. Bradykinin sequesters B2 bradykinin receptors and the receptor-coupled G_α subunits $G_{\alpha q}$ and $G_{\alpha i}$ in caveolae in DDT1 MF-2 smooth muscle cells. *J Biol Chem*, 272(28):17858–66, 1997.

[54] O. Feron, T. W. Smith, T. Michel, and R. A. Kelly. Dynamic targeting of the agonist-stimulated M2 muscarinic acetylcholine receptor to caveolae in cardiac myocytes. *J Biol Chem*, 272(28):17744–8, 1997.

[55] P. C. Leclerc, M. Auger-Messier, P. M. Lanctot, E. Escher, R. Leduc, and G. Guillemette. A polyaromatic caveolin-binding-like motif in the cytoplasmic tail of the type 1 receptor for angiotensin II plays an important role in receptor trafficking and signaling. *Endocrinology*, 143(12):4702–10, 2002.

[56] K. Peppel, I. Boekhoff, P. McDonald, H. Breer, M. G. Caron, and R. J. Lefkowitz. G protein-coupled receptor kinase 3 (GRK3) gene disruption leads to loss of odorant receptor desensitization. *J Biol Chem*, 272(41):25425–8, 1997.

[57] S. Schleicher, I. Boekhoff, J. Arriza, R. J. Lefkowitz, and H. Breer. A β-adrenergic receptor kinase-like enzyme is involved in olfactory signal termination. *Proc Natl Acad Sci U S A*, 90(4):1420–4, 1993.

[58] T. M. Dawson, J. L. Arriza, D. E. Jaworsky, F. F. Borisy, H. Attramadal, R. J. Lefkowitz, and G. V. Ronnett. β-adrenergic receptor kinase-2 and β-arrestin-2 as mediators of odorant-induced desensitization. *Science*, 259(5096):825–9, 1993.

[59] P. Nef, I. Hermans-Borgmeyer, H. Artieres-Pin, L. Beasley, V. E. Dionne, and S. F. Heinemann. Spatial pattern of receptor expression in the olfactory epithelium. *Proc Natl Acad Sci U S A*, 89(19):8948–52, 1992.

[60] J. Strotmann, I. Wanner, J. Krieger, K. Raming, and H. Breer. Expression of odorant receptors in spatially restricted subsets of chemosensory neurones. *Neuroreport*, 3(12):1053–6, 1992.

[61] K. J. Ressler, S. L. Sullivan, and L. B. Buck. A zonal organization of odorant receptor gene expression in the olfactory epithelium. *Cell*, 73(3):597–609, 1993.

[62] R. Vassar, J. Ngai, and R. Axel. Spatial segregation of odorant receptor expression in the mammalian olfactory epithelium. *Cell*, 74(2):309–18, 1993.

[63] N. E. Rawson, J. Eberwine, R. Dotson, J. Jackson, P. Ulrich, and D. Restrepo. Expression of mRNAs encoding for two different olfactory receptors in a subset of olfactory receptor neurons. *J Neurochem*, 75(1):185–95, 2000.

[64] K. J. Ressler, S. L. Sullivan, and L. B. Buck. Information coding in the olfactory system: Evidence for a stereotyped and highly organized epitope map in the olfactory bulb. *Cell*, 79(7):1245–55, 1994.

[65] P. Mombaerts, F. Wang, C. Dulac, S. K. Chao, A. Nemes, M. Mendelsohn, J. Edmondson, and R. Axel. Visualizing an olfactory sensory map. *Cell*, 87(4):675–86, 1996.

[66] B. Malnic, J. Hirono, T. Sato, and L. B. Buck. Combinatorial receptor codes for odors. *Cell*, 96(5):713–23., 1999.

[67] M. Lu, F. Echeverri, and B. D. Moyer. Endoplasmic reticulum retention, degradation, and aggregation of olfactory G-protein coupled receptors. *Traffic*, 4(6):416–33, 2003.

[68] P. Sengupta, J. H. Chou, and C. I. Bargmann. *odr*-10 encodes a seven transmembrane domain olfactory receptor required for responses to the odorant diacetyl. *Cell*, 84(6):899–909., 1996.

[69] Y. Zhang, J. H. Chou, J. Bradley, C. I. Bargmann, and K. Zinn. The *Caenorhabditis elegans* seven-transmembrane protein ODR-10 functions as an odorant receptor in mammalian cells. *Proc Natl Acad Sci U S A*, 94(22):12162–7., 1997.

[70] H. Zhao, L. Ivic, J. M. Otaki, M. Hashimoto, K. Mikoshiba, and S. Firestein. Functional expression of a mammalian odorant receptor. *Science*, 279(5348):237–42, 1998.

[71] R. C. Araneda, A. D. Kini, and S. Firestein. The molecular receptive range of an odorant receptor. *Nat Neurosci*, 3(12):1248–55., 2000.

[72] K. Touhara, S. Sengoku, K. Inaki, A. Tsuboi, J. Hirono, T. Sato, H. Sakano, and T. Haga. Functional identification and reconstitution of an odorant receptor in single olfactory neurons. *Proc Natl Acad Sci U S A*, 96(7):4040–5, 1999.

[73] T. Bozza, P. Feinstein, C. Zheng, and P. Mombaerts. Odorant receptor expression defines functional units in the mouse olfactory system. *J Neurosci*, 22(8):3033–43, 2002.

[74] D. Krautwurst, K. W. Yau, and R. R. Reed. Identification of ligands for olfactory receptors by functional expression of a receptor library. *Cell*, 95(7):917–26., 1998.

[75] C. H. Wetzel, M. Oles, C. Wellerdieck, M. Kuczkowiak, G. Gisselmann, and H. Hatt. Specificity and sensitivity of a human olfactory receptor functionally expressed in human embryonic kidney 293 cells and *Xenopus Laevis* oocytes. *J Neurosci*, 19(17):7426–33., 1999.

[76] M. Jordan, A. Schallhorn, and F. M. Wurm. Transfecting mammalian cells: optimization of critical parameters affecting calcium-phosphate precipitate formation. *Nucleic Acids Res*, 24(4):596–601, 1996.

[77] M. Hansen, S. Boitano, E. R. Dirksen, and M. J. Sanderson. Intercellular calcium signaling induced by extracellular adenosine 5'-triphosphate and mechanical stimulation in airway epithelial cells. *J Cell Sci*, 106 (Pt 4):995–1004, 1993.

[78] G. Vargas and M. T. Lucero. A method for maintaining odor-responsive adult rat olfactory receptor neurons in short-term culture. *Chem Senses*, 24(2):211–6, 1999.

[79] K. Kajiya, K. Inaki, M. Tanaka, T. Haga, H. Kataoka, and K. Touhara. Molecular bases of odor discrimination: Reconstitution of olfactory receptors that recognize overlapping sets of odorants. *J Neurosci*, 21(16):6018–25., 2001.

[80] C. Wellerdieck, M. Oles, L. Pott, S. Korsching, G. Gisselmann, and H. Hatt. Functional expression of odorant receptors of the zebrafish *Danio rerio* and of the nematode *C. elegans* in HEK293 cells. *Chem Senses*, 22(4):467–76., 1997.

[81] J. R. Murrell and D. D. Hunter. An olfactory sensory neuron line, *odora*, properly targets olfactory proteins and responds to odorants. *J Neurosci*, 19(19):8260–70., 1999.

[82] A. A. Gimelbrant, S. L. Haley, and T. S. McClintock. Olfactory receptor trafficking involves conserved regulatory steps. *J Biol Chem*, 276(10):7285–90., 2001.

[83] A. E. Brady and L. E. Limbird. G protein-coupled receptor interacting proteins: Emerging roles in localization and signal transduction. *Cell Signal*, 14(4):297–309, 2002.

[84] P. A. Ferreira, T. A. Nakayama, W. L. Pak, and G. H. Travis. Cyclophilin-related protein RanBP2 acts as chaperone for red/green opsin. *Nature*, 383(6601):637–40, 1996.

[85] L. M. McLatchie, N. J. Fraser, M. J. Main, A. Wise, J. Brown, N. Thompson, R. Solari, M. G. Lee, and S. M. Foord. RAMPs regulate the transport and ligand specificity of the calcitonin-receptor-like receptor. *Nature*, 393(6683):333–9, 1998.

[86] J. Loconto, F. Papes, E. Chang, L. Stowers, E. P. Jones, T. Takada, A. Kumanovics, K. Fischer Lindahl, and C. Dulac. Functional expression of murine V2R pheromone receptors involves selective association with the M10 and M1 families of MHC class Ib molecules. *Cell*, 112(5):607–18, 2003.

[87] M. C. Larsson, A. I. Domingos, W. D. Jones, M. E. Chiappe, H. Amrein, and L. B. Vosshall. Or83b encodes a broadly expressed odorant receptor essential for drosophila olfaction. *Neuron*, 43(5):703–14, 2004.

[88] N. D. Dwyer, E. R. Troemel, P. Sengupta, and C. I. Bargmann. Odorant receptor localization to olfactory cilia is mediated by ODR-4, a novel membrane-associated protein. *Cell*, 93(3):455–66, 1998.

[89] H. Saito, M. Kubota, R. W. Roberts, Q. Chi, and H. Matsunami. RTP family members induce functional expression of mammalian odorant receptors. *Cell*, 119(5):679–91, 2004.

[90] S. Angers, A. Salahpour, and M. Bouvier. Dimerization: an emerging concept for G protein-coupled receptor ontogeny and function. *Annu Rev Pharmacol Toxicol*, 42:409–35, 2002.

[91] S. Bulenger, S. Marullo, and M. Bouvier. Emerging role of homo- and heterodimerization in G-protein-coupled receptor biosynthesis and maturation. *Trends in Pharmacological Sciences*, 26(3):131–137, 2005.

[92] L. F. Agnati, S. Ferre, C. Lluis, R. Franco, and K. Fuxe. Molecular mechanisms and therapeutical implications of intramembrane receptor/receptor interactions among heptahelical receptors with examples from the striatopallidal gaba neurons. *Pharmacol Rev*, 55(3):509–550, 2003.

[93] M. Pfeiffer, S. Kirscht, R. Stumm, T. Koch, D. Wu, M. Laugsch, H. Schroder, V. Hollt, and S. Schulz. Heterodimerization of substance P and μ-opioid receptors regulates receptor trafficking and resensitization. *J Biol Chem*, 278(51):51630–7, 2003.

[94] C. Hague, M. A. Uberti, Z. Chen, C. F. Bush, S. V. Jones, K. J. Ressler, R. A. Hall, and K. P. Minneman. Olfactory receptor surface expression is driven by association with the β_2-adrenergic receptor. *PNAS*, 101(37):13672–13676, 2004.

[95] G. Turcatti, K. Nemeth, M. D. Edgerton, U. Meseth, F. Talabot, M. Peitsch, J. Knowles, H. Vogel, and A. Chollet. Probing the structure and function of the tachykinin neurokinin-2 receptor through biosynthetic incorporation of fluorescent amino acids at specific sites. *J Biol Chem*, 271(33):19991–8, 1996.

[96] R. Y. Tsien. The green fluorescent protein. *Annu Rev Biochem*, 67:509–44, 1998.

[97] B. A. Griffin, S. R. Adams, and R. Y. Tsien. Specific covalent labeling of recombinant protein molecules inside live cells. *Science*, 281(5374):269–72., 1998.

[98] A. Keppler, S. Gendreizig, T. Gronemeyer, H. Pick, H. Vogel, and K. Johnsson. A general method for the covalent labeling of fusion proteins with small molecules in vivo. *Nat Biotechnol*, 21, 2003.

[99] N. George, H. Pick, H. Vogel, N. Johnsson, and K. Johnsson. Specific labeling of cell surface proteins with chemically diverse compounds. *J Am Chem Soc*, 126(29):8896–7, 2004.

[100] E. G. Guignet, R. Hovius, and H. Vogel. Reversible site-selective labeling of membrane proteins in live cells. *Nat Biotechnol*, 22(4):440–4, 2004.

[101] K. M. Marks, P. D. Braun, and G. P. Nolan. A general approach for chemical labeling and rapid, spatially controlled protein inactivation. *Proc Natl Acad Sci U S A*, 101(27):9982–7, 2004.

[102] I. Chen and A. Y. Ting. Site-specific labeling of proteins with small molecules in live cells. *Curr Opin Biotechnol*, 16(1):35–40, 2005.

[103] R. H. Lambalot, A. M. Gehring, R. S. Flugel, P. Zuber, M. LaCelle, M. A. Marahiel, R. Reid, C. Khosla, and C. T. Walsh. A new enzyme superfamily - the phosphopantetheinyl transferases. *Chem Biol*, 3(11):923–36, 1996.

[104] S. Katada, M. Tanaka, and K. Touhara. Structural determinants for membrane trafficking and G protein selectivity of a mouse olfactory receptor. *J Neurochem*, 90(6):1453–63, 2004.

[105] L. Ivic, C. Zhang, X. Zhang, S. O. Yoon, and S. Firestein. Intracellular trafficking of a tagged and functional mammalian olfactory receptor. *J Neurobiol*, 50(1):56–68, 2002.

[106] L. Kallal and J. L. Benovic. Using green fluorescent proteins to study G-protein-coupled receptor localization and trafficking. *Trends Pharmacol Sci*, 21(5):175–80, 2000.

[107] J. Lippincott-Schwartz and C. L. Smith. Insights into secretory and endocytic membrane traffic using green fluorescent protein chimeras. *Curr Opin Neurobiol*, 7(5):631–9, 1997.

[108] Z Fan, Y Lu, X Wu, and J Mendelsohn. Antibody-induced epidermal growth factor receptor dimerization mediates inhibition of autocrine proliferation of A431 squamous carcinoma cells. *J. Biol. Chem.*, 269(44):27595–27602, 1994.

[109] M Spaargaren, LH Defize, J Boonstra, and SW de Laat. Antibody-induced dimerization activates the epidermal growth factor receptor tyrosine kinase. *J. Biol. Chem.*, 266(3):1733–1739, 1991.

[110] C. W. Lehman, J. D. Lee, and C. F. Komives. Ubiquitously expressed GPCR membrane-trafficking orthologs. *Genomics*, 85(3):386–91, 2005.

[111] J. Krieger, S. Schleicher, J. Strotmann, I. Wanner, I. Boekhoff, K. Raming, P. De Geus, and H. Breer. Probing olfactory receptors with sequence-specific antibodies. *Eur J Biochem*, 219(3):829–35, 1994.

[112] H. Koshimoto, K. Katoh, Y. Yoshihara, and K. Mori. Distribution of putative odour receptor proteins in olfactory epithelium. *Neuroreport*, 3(6):521–3, 1992.

[113] K. Schwarzenbacher, J. Fleischer, and H. Breer. Formation and maturation of olfactory cilia monitored by odorant receptor-specific antibodies. *Histochem Cell Biol*, 123(4-5):419–28, 2005.

[114] T. S. McClintock, T. M. Landers, A. A. Gimelbrant, L. Z. Fuller, B. A. Jackson, C. K. Jayawickreme, and M. R. Lerner. Functional expression of olfactory-adrenergic receptor chimeras and intracellular retention of heterologously expressed olfactory receptors. *Brain Res Mol Brain Res*, 48(2):270–8, 1997.

[115] J. E. Heuser and R. G. Anderson. Hypertonic media inhibit receptor-mediated endocytosis by blocking clathrin-coated pit formation. *J Cell Biol*, 108(2):389–400, 1989.

[116] M. S. Singer, G. M. Shepherd, and C. A. Greer. Olfactory receptors guide axons. *Nature*, 377(6544):19–20, 1995.

[117] A. A. Gimelbrant, T. D. Stoss, T. M. Landers, and T. S. McClintock. Truncation releases olfactory receptors from the endoplasmic reticulum of heterologous cells. *J Neurochem*, 72(6):2301–11., 1999.

[118] D. P. Morris, R. R. Price, M. P. Smith, B. Lei, and D. A. Schwinn. Cellular trafficking of human α_{1a}-adrenergic receptors is continuous and primarily agonist-independent. *Mol Pharmacol*, 66(4):843–54, 2004.

[119] A. G. Roseberry and M. M. Hosey. Trafficking of M2 muscarinic acetylcholine receptors. *J Biol Chem*, 274(47):33671–6, 1999.

[120] N. Signoret, J. Oldridge, A. Pelchen-Matthews, P. J. Klasse, T. Tran, L. F. Brass, M. M. Rosenkilde, T. W. Schwartz, W. Holmes, W. Dallas, M. A. Luther, T. N. Wells, J. A. Hoxie, and M. Marsh. Phorbol esters and SDF-1 induce rapid endocytosis and down modulation of the chemokine receptor CXCR4. *J Cell Biol*, 139(3):651–64, 1997.

[121] C. Leterrier, D. Bonnard, D. Carrel, J. Rossier, and Z. Lenkei. Constitutive endocytic cycle of the CB1 cannabinoid receptor. *J Biol Chem*, 279(34):36013–21, 2004.

[122] M. J. Shapiro, J. Trejo, D. Zeng, and S. R. Coughlin. Role of the thrombin receptor's cytoplasmic tail in intracellular trafficking. Distinct determinants for agonist-triggered versus tonic internalization and intracellular localization. *J Biol Chem*, 271(51):32874–80, 1996.

[123] A. Fraile-Ramos, T. N. Kledal, A. Pelchen-Matthews, K. Bowers, T. W. Schwartz, and M. Marsh. The human cytomegalovirus US28 protein is located in endocytic vesicles and undergoes constitutive endocytosis and recycling. *Mol Biol Cell*, 12(6):1737–49, 2001.

[124] E. J. Adie, S. Kalinka, L. Smith, M. J. Francis, A. Marenghi, M. E. Cooper, M. Briggs, N. P. Michael, G. Milligan, and S. Game. A pH-sensitive fluor, CypHer 5, used to monitor agonist-induced G protein-coupled receptor internalization in live cells. *Biotechniques*, 33(5):1152–4, 1156–7, 2002.

[125] M von Zastrow and BK Kobilka. Ligand-regulated internalization and recycling of human β_2- adrenergic receptors between the plasma membrane and endosomes containing transferrin receptors. *J. Biol. Chem.*, 267(5):3530–3538, 1992.

[126] M. Weber, E. Blair, C. V. Simpson, M. O'Hara, P. E. Blackburn, A. Rot, G. J. Graham, and R. J. Nibbs. The chemokine receptor D6 constitutively traffics to and from the cell surface to internalize and degrade chemokines. *Mol Biol Cell*, 15(5):2492–508, 2004.

[127] L. B. Dale, M. Bhattacharya, J. L. Seachrist, P. H. Anborgh, and S. S. Ferguson. Agonist-stimulated and tonic internalization of metabotropic glutamate receptor 1a in human embryonic kidney 293 cells: Agonist-stimulated endocytosis is β-arrestin1 isoform-specific. *Mol Pharmacol*, 60(6):1243–53, 2001.

[128] C. Theriault, M. D. Rochdi, and J. L. Parent. Role of the Rab11-associated intracellular pool of receptors formed by constitutive endocytosis of the β isoform of the thromboxane A2 receptor (TPβ). *Biochemistry*, 43(19):5600–7, 2004.

[129] J. L. Parent, P. Labrecque, M. Driss Rochdi, and J. L. Benovic. Role of the differentially spliced carboxyl terminus in thromboxane A2 receptor trafficking: Identification of a distinct motif for tonic internalization. *J Biol Chem*, 276(10):7079–85, 2001.

[130] V. Segredo, N. T. Burford, J. Lameh, and W. Sadee. A constitutively internalizing and recycling mutant of the μ-opioid receptor. *J Neurochem*, 68(6):2395–404, 1997.

[131] M. Waldhoer, P. Casarosa, M. M. Rosenkilde, M. J. Smit, R. Leurs, J. L. Whistler, and T. W. Schwartz. The carboxyl terminus of human cytomegalovirus-encoded 7 transmembrane receptor US28 camouflages agonism by mediating constitutive endocytosis. *J Biol Chem*, 278(21):19473–82, 2003.

[132] J. L. Whistler, B. O. Gerber, E. C. Meng, T. J. Baranski, M. von Zastrow, and H. R. Bourne. Constitutive activation and endocytosis of the complement factor 5a receptor: Evidence for multiple activated conformations of a G protein-coupled receptor. *Traffic*, 3(12):866–77, 2002.

[133] S. Tsunoda, J. Sierralta, Y. Sun, R. Bodner, E. Suzuki, A. Becker, M. Socolich, and C. S Zuker. A multivalent PDZ-domain protein assembles signalling complexes in a G-protein-coupled cascade. *Nature*, 388(6639):243–249, 1997.

[134] W. R. Burack and A. S. Shaw. Signal transduction: Hanging on a scaffold. *Current Opinion in Cell Biology*, 12(2):211–216, 2000.

[135] R. V. Rebois and T. E. Hebert. Protein complexes involved in heptahelical receptor-mediated signal transduction. *Receptors Channels*, 9(3):169–94, 2003.

[136] R. R. Neubig. Membrane organization in G-protein mechanisms. *Faseb J*, 8(12):939–46, 1994.

[137] R. S. Ostrom, S. R. Post, and P. A. Insel. Stoichiometry and compartmentation in G protein-coupled receptor signaling: Implications for therapeutic interventions involving G_s. *J Pharmacol Exp Ther*, 294(2):407–12, 2000.

[138] S. J. Singer and G. L. Nicolson. The fluid mosaic model of the structure of cell membranes. *Science*, 175(23):720–31, 1972.

[139] K. Jacobson, E. D. Sheets, and R. Simson. Revisiting the fluid mosaic model of membranes. *Science*, 268(5216):1441–2, 1995.

[140] A. Kusumi and Y. Sako. Cell surface organization by the membrane skeleton. *Curr Opin Cell Biol*, 8(4):566–74, 1996.

[141] A. Kusumi, H. Ike, C. Nakada, K. Murase, and T. Fujiwara. Single-molecule tracking of membrane molecules: Plasma membrane compartmentalization and dynamic assembly of raft-philic signaling molecules. *Semin Immunol*, 17(1):3–21, 2005.

[142] J. Hwang, L. A. Gheber, L. Margolis, and M. Edidin. Domains in cell plasma membranes investigated by near-field scanning optical microscopy. *Biophys J*, 74(5):2184–90, 1998.

[143] M. Edidin. Lipid microdomains in cell surface membranes. *Curr Opin Struct Biol*, 7(4):528–32, 1997.

[144] K. Simons and D. Toomre. Lipid rafts and signal transduction. *Nat Rev Mol Cell Biol*, 1(1):31–9, 2000.

[145] K. Simons and W. L. Vaz. Model systems, lipid rafts, and cell membranes. *Annu Rev Biophys Biomol Struct*, 33:269–95, 2004.

[146] P. H. Lommerse, G. A. Blab, L. Cognet, G. S. Harms, B. E. Snaar-Jagalska, H. P. Spaink, and T. Schmidt. Single-molecule imaging of the H-Ras membrane-anchor reveals domains in the cytoplasmic leaflet of the cell membrane. *Biophys J*, 86(1 Pt 1):609–16, 2004.

[147] E. D. Sheets, G. M. Lee, R. Simson, and K. Jacobson. Transient confinement of a glycosylphosphatidylinositol-anchored protein in the plasma membrane. *Biochemistry*, 36(41):12449–58, 1997.

[148] Y. Sako and A. Kusumi. Compartmentalized structure of the plasma membrane for receptor movements as revealed by a nanometer-level motion analysis. *J Cell Biol*, 125(6):1251–64, 1994.

[149] A. Kusumi, Y. Sako, and M. Yamamoto. Confined lateral diffusion of membrane receptors as studied by single particle tracking (nanovid microscopy). Effects of calcium-induced differentiation in cultured epithelial cells. *Biophys J*, 65(5):2021–40, 1993.

[150] S. Mukherjee and F. R. Maxfield. Membrane domains. *Annu Rev Cell Dev Biol*, 20:839–66, 2004.

[151] T. Fujiwara, K. Ritchie, H. Murakoshi, K. Jacobson, and A. Kusumi. Phospholipids undergo hop diffusion in compartmentalized cell membrane. *J Cell Biol*, 157(6):1071–81, 2002.

[152] K. Ritchie, R. Iino, T. Fujiwara, K. Murase, and A. Kusumi. The fence and picket structure of the plasma membrane of live cells as revealed by single molecule techniques (review). *Mol Membr Biol*, 20(1):13–8, 2003.

[153] F. Daumas, N. Destainville, C. Millot, A. Lopez, D. Dean, and L. Salome. Confined diffusion without fences of a G protein-coupled receptor as revealed by single particle tracking. *Biophys J*, 84(1):356–66, 2003.

[154] M. J. Saxton and K. Jacobson. Single-particle tracking: applications to membrane dynamics. *Annu Rev Biophys Biomol Struct*, 26:373–99, 1997.

[155] R. N. Ghosh and W. W. Webb. Automated detection and tracking of individual and clustered cell surface low density lipoprotein receptor molecules. *Biophys J*, 66(5):1301–18, 1994.

[156] G. J. Schutz, H. Schindler, and T. Schmidt. Single-molecule microscopy on model membranes reveals anomalous diffusion. *Biophys J*, 73(2):1073–80, 1997.

[157] H. Geerts, M. de Brabander, and R. Nuydens. Nanovid microscopy. *Nature*, 351(6329):765–6, 1991.

[158] T. Schmidt, G. J. Schutz, W. Baumgartner, H. J. Gruber, and H. Schindler. Imaging of single molecule diffusion. *Proc Natl Acad Sci U S A*, 93(7):2926–9, 1996.

[159] A. Yildiz, J. N. Forkey, S. A. McKinney, T. Ha, Y. E. Goldman, and P. R. Selvin. Myosin V walks hand-over-hand: Single fluorophore imaging with 1.5-nm localization. *Science*, 300(5628):2061–5, 2003.

[160] R. E. Thompson, D. R. Larson, and W. W. Webb. Precise nanometer localization analysis for individual fluorescent probes. *Biophys. J.*, 82(5):2775–2783, 2002.

[161] F. Daumas, N. Destainville, C. Millot, A. Lopez, D. Dean, and L. Salome. Interprotein interactions are responsible for the confined diffusion of a G-protein-coupled receptor at the cell surface. *Biochem Soc Trans*, 31(Pt 5):1001–5, 2003.

[162] L. S. Barak, S. S. Ferguson, J. Zhang, C. Martenson, T. Meyer, and M. G. Caron. Internal trafficking and surface mobility of a functionally intact β_2-adrenergic receptor-green fluorescent protein conjugate. *Mol Pharmacol*, 51(2):177–84, 1997.

[163] L. Cezanne, S. Lecat, B. Lagane, C. Millot, J. Y. Vollmer, H. Matthes, J. L. Galzi, and A. Lopez. Dynamic confinement of NK2 receptors in the plasma membrane. improved FRAP analysis and biological relevance. *J Biol Chem*, 279(43):45057–67, 2004.

[164] R. D. Horvat, D. A. Roess, S. E. Nelson, B. G. Barisas, and C. M. Clay. Binding of agonist but not antagonist leads to fluorescence resonance energy transfer between intrinsically fluorescent gonadotropin-releasing hormone receptors. *Mol Endocrinol*, 15(5):695–703, 2001.

[165] K. Ritchie and A. Kusumi. Role of the membrane skeleton in creation of microdomains. *Subcell Biochem*, 37:233–45, 2004.

[166] K. Suzuki, K. Ritchie, E. Kajikawa, T. Fujiwara, and A. Kusumi. Rapid hop diffusion of a G-protein-coupled receptor in the plasma membrane as revealed by single-molecule techniques. *Biophys J*, 88(5):3659–80, 2005.

[167] F. Santini, I. Gaidarov, and J. H. Keen. G protein-coupled receptor/arrestin3 modulation of the endocytic machinery. *J Cell Biol*, 156(4):665–76, 2002.

[168] M. G. Scott, A. Benmerah, O. Muntaner, and S. Marullo. Recruitment of activated G protein-coupled receptors to pre-existing clathrin-coated pits in living cells. *J Biol Chem*, 277(5):3552–9, 2002.

[169] C. J. Merrifield, M. E. Feldman, L. Wan, and W. Almers. Imaging actin and dynamin recruitment during invagination of single clathrin-coated pits. *Nat Cell Biol*, 4(9):691–8, 2002.

[170] T. T. Cao, R. W. Mays, and M. von Zastrow. Regulated endocytosis of G-protein-coupled receptors by a biochemically and functionally distinct subpopulation of clathrin-coated pits. *J Biol Chem*, 273(38):24592–602, 1998.

[171] I. Gaidarov, F. Santini, R. A. Warren, and J. H. Keen. Spatial control of coated-pit dynamics in living cells. *Nat Cell Biol*, 1(1):1–7, 1999.

[172] Y. Lill, K. L. Martinez, M. A. Lill, B. H. Meyer, H. Vogel, and B. Hecht. Kinetics of the initial steps of G protein-coupled receptor-mediated cellular signaling revealed by single-molecule imaging. *Chemphyschem*, 6(8):1633–40, 2005.

[173] B. F. Roettger, D. Ghanekar, R. Rao, C. Toledo, J. Yingling, D. Pinon, and L. J. Miller. Antagonist-stimulated internalization of the G protein-coupled cholecystokinin receptor. *Mol Pharmacol*, 51(3):357–62, 1997.

[174] I. Gaillard, S. Rouquier, J. P. Pin, P. Mollard, S. Richard, C. Barnabe, J. Demaille, and D. Giorgi. A single olfactory receptor specifically binds a set of odorant molecules. *Eur J Neurosci*, 15(3):409–18, 2002.

[175] E. Shirokova, K. Schmiedeberg, P. Bedner, H. Niessen, K. Willecke, J. D. Raguse, W. Meyerhof, and D. Krautwurst. Identification of specific ligands for orphan olfactory receptors. G protein-dependent agonism and antagonism of odorants. *J Biol Chem*, 280(12):11807–15, 2005.

[176] M. Spehr, G. Gisselmann, A. Poplawski, J. A. Riffell, C. H. Wetzel, R. K. Zimmer, and H. Hatt. Identification of a testicular odorant receptor mediating human sperm chemotaxis. *Science*, 299(5615):2054–2058, 2003.

[177] Y. Oka, A. Nakamura, H. Watanabe, and K. Touhara. An odorant derivative as an antagonist for an olfactory receptor. *Chem Senses*, 29(9):815–22, 2004.

[178] G. Sanz, C. Schlegel, J. C. Pernollet, and L. Briand. Comparison of odorant specificity of two human olfactory receptors from different phylogenetic classes and evidence for antagonism. *Chem Senses*, 30(1):69–80, 2005.

[179] H. Pick, E. L. Schmid, A. P. Tairi, E. Ilegems, R. Hovius, and H. Vogel. Investigating cellular signaling reactions in single attoliter vesicles. *J Am Chem Soc*, 127(9):2908–12, 2005.

[180] H. Pick, A. K. Preuss, M. Mayer, T. Wohland, R. Hovius, and H. Vogel. Monitoring expression and clustering of the ionotropic 5HT3 receptor in plasma membranes of live biological cells. *Biochemistry*, 42(4):877–84, 2003.

[181] H. Hamana, J. Hirono, M. Kizumi, and T. Sato. Sensitivity-dependent hierarchical receptor codes for odors. *Chem Senses*, 28(2):87–104, 2003.

[182] T. Nagai, K. Ibata, E. S. Park, M. Kubota, K. Mikoshiba, and A. Miyawaki. A variant of yellow fluorescent protein with fast and efficient maturation for cell-biological applications. *Nat Biotechnol*, 20(1):87–90, 2002.

[183] C. Yoshina-Ishii and S. G. Boxer. Arrays of mobile tethered vesicles on supported lipid bilayers. *J Am Chem Soc*, 125(13):3696–7, 2003.

[184] F. F. Rossetti, M. Bally, R. Michel, M. Textor, and I. Reviakine. Interactions between titanium dioxide and phosphatidyl serine-containing liposomes: Formation and patterning of supported phospholipid bilayers on the surface of a medically relevant material. *Langmuir*, 21(14):6443–50, 2005.

[185] C. Bieri, O. P. Ernst, S. Heyse, K. P. Hofmann, and H. Vogel. Micropatterned immobilization of a G protein-coupled receptor and direct detection of G protein activation. *Nat Biotechnol*, 17(11):1105–8, 1999.

[186] G. M. Whitesides. The 'right' size in nanobiotechnology. *Nat Biotechnol*, 21(10):1161–5, 2003.

[187] J. P. Renault, A. Bernard, D. Juncker, B. Michel, H. R. Bosshard, and E. Delamarche. Fabricating microarrays of functional proteins using affinity contact printing. *Angew Chem Int Ed Engl*, 41(13):2320–3, 2002.

Acknowledgements

Je tiens à exprimer ma plus profonde gratitude à toutes les personnes qui ont, de près ou de loin, participé à l'élaboration de cette thèse:

Je remercie mon directeur de thèse, le Professeur Horst Vogel, pour m'avoir proposé ce sujet et m'avoir permis d'intégrer son groupe, ainsi que pour ses conseils et sa confiance. Travailler dans son laboratoire, au sein d'un environnement interdisciplinaire et aux intérêts scientifiques divers, a été une expérience très enrichissante.

Je tiens à exprimer ma reconnaissance au docteur Horst Pick, qui a supervisé mon travail tout au long de ces années avec beaucoup d'intérêt et d'engagement. Il m'a initiée à la biologie moléculaire et cellulaire, a corrigé ma thèse de manière critique et a toujours été présent pour répondre à mes questions. Je le remercie de tout coeur pour son soutien constant, sa patience et son amabilité.

Je suis aussi reconnaissante envers le docteur Michael Prummer, qui m'a appris l'imagerie de molécules uniques, et qui a corrigé une partie de cette thèse. Je le remercie pour sa patience et pour son optimisme.

Je remercie Cédric Deluz pour son aide, en particulier à la fin de ma thèse. C'est avec enthousiasme qu'il a entrepris de nouvelles cultures cellulaires.

Merci également au docteur Jean-Manuel Segura pour être toujours ouvert aux discussions et pour ses commentaires critiques lors de la rédaction de ma thèse.

Je remercie le Professeur Kai Johnsson, Nathalie George, Frédéric Grosjean, Estelle Devèvre, Maurice Perrinjaquet, Andreas Peer, Bruno Meyer, Christoph Schreiter, Paulina Izewska et Sylvain Etter pour leur collaboration et leur aide durant ma thèse.

Merci à Verena Tabet pour sa gentillesse et son aide concernant les tâches administratives.

Merci à tous les membres du LCPPM, anciens et nouveaux, pour leur amitié et pour avoir contribué à faire du laboratoire un endroit agréable où travailler.

Enfin, je remercie ma famille pour son amour, sa présence et son soutien tout au long de ces années.

Curriculum Vitae

Valérie Jacquier

Born on the 4th of October 1976 in Martigny (VS), Switzerland

1991 – 1996	Lycée-Collège de St-Maurice (VS), Switzerland. Degree: Maturité B' (latin-sciences).
1996 – 2001	Studies in Physics at the Swiss Federal Institute of Technology (EPFL), Lausanne, Switzerland. Degree: Ingénieure Physicienne.
1998 – 1999	Erasmus Student Exchange at the Royal Institute of Technology (KTH), Stockholm, Sweden.
2000 – 2001	Diploma Work in the group of Prof. R. Glockshuber, Insitute for Molecular Biology and Biophysics, ETHZ, Zurich, Switzerland.
since 2001	Preparation of this PhD thesis in Biophysics of Membrane Proteins under supervision of Prof. Horst Vogel at the Swiss Federal Insitute of Technology (EPFL), Lausanne, Switzerland.